Scalable Polymeric Nanoparticles for Potential Nose-to-Brain Delivery Applications

Dissertation
zur Erlangung des Grades
des Doktors der Naturwissenschaften
der Naturwissenschaftlich-Technischen Fakultät
der Universität des Saarlandes

von

Selin Akpinar Adscheid

Saarbrücken

2025

Tag des Kolloquiums:	11. Juli 2025
Dekan	Prof. Dr. Dirk Bähre
Berichterstatter:	Prof. Dr. Marc Schneider
	Prof. Dr. Claus Jacob
Vorsitz:	Prof. Dr. Guido Kickelbick
Akad. Mitarbeiter:	Dr. Brigitta Loretz

This work was performed at MyBiotech GmbH located in Überherrn, Germany and Saarland University located in Saarbrücken, Germany between October 2021 and September 2024 under the supervision of Dr. Nazende Günday-Türeli and Prof. Dr. Marc Schneider.

This work was carried out as part of the Bio2Brain project which has received funding from the European Union's Horizon 2020 research and innovation programme under the Marie Skłodowska-Curie grant agreement No 956977.

Table of Content

Contents

List of Figures 7
List of Tables 10
Abstract 11
Kurzzusammenfassung 12
Abbreviation list 13
1. Introduction 14
1.1. Scientific Background 15
1.1.1. CNS Diseases 15
1.1.2. Brief introduction to Drug Delivery Systems 17
1.1.3. Strategies for Effective Non-invasive Brain Delivery 19
1.1.4. Delivery of Biopharmaceuticals 25
1.1.5. Manufacturing DDS for Brain Delivery 28
1.1.6. GMP-compliant Downstreaming Methods 38
1.2. Techniques of Interests 41
1.2.1. Emulsification/Solvent Evaporation (Double Emulsion) Method 41
1.2.2. Spinning Disc System 44
1.2.3. Micro-spray-reactor System 47
2. Aim and Scope of the Dissertation 49
3. Formulating and Manufacturing Scalable Polymeric NPs 52
3.1. Introduction 53
3.2. Materials and Method 54
3.2.1. SDS Design and Functionality: Prototype I 54

3.2.2. Preparation of PLGA NPs with the SDS by the modified nanoprecipitation method 55

3.2.3. Preparing Curcumin-loaded PLGA NPs by SDS 58

3.2.4. Preparation of PLGA NPs as double emulsions by the emulsification/solvent evaporation method 61

3.2.5. Screening of possible process parameters to produce PLGA NPs with the double emulsion method by the SDS. 64

3.2.6. Preparation of PLGA NPs by the MSR-system 71

3.2.6.7. Cryo-SEM Imaging of PLGA NPs in suspension and lyophilized form 79

3.3. Results and Discussion 80

3.3.1. Screening of possible process parameters to produce PLGA NPs with the SDS by the modified nanoprecipitation method. 80

3.3.2. Preparing and Optimizing Curcumin-loaded PLGA NPs 85

3.3.3. Preparation of PLGA NPs as double emulsions by the emulsification/solvent evaporation method 90

3.3.4. Screening of the SDS to prepare PLGA NPs as double emulsions. .. 93

3.3.5. Preparation of PLGA NPs by the MSR 99

3.4. Conclusion 106

4. Scalable PLGA NPs for the potential N2B delivery: The proof-of-concept 108

4.1. Introduction 109

4.2. Materials and Methods 110

4.2.1. Preparing Scalable Fluorescent PLGA NPs 110

4.2.2. Colloidal Characteristics, Biocompatibility and Release Profiles of Fluorescent PLGA NPs 115

4.3. Results and Discussions 120

4.4. Conclusions 132

5. Summary and Outlook 133

6. Annexes 137

6.1. References 138

6.2. Scientific Output 152

6.3. Curriculum Vitae 154

6.4. Acknowledgements 155

List of Figures

Figure 1. Structure of the BBB. 16

Figure 2. DDS for Brain Delivery. 18

Figure 3. Schematic representation of different brain delivery routes. 19

Figure 4. Advantages and limitations of N2B delivery 21

Figure 5. Nasal Anatomy: Nasal vestibule olfactory and respiratory region. 23

Figure 6. The anatomy of the nasal cavity and the suggested direct and indirect transport mechanisms for the N2B delivery. 25

Figure 7. Schematic representation of essential steps for transition of nano-pharmaceutical DDS from bench to bedside. 28

Figure 8. Nanoprecipitation method. 32

Figure 9. Emulsification/solvent evaporation method. 33

Figure 10. Salting-out method. 35

Figure 11. Illustration of a simple cross-flow filtration setup 40

Figure 12. Preparation of polymeric NPs by double emulsion method 41

Figure 13. Illustration of SDS set-up. 46

Figure 14. Illustration of MSR-system 48

Figure 15. Preparation of the PLGA NPs by the SDS with the modified nanoprecipitation method 55

Figure 16. Different disc materials and surface structures for polyamide (PA), polypropylene (PP), and concave shaped polypropylene (CA) discs 57

Figure 17. Preparing curcumin-loaded PLGA NPs by the SDS 59

Figure 18. Illustration of the W/O/W Double emulsion structure 62

Figure 19. Further method development for preparation of PLGA NPs with the double emulsion method 63

Figure 20. Final preparation of the PLGA NPs by the double emulsion method 64

Figure 21. Second SDS Prototype for preparing PLGA NPs by the double emulsion method..... 65

Figure 22. Representation of different connector types for the SDS 71

Figure 23. Preparing PLGA NPs by the MSR system 72

Figure 24. Final preparation protocol for PLGA NPs by the MSR-system by the double emulsion method 74

Figure 25. Illustration of the Nanosep® centrifugal devices..... 75

Figure 26. Preparation of albumin-loaded PLGA NPs (reactor and bench top preparations) 77

Figure 27. Representation of how different disc types influence the particle size and distribution properties of the PLGA NPs 81

Figure 28. Representation of the effect of different disc surface patterns on PLGA NPs with PA-1 having a flat surface while PA-3 and PA-9 featuring non-flat surface structures..... 82

Figure 29. Effect of motor voltage on PLGA NPs..... 83

Figure 30. Influence of needle diameter on the properties of PLGA NPs 84

Figure 31. Contour plot for effect of disc speed and flow rate on particle size 87

Figure 32. Contour plots for the effect of disc speed and polymer concentration on PDI as well as effect of droplet size and flow rate on PDI 88

Figure 33. Contour plots for the effect of disc speed and flow rate, droplet size and polymer concentration, and the flow rate and polymer concentration on the EE% ... 89

Figure 34. PLGA NPs, double emulsion optimization, influence of W:O:W ratio and surfactant concentration 91

Figure 35. PLGA NP as double emulsion method development optimization: the effect of W:O:W ratio and surfactant concentrations in the outer phase..... 92

Figure 36. DLS measurements for particles produced with different disc types..... 93

Figure 37. DLS measurements for different disc rotation speeds. The legends were labelled with different colors corresponding to different disc rotation speeds. 95

Figure 38. DLS measurement obtained for different connector types. 96

Figure 39. DLS measurement for different phase ratios 98

Figure 40. Cryo-SEM image of lyophilized PLGA NPs..... 106

Figure 41. Illustrative summary of aim of the chapter 109

Figure 42. Synthetic Pathway to Rhod-PLGA 110

Figure 43. Preparation of the albumin-FITC-loaded Rhod-PLGA NPs..... 112

Figure 44. Preparation of the WGA488-loaded PLGA NPs..... 114

Figure 45. Ratio Measurement 119

Figure 46. Correlation between the kinetics profiles.. 122

Figure 47. MTT assay results after 4 h of incubation for varying concentrations. .. 123

Figure 48. Rhod-PLGA NPs localization after 24 h of incubation..... 124

Figure 49. Cumulative release profile from the albumin-FITC loaded PLGA NPs.. 126

Figure 50. Albumin-FITC loaded Rhod-PLGA NPs localization and release. 127

Figure 51. WGA488-loaded PLGA NPs release studies.. 129

Figure 52. Comparison of the cargo release in 24 h. 131

List of Tables

Table 1. Screened process parameters for the PLGA NPs prepared by the SDS.... 56

Table 2. Factors in Box-Behnken design space for process optimization of curcumin-loaded PLGA NP formulation..... 60

Table 3. Screening of effect of different disc types to prepare PLGA NPs by the double emulsion method with the SDS..... 66

Table 4. Screening of effect of different disc rotation speeds to prepare PLGA NPs by the double emulsion method with the SDS..... 67

Table 5. Screening of effect on different primary emulsion-to-W_2 phase ratios to prepare PLGA NPs as double emulsions by the SDS 69

Table 6. Screening of effect on different connector types to prepare PLGA NPs as double emulsions by SDS..... 70

Table 7. HPLC-UV Method, Ciprofloxacin HCl 76

Table 8. Box-Behnken design coefficient table for the NPs 85

Table 9. Characterization of the Ciprofloxacin-HCl-loadedPLGA NPs, Before CFF 101

Table 10. Characterization of Ciprofloxacin-HCl-loaded PLGA NPs, After CFF..... 102

Table 11. Particle size measurements: PLGA NPs by bench top vs MSR 103

Table 12. Assay results of the Albumin-FITC-loaded PLGA NPs. 104

Table 13. Albumin-FITC PLGA NPs Assay Results 104

Abstract

Nose-to-brain (N2B) delivery offers a non-invasive route to treat central nervous system (CNS) diseases via bypassing the blood-brain barrier (BBB). Polymeric nanoparticles (NPs) such as poly*(lactic-co-glycolic acid*) (PLGA) NPs are biodegradable, making them promising carriers. Incorporating hydrophobic and hydrophilic small and large molecular weight (Mw) substances with innovative methods could enhance bioavailability. However, scalable manufacturing of these NPs remains a challenge. Therefore, this study investigates encapsulating model substances with different Mw into these PLGA NPs using two continuous manufacturing technologies: the spinning disc system (SDS) and the micro-spray-reactor (MSR). By employing the modified-nanoprecipitation method with the SDS, a small Mw hydrophobic substance (curcumin), and by the double emulsion method and MSR, small and large Mw drugs (Ciprofloxacin HCl and albumin-FITC) were successfully encapsulated with high encapsulation efficiencies. Blank and model-substance-loaded (albumin-FITC and wheat germ agglutinin-488 (WGA488)) fluorescent PLGA NPs were prepared using the MSR system to assess their potential for future N2B delivery applications. The NPs showed biocompatibility and sustained drug release profiles and were not internalized in test cells, which is ideal for N2B delivery. Overall**,** these proof-of-concept studies show scalable NP manufacturing and flexible drug loading for future applications such as N2B delivery.

Kurzzusammenfassung

Das Delivery von Wirkstoffen über die Nase zum Gehirn (N2B) bietet einen nicht-invasiven Weg zur Behandlung von Erkrankungen des zentralen Nervensystems durch Umgehung der Blut-Hirn-Schranke. Polymere Nanopartikel (NP) wie PLGA NP sind bioabbaubar und daher vielversprechende Träger. Die Einbindung hydrophober und hydrophiler Substanzen mit kleinen und großen Molekulargewichten (Mw) mittels innovativer Technologien könnte die Bioverfügbarkeit verbessern. Die skalierbare Produktion dieser NPs bleibt jedoch eine Herausforderung. Diese Studie untersucht die kontinuierliche Herstellung von PLGA NPs mit Modellsubstanzen unterschiedlichen Mw mittels Spinning-Disc-System (SDS) und Micro-Spray-Reactor (MSR). Mit der modifizierten Nanopräzipitationsmethode mit SDS und einer hydrophoben Substanz mit kleinem Mw (Curcumin) sowie der Doppelemulsionsmethode und dem MSR wurden Substanzen mit kleinem und großem Mw (Ciprofloxacin HCl und Albumin-FITC) erfolgreich mit hoher Verkapselungseffizienz verkapselt. Leere und mit Albumin-FITC und WGA488 beladene fluoreszierende PLGA NP wurden mit dem MSR-System hergestellt, um ihr Potenzial für künftige N2B-Transportanwendungen zu bewerten. Die NPs wiesen Biokompatibilitäts- und anhaltende Wirkstofffreisetzungsprofile auf und wurden nicht zellular internalisiert, was für die N2B-Verabreichung ideal ist. Insgesamt zeigen diese Studien, dass die Herstellung von NPs mit verschiedenen Wirkstoffmolekülen für zukünftige Anwendungen skalierbar machbar ist.

Abbreviation list

BBB	Blood-Brain Barrier
BSA	Bovine Serum Albumin
CFF	Cross-flow Filtration
CLSM	Confocal Laser Scanning Microscopy
CNS	Central Nervous System
DCM	Dichloromethane
DDS	Drug Delivery System
DLS	Dynamic Light Scattering
DoE	Design of Experiment
EA	Ethyl Acetate
EE%	Encapsulation Efficiency
EMEM	Eagle's Minimum Essential Medium
FITC	Fluorescein isothiocyanate
GMP	Good Manufacturing Practices
HBSS	Hanks' Balanced Salt Solution
Mw	Molecular weight
MSR	Micro-spray-reactor
NP	Nanoparticle
NS	Non-solvent
PBS	Phosphate-buffered Saline
PDI	Polydispersity Index
PLGA	Poly (lactic-co-glycolic acid)
PVA	Polyvinyl alcohol
RCF	Relative Centrifugal Force
RPM	Revolutions per minute
ROI	Region of Interest
SDS	Spinning Disc System
NS	Non-solvent
WGA	Wheat Germ Agglutinin

1. Introduction

Part of this chapter has been published in Beilstein Journal of Nanotechnology as part of the thematic issue “Emerging targeting strategies and next generation of nanomedicines” as a review article following: Akpinar Adscheid, A.E. Türeli, N. Günday-Türeli, M. Schneider, Nanotechnological approaches for efficient N2B delivery: from small-molecule drugs to biopharmaceuticals, Beilstein J. Nanotechnol. 15 (2024) 1400–1414. https://doi.org/10.3762/bjnano.15.113.

Part of this chapter has been submitted to Taylor & Francis as a book chapter as follows: Akpinar Adscheid, S.; Türeli, A.E.; Günday-Türeli, N. Industrial Aspects to be considered for drug delivery for brain.

The figures in this chapter have been created with Biorender.com in scope of student licensing plan.

1.1. Scientific Background

1.1.1. CNS Diseases

Central nervous system (CNS) consists of the brain and the spinal cord and is considered the body's processing and control center. While the brain controls most of the functions in the body, the spinal cord carries messages from the brain to the other parts of the body [1]. Like other systems and parts of the human body, the CNS is susceptible to various disorders [2]. CNS diseases are a group of challenging pathological conditions which can be originated to ischemic, neurodegenerative, inflammatory or developmental disorders [3]. Among them, neurodegenerative diseases can be explained by progressive loss of neurons, and lead to diseases such as Multiple Sclerosis (MS), Alzheimer's, Huntington´s, and Parkinson's Diseases [4,5].

In broader perspective, CNS diseases affects both patients and society and causes one in nine deaths worldwide [6]. For example, solely in 2019, there were nearly 10 million deaths, and 349 million disability-adjusted life years (DALYs) were estimated due to neurological diseases [7]. The estimated cost of these diseases to the European healthcare budget is around 800 billion Euros per year [8]. The World Health Organization (WHO) highlights that every year almost 8 million new cases of Alzheimer's disease are reported [9]. In addition, the Global Burden of Diseases, Injuries, and Risk Factors Study (GBD) reported, there were 2.2 million cases of MS worldwide in 2016 [10]. While the importance of providing efficient therapies for CNS diseases is clear, from a pharmaceutical perspective it is considered as a significant challenge [11–13]. Therefore, the next sections will focus on these challenges from physiology of brain to formulation development perspectives, with possible innovative solutions.

1.1.1.2. Pharmaceutical Challenges to CNS Diseases: Blood-Brain Barrier

From a pharmaceutical point of view, although there is an immense network of cerebral vascularization, providing therapeutics for CNS diseases is considered a challenge because of the existence of the blood-brain barrier (BBB) (Figure 1) which is composed of several cell types [14].

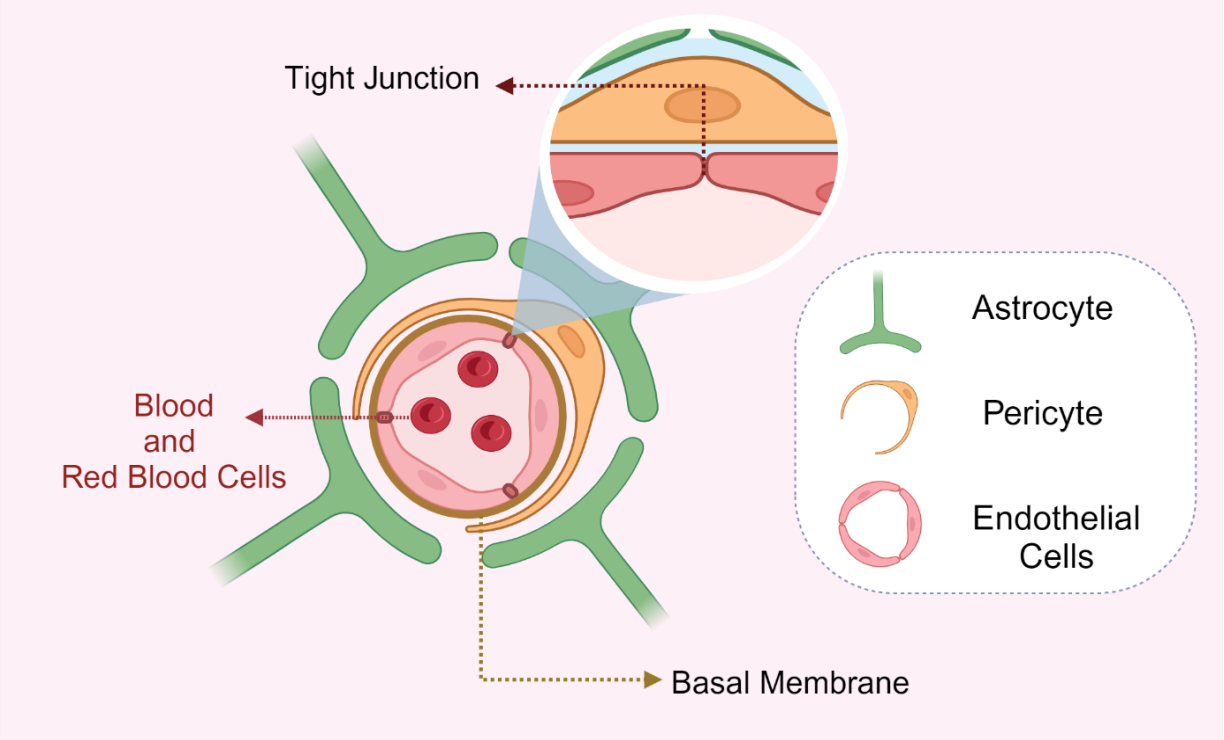

Figure 1. Structure of the BBB. The endothelial cells joined by tight junctions to form a barrier for metabolic functions. The barrier is formed by a basal membrane, pericytes, and astrocytes. The figure is modified from [15].

The BBB is a dynamic and selective interface between the systemic circulation and the brain [16]. The structure of the healthy BBB relies on the endothelial cells and the tight barrier formed using tight junctions [17–19]. These are surrounded by other cell types, such as astrocytes and pericytes. Astrocytes are crucial for the formation and maintenance of the BBB, which leads to an adequate association between the cells

and the BBB. Pericytes are also important regulatory cells for the homeostasis of the BBB. The interaction between astrocytes and pericytes plays a vital role in brain vasculogenesis and the maintenance of the BBB [20]. Overall, the high selectivity of the BBB provides optimal conditions for CNS homeostasis [21].

Due to the presence of the BBB, most systemically administered drugs cannot reach the site of action, the brain. The BBB is reported to limit the passage of 98% of small-molecule drugs and almost all large-molecule therapeutics to the brain [22]. The high density of the intact barrier prevents easy overcoming of the barrier. Thus, different invasive methods, such as disruption of the BBB with osmotic pressure or intrathecal delivery, have been proposed [23]. On the other sides, drug delivery systems (DDS) can offer non-invasive methods to overcome BBB, therefore effectively delivery the drugs to the site of action, the brain.

1.1.2. Brief introduction to Drug Delivery Systems

Drug delivery systems (DDS) are considered as a formulation or device assisting in introducing the therapeutic substance into the body to improve its efficacy and safety while giving possibilities on controlling the release rate and promoting targeting capacities [5].

Regarding particulate formulations, polymeric NPs, lipid NPs (*e.g.*, liposomes, nanostructured lipid carriers (NLCs), and solid-lipid NPs (SLNs)), inorganic NPs, and hybrid NPs stand out due to their various advantages to different drug delivery strategies (Figure 2) [24]. As an example of these advantages, lipid NPs could offer biocompatibility and biodegradability, and ability to be a reservoir to both hydrophobic and hydrophilic substances [25,26]. Polymeric NPs, on the other hand, can further present extensive tunable characteristics and can be of biological or synthetic origin [27]. Among synthetic polymers, PLGA has been studied intensively due to its

biocompatible and biodegradable structure, which has enabled the FDA approval of PLGA for therapeutic use [28,29]. Moreover, polymeric NPs can be employed to modify the release profile of the drugs when administrated to the body by carefully choosing the polymer properties while preparing NPs [30].

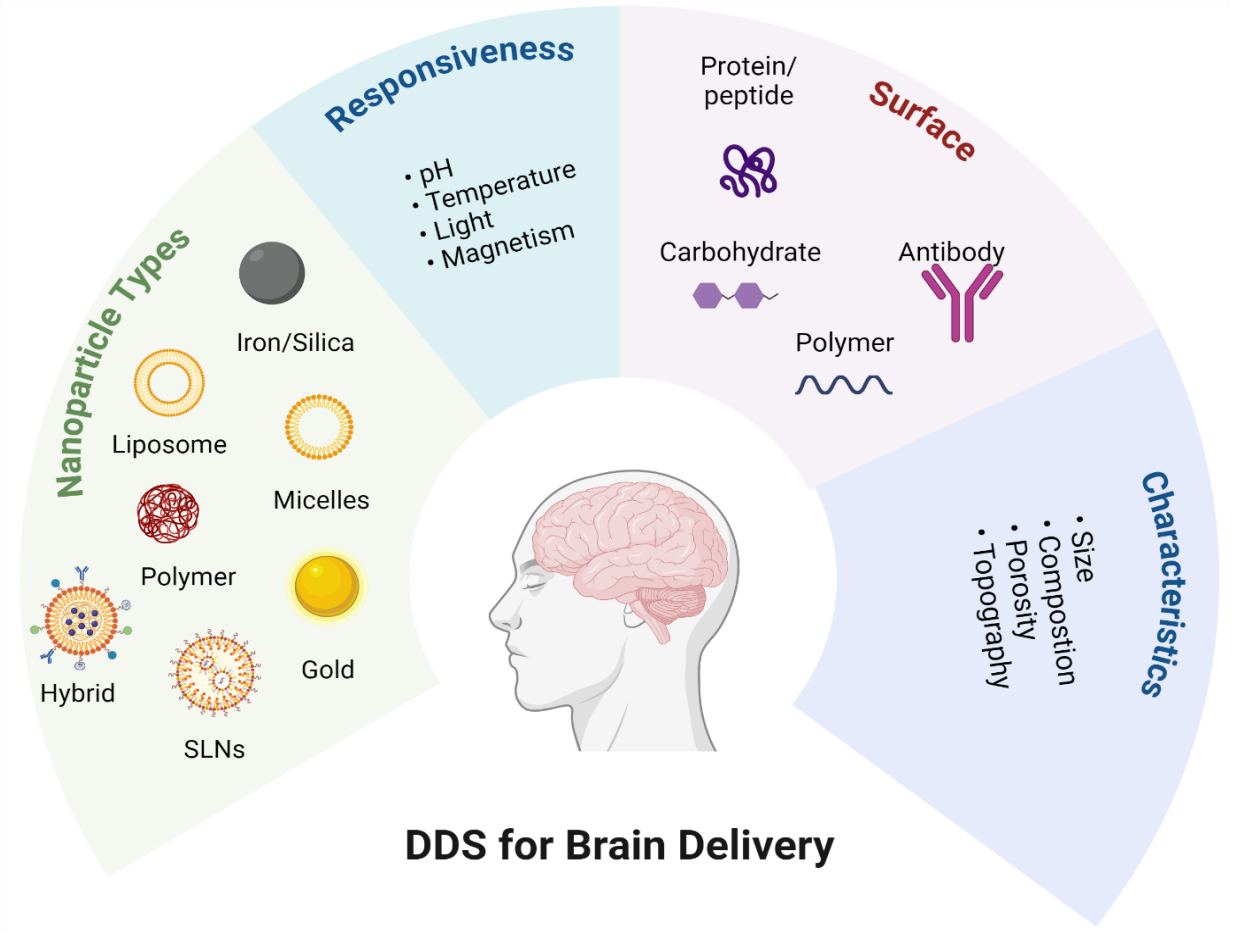

Figure 2. DDS for Brain Delivery. There are many different NP types, and they can exhibit responsive properties. The surface of the NPs can be decorated with different materials to tailor them for therapeutic needs. Their physicochemical and morphological properties play a critical role in drug delivery, especially in brain delivery.

Inorganic NPs, on the other hand, employ a wide range of materials such as gold, silver, and silica. Thanks to these wide range of material types and their unique physicochemical, optical, and electrical properties, they can be used in various applications such as imaging and photothermal therapy [31]. Moreover, these unique

properties allow researchers to tailor these NPs with high functionalization abilities for targeted drug delivery. In addition, when the surface of these DDS is decorated with proteins, peptides, polymers, and carbohydrates, it can exhibit additional targeting abilities [32].

1.1.3. Strategies for Effective Non-invasive Brain Delivery

As mentioned in previous sections, techniques for overcoming the BBB can be invasive (*e.g.*, disruption of the BBB and surgical interventions to administrate the drug at the site of action focusing on the local delivery) or non-invasive (Figure 3) [33].

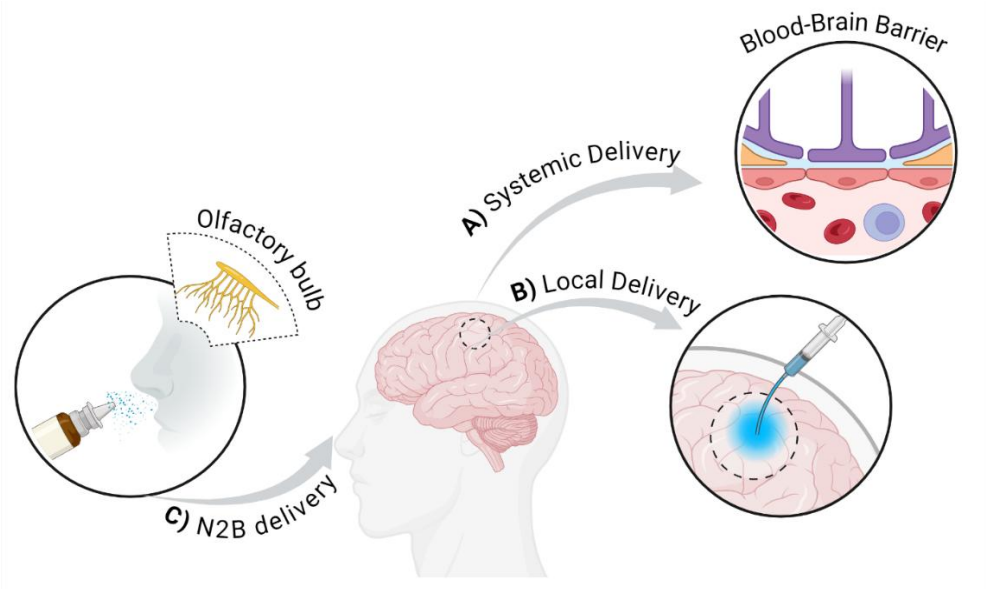

Figure 3. Schematic representation of different brain delivery routes. A) The NPs meet the requirements to cross the BBB can deliver the therapeutics through systemic delivery. B) The local delivery focuses on the direct delivery/injection of the drug at the site of action. C) The N2B delivery can exploit the direct anatomical interaction between the nasal cavity and the brain. The figure is modified from [34].

The use of DDS as an option to treat CNS diseases includes different non-invasive methods including but not limited to intranasal drug delivery, systemic administration by using DDS to overcome BBB, and ultrasound-mediated-drug delivery [35,36]. The systemic route of administration combined with the DDS has interested researchers

who want to cross the BBB [34]. While NPs hold great promise for drug delivery to the brain, their systemic administration faces significant challenges related to BBB penetration, targeting specificity, and their particle size and surface properties requires tailoring that are crucial for crossing the BBB [35,37].

In another technique, ultrasound-mediated drug delivery for brain diseases, researchers employ ultrasound to open the BBB and simultaneously enhance the triggered release of the drugs from the loaded NPs [38]. While ultrasound mediation involves a non-invasive approach to successfully delivering the drug to the brain, one of the main challenges of obtaining clinically relevant results is the establishment of setups that are relevant in the transition from *in vitro* to *in vivo* providing efficiently the acoustic energy needed [39].

In another perspective, the intranasal route of administration to administrate the drugs efficiently to the brain has been gaining interest. The N2B delivery exploits the direct anatomical pathway between the nasal cavity and the brain [40]. This approach highlights the advantages of bypassing the BBB, therefore enabling more efficient delivery of drug substances to the site of action, the brain. While N2B delivery has multiple benefits, such as enhanced drug delivery and bioavailability and reduced systemic side effects it has also limitations due to the high nasal clearance in the nasal cavity and the limited dosage due to the limited surface area that the intranasal route offers (Figure 4) [41–43]. Regardless of the limitations, N2B delivery offers a non-invasive way to bypass the BBB with high patient compliance and with increased CNS bioavailability. Therefore, the next sections focus on this effective strategy to deliver the therapeutics to the brain.

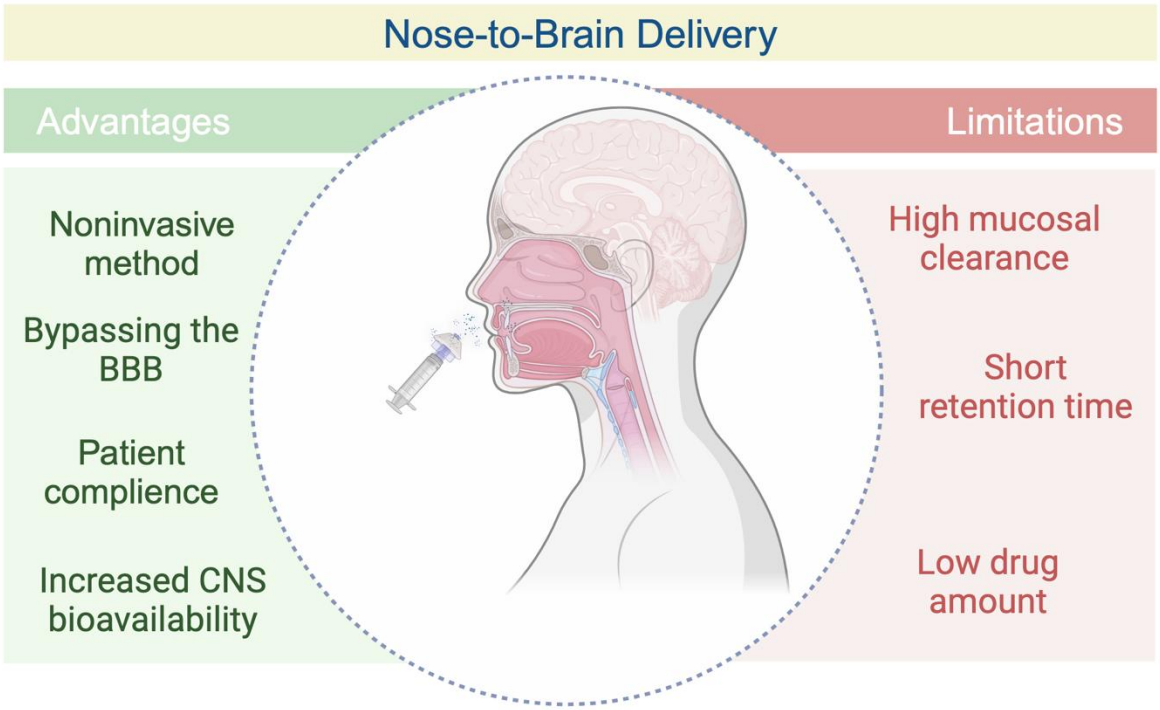

Figure 4. Advantages and limitations of N2B delivery

1.1.3.1. N2B Delivery

The nasal route of drug administration has gained attention over the last decade and has become more attractive, especially with the COVID-19 pandemic vaccine development research [44]. The anatomy of the nose allows non-invasive administration and plays a critical role in intranasal delivery [45]. The nasal cavity has a highly vascularized anatomy and offers a relatively large surface area [46]. Compared to the many other routes of administration, it also has a more permeable structure [47]. These advantages make the nasal route suitable for local delivery and systemic administration [48]. It offers various benefits, including but not limited to a fast onset of action [49]. Intranasal delivery can be used to target a limitedly available site, the brain [50]. The direct anatomical interaction between the nasal cavity and the brain make the olfactory region the primary target for N2B delivery and bypass the BBB [51,52].

When combined with nanotechnology, the N2B delivery becomes an even more attractive route to bypass the BBB since nanotechnology-driven drug delivery systems (DDS) have demonstrated improved drug accumulation at the target site [53]. DDS, such as polymeric or lipid-based NPs, can provide an opportunity to modify the release profile of the drugs, enhance targeting efficiency, and improve nasal permeation during intranasal administration [51,54–56]. In general, the active pharmaceutical ingredients (API) encapsulation into mucoadhesive DDS could eliminate rapid mucosal clearance [57,58] and protect the drug from biological or chemical degradation or deactivation, which results in increasing the bioavailability in the brain [59,60].

The physicochemical characteristics of the DDS are important in determining the success of drug carriers for CNS targeting. For example, the DDS's size, shape, and surface characteristics directly affect cellular transport and uptake, biodistribution, and their interaction with biological interfaces [61,62]. In terms of the effect of particle size, NPs with a size of approx. 15 nm or below were observed to penetrate the olfactory bulb thanks to the paracellular space in the olfactory epithelium [63]. Moreover, NPs with sizes up to 300 nm were found and considered suitable for intranasal delivery [64,65]. Among them, the significant portions of the NPs studied for N2B delivery are approx. 200 nm, which is the average size of olfactory exons [52,66]. Rejman et al. demonstrated that the clathrin-mediated pathway of endocytosis has an upper limit for internalization of approximately 200 nm. Their study also revealed that an increase in particle size led to a shift towards caveolae-mediated internalization, the primary pathway for particles sized around 500 nm [67]. This shows the possibility of an even more extended particle size range to be considered for N2B delivery [67]. Regarding surface characteristics, chitosan-coated NPs can be a good example, as positively charged chitosan and its derivatives interact with negatively charged mucin. This

interaction can enhance the NPs residence time in the nasal cavity [68] increasing the likelihood to be uptaken or overcome the barrier.

As represented by the examples the combination of intranasal delivery with DDS, N2B delivery already has been studied with different perspectives. However, understanding nasal anatomy and N2B delivery transport mechanisms could lead to better exploitation of the technique. Therefore, the next section focuses on these important aspects.

1.1.3.2. Nasal Anatomy

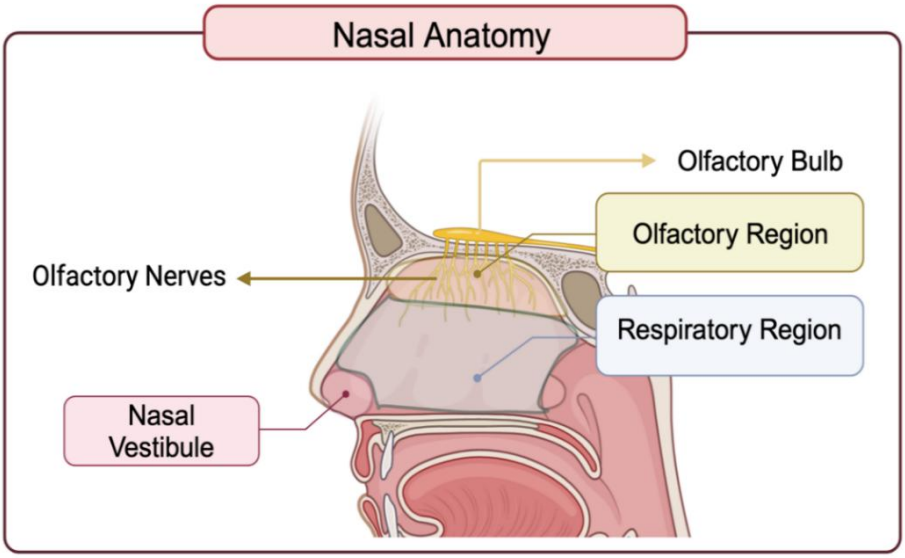

Figure 5. Nasal Anatomy: Nasal vestibule olfactory and respiratory region. Adapted from [69].

The nose has a complex anatomical structure and is responsible for the olfactory and respiratory actions of the human body. The nasal cavity comprises the vestibule, olfactory, and respiratory regions [70] (Figure 5). The nasal vestibule is the anterior part of the nasal cavity. The latter parts, olfactory and respiratory regions, have the possibility for further drug absorption but differ in their routes of drug delivery pathways. While the olfactory mucosa is predominantly targeted for N2B delivery applications, respiratory mucosa is also being investigated due to respiratory mucosa intervening in

the trigeminal nerve and providing a possible indirect transport of the drugs to the brain with a systemic pathway [40].

The central focus of the research interest is the olfactory region in the upper part of the nasal cavity lined up with the olfactory epithelium. It consists of three primary parts: olfactory epithelium, lamina propria, and the basal membrane [71]. The olfactory epithelium is the specialized epithelial tissue mainly formed by basal, supporting, and olfactory sensory neurons [72]. The olfactory sensory neurons are bipolar neurons and chemoreceptors that play an essential role in recognizing odor [73]. They deliver information to the olfactory bulb, where it is processed [74]. Below the olfactory epithelium is another part of the olfactory region, the lamina propria, which contains different cell types, including Bowman's Glands, responsible for producing mucus [75]. The lamina propria is also the region where the olfactory sensory neurons start and form the installments of the olfactory sensory neurons [76]. The respiratory mucosa, on the other hand, lines with the respiratory epithelium and contains mainly ciliated cells, goblet cells, and basal cells [77].

1.1.3.3. Transport Mechanisms for N2B Delivery

The transport mechanisms for the N2B delivery are yet to be fully understood. It is suggested that olfactory and trigeminal nerves are responsible for direct transport to the brain through the nasal route (Figure 6). For the olfactory pathway, the drugs pass through the cribriform plate and are projected to the olfactory bulb [51]. In addition to the olfactory path, there is the trigeminal pathway, the largest and fifth cranial nerve [78]. Even though the trigeminal pathway is less explored than the olfactory pathway, a study by Li et al. showed that the trigeminal pathway could be the dominant pathway for the N2B delivery of intact polymeric NPs [79]. Furthermore, due to the highly

vascularized nature of the respiratory region of the nose, drug transport can also follow a systemic pathway through this region [80].

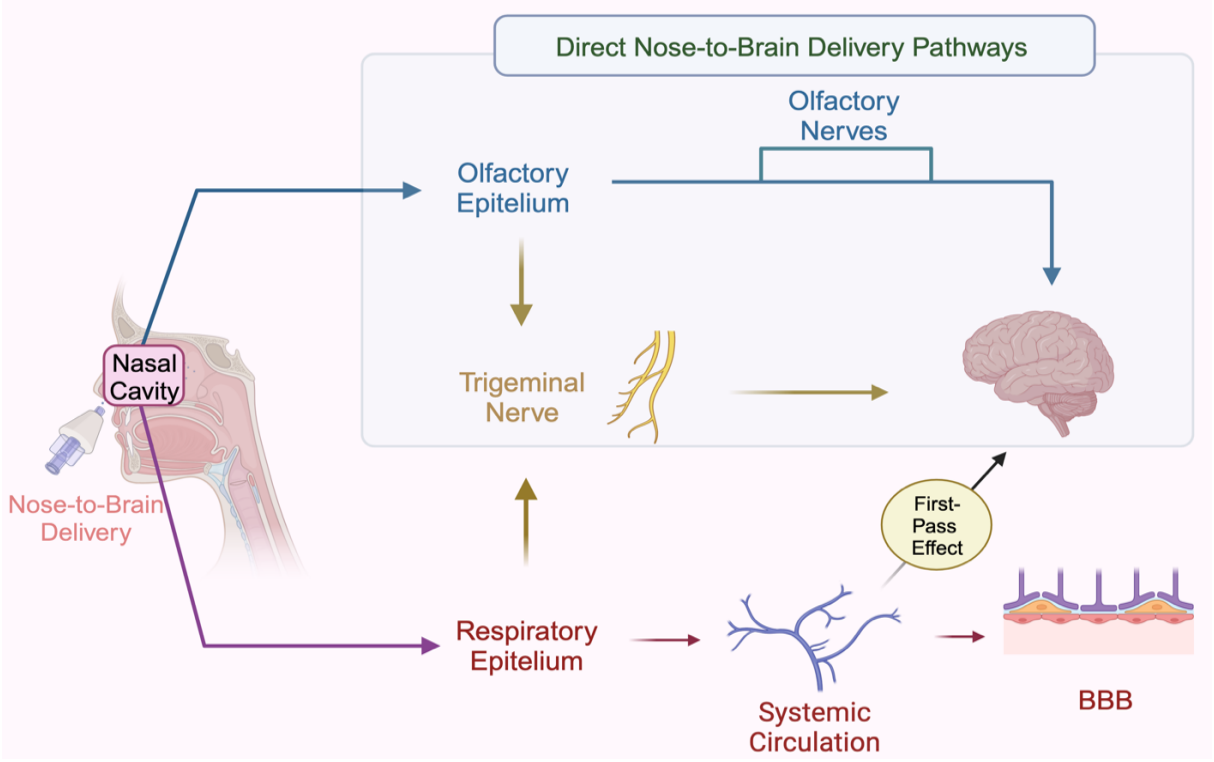

Figure 6. The anatomy of the nasal cavity and the suggested direct and indirect transport mechanisms for the N2B delivery. The direct transport of the drugs can be within the olfactory epithelium or trigeminal nerve. The figure is inspired by [66].

Drug transport through N2B mainly includes intracellular and extracellular mechanisms [50]. While the intracellular pathway is based on the drug's internalization by the neurons followed by axonal transport, the extracellular pathway is based on the drugs' transport through the paracellular space [81,82].

1.1.4. Delivery of Biopharmaceuticals

Biopharmaceuticals have been described in the literature as an advanced therapeutic option for CNS diseases. One of these advanced therapeutics is molecular antibodies (mAbs) which are generated from B cells and are antigen-specific [83]. The advantages, like high specificity and affinity towards target antigens, make therapeutic

monoclonal antibodies one of the highlights of pharmaceutical industry [84]. As a result, an increasing number of FDA-approved mAb-based therapeutics are on the market for treating CNS diseases. For example, for treating MS, Ocrevus, based on CD-20 targeting mAb ocrelizumab, is projected to have the highest growth in sales by 2025 [85]. Moreover, aducanumab, a mAb IgG1, was approved for treating Alzheimer's Disease in 2021 [86]. Even though there are successful examples, using the full potential of mAbs for treating CNS diseases is limited. It is estimated that only 1 in 1000 antibodies can reach the brain with a concentration as low as 0.1% of the injected dose [87]. As an example, aducanumab can be mentioned. Although it has low BBB passage, it targets the brain amyloid plaque at high injection doses. However, these doses can also cause BBB disruption [88]. Researchers are working on the focused-ultrasound-mediated delivery of aducanumab by shortly opening the BBB, indicating the need for novel targeting strategies for mAbs [89]. As another example, ocrelizumab showed modest disease progress in clinical trials [90,91] although only a limited amount of the Cd20 antibodies can cross the BBB. This can be attributed to their large size and degradation-prone nature [92,93].

In addition, siRNA therapy is also considered a powerful tool for modulating gene expression through gene silencing, and it can open new doors for disease treatments [94]. Currently, *patisiran*, *givosiran*, *lumasiran*, *inclisiran*, nedosiran, and *vutrisiran* are siRNA-based drugs approved by FDA for treating different diseases [95]. Besides these successful efforts, their delivery to the site of action with the highest efficiency and without toxicity or enzymatic degradation is considered a challenge [96]. Therefore, using DDS to deliver biopharmaceuticals along N2B will provide increased stability and targeting potential. Thus, new possibilities for their use in treating CNS diseases will arise.

Despite the advantages of mAbs, limited number of studies is available in literature with respect to N2B delivery for treating CNS diseases. The challenge of delivering these molecules and the lack of extensive research compared to other biopharmaceuticals could be attributed to their large molecular size, low stability and high required doses, which limit their formulation options with DDS [97]. On the other hand, the trend has been changing, and more research highlighting nanotechnological approaches for delivering mAbs via the nasal route has been available [98]. For instance, Musumeci et al. worked on the absorption of the anti-TRAIL (Tumor necrosis factor (TNF)-Related Apoptosis Inducing Ligand)-neutralizing mAbs on the surfaces of polymeric NPs and NLCs for the treatment of Alzheimer's Disease. The *in vivo* studies in a mouse model showed that polymeric NPs and NLCs reached the brain via N2B delivery. They also showed that the adsorption of the monoclonal antibody onto the NPs led to an increase in particle size and influenced the distribution of NPs in the hippocampus, indicating another critical factor for N2B delivery: the particle size of NPs [99].

In another study with mAbs, Ferreira et al. developed and optimized PLGA and oligomeric chitosan NP system for the co-delivery of alpha-cyano-4-hydroxycinnamic acid and the monoclonal antibody cetuximab to the brain for glioblastoma therapy. The cetuximab conjugation on the NP surface improved the cytotoxicity profile, and a chicken chorioallantoic membrane assay showed enhanced antiangiogenic effects for the mAbs-conjugated NPs. They showed that mucoadhesive NPs with enhanced antiangiogenic effects could be a good candidate for nasal delivery [100].

Additionally, Chu et al. reported Ephrin type-A receptor 3 (EPHA3) tyrosine kinase antibody-modified PLGA NPs. The NPs were coated with N-trimethylated chitosan (TMC), a modified chitosan, which stands out with its water solubility and safety [101]

to overcome nasal clearance and thus increase brain delivery [102]. As a result, TMC-coated NPs showed increased cellular uptake compared to the non-coated NPs in cell uptake studies with C6 glioma cells. Moreover, when Glioma-bearing rats were treated with the NPs, the median survival was increased by 1.37-fold compared to the regular PLGA NPs [102]. In addition to these research efforts, EU-funded consortiums such as N2B-patch (EU's Horizon 2020 grant agreement No: 721098) [103], and Bio2Brain (EU's Horizon 2020 MSCA grant agreement No:956977) have been funded to study N2B delivery of biopharmaceuticals such as mAbs underlining the research activities in the field.

1.1.5. Manufacturing DDS for Brain Delivery

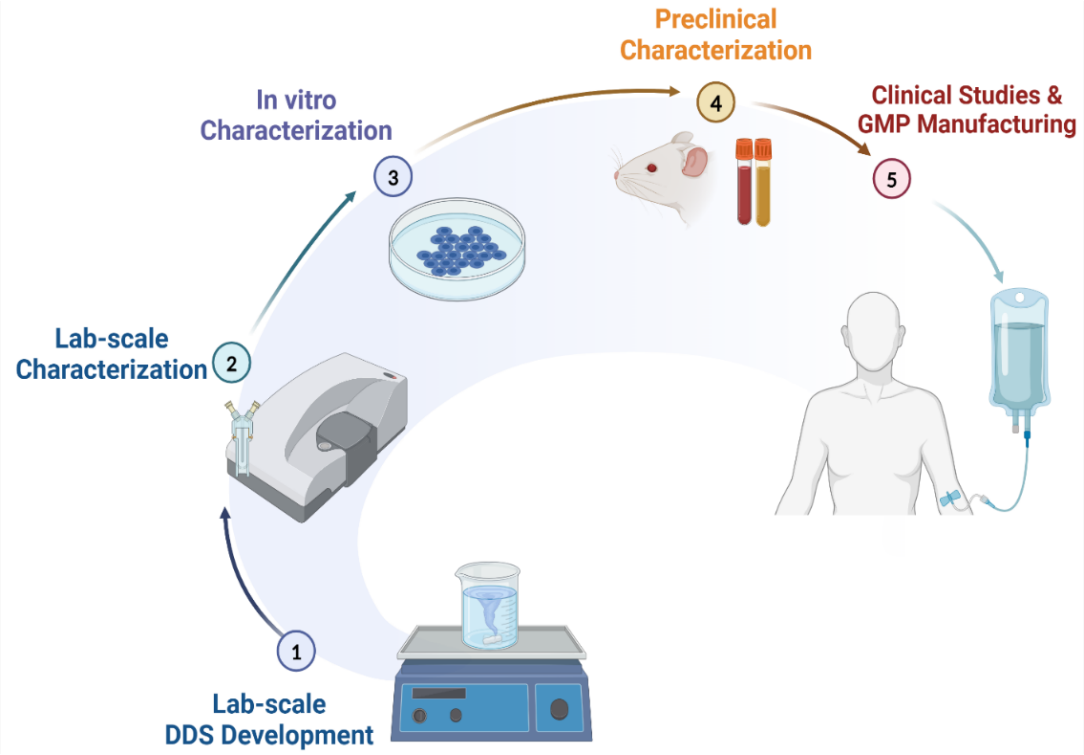

Figure 7. Schematic representation of essential steps for transition of nano-pharmaceutical DDS from bench to bedside. The figure is modified from [104].

As mentioned, each technique and delivery approach have different advantages and disadvantages when successfully delivering the drug to the brain. The manufacturing

techniques used to prepare these DDS determine the fate of the physicochemical properties (such as stability and surface properties) as well as the scalability of the NPs that have been prepared [105]. Therefore, in addition to the route of administration in focus, manufacturing techniques, including both traditional and innovative methods, play a critical role to obtain clinical relevance and transition from bench to bedside [106]. This transition involves multiple steps from developing lab-scale production protocols to good manufacturing practices (GMP) manufacturing (Figure 7). Thus, in the following sections, we introduce both traditional bench top methods and innovative methods to prepare these DDS; while focusing on scalability, and different down-streaming techniques.

1.1.5.1. Polymeric NPs

Due to their tunable physicochemical characteristics, polymeric NPs are a potential vehicle for different drug delivery applications [107]. They can be prepared with easy-to-fabricate production methods [108] and there are also efforts made for reasonable upscaling [109–112]. Among the natural polymers, chitosan and its derivatives could provide many advantages to brain delivery due to their mucoadhesive properties, which increase mucosal retention [113]. In addition to biopolymers, synthetic biodegradable and biocompatible polymers such as poly (lactic acid) (PLA) and poly(lactic-co-glycolic acid) (PLGA), which are approved by the US Food and Drug Administration (FDA) for human administration [114] are relevant options.

Extensive testing has been conducted for polymeric nanoparticles to understand their role in N2B delivery. For instance, Gabold et al. reported the preparation of protein-loaded chitosan NPs decorated with transferrin as a proof-of-concept study to demonstrate a versatile surface functionalization that can also be suitable for N2B delivery. They showed that the transferrin-decorated with the highest amount of

targeting ligand exhibited the highest cellular uptake in the RPMI 2650 human epithelium cell line [115].

In another study, the researchers studied the chitosan coating of PLGA NPs to study the mucosal uptake. Chatzitaki et al. reported the encapsulation of ropinirole hydrochloride (RH), an anti-Parkinson drug, into the chitosan-coated PLGA NPs by the nanoprecipitation method to enhance drug delivery through the nasal mucosa. The researchers assessed the mucoadhesive properties by observing the ability of the NPs to adsorb mucin. While the presence of the mucin did not significantly alter the surface negative charge of the PLGA NPs, the surface zeta potential for the PLGA-chitosan NPs towards more negative values showed that there was an interaction with the mucin. Following this, the RH-loaded NPs showed 3.22-fold enhanced drug permeation through sheep nasal mucosa compared to their non-coated PLGA counterparts [116]. In another study by Spindler et al., the researchers prepared PLGA NPs with batches of different sizes as well as chitosan-coated PLGA NPs to study the uptake mechanisms of these particles into the olfactory mucosa through *ex vivo* permeation studies. As a result, PLGA NPs showed size-time-dependent uptake mechanisms. For instance, PLGA NPs with a particle size of 80 and 175 nm were taken up only after 5 min in the lamina propria, and after 15 min, PLGA NPs with a particle size of 520 nm were associated with nuclei. Additionally, they presented that PLGA NPs with larger particle sizes (520 nm) were accumulated in neural bundles. They showed that this accumulation could enable intracellular uptake in neuronal axons and further provided transcellular transport with the olfactory or trigeminal nerve pathways [117]. It should be noted that while e*x vivo* studies provide advantages such as simplicity in the procedures and offer high tissue availability, differences in tissue morphologies should be considered [118].

Although these results regarding larger particle size (520 nm) are particularly interesting since the particle size generally is considered suitable and reported for N2B delivery for deposition at the olfactory region focuses on 200 nm and below [119], a computational study revealed that NPs size of 500 nm could also be deposited at the olfactory region (less than the smaller NPs) but it should be noted that the computational model only provides limited insights as some factors such as injection position and the effect of the mucus layer was not considered [120]. In addition to these, the study highlighted that the chitosan coating favored the penetration in the mucosa, and this was attributed to the swelling of chitosan at the healthy pH of the nose, and due to well-studied tight junction opening abilities of chitosan [121].

In another study on the mucoadhesion and permeation properties of materials, a thiolated-cellulose was synthesized and used for delivering a model drug, enoxaparin. They reported that thiolation increased mucoadhesion by 9.6-fold in the porcine intestinal mucosa, while the apparent permeability was increased by 2.2-fold. These results showed that thiolated-cellulose could also be a candidate for favoring mucoadhesion and permeability and the polymer can be studied also for nasal mucosa permeation properties in the future [122].

1.1.5.1.1. Bench top Preparation Methods for Polymeric NPs

Polymeric NPs can be prepared by different traditional bench top methods such as nanoprecipitation, emulsification/solvent evaporation, emulsification/solvent diffusion and salting-out. Nanoprecipitation is one of the common and straightforward methods to prepare polymeric NPs. The method requires two miscible solvents. In the bench top nanoprecipitation method, the NP precursor solution containing the polymer dissolved in a water-miscible organic solvent phase is added into the non-solvent

(aqueous phase) (Figure 8). The rapid mixture further supports the polymer assembly and formation of the NPs [123]. Unlike the high-pressure homogenization methods, this simple and cost-effective method does not require high energy input [124].

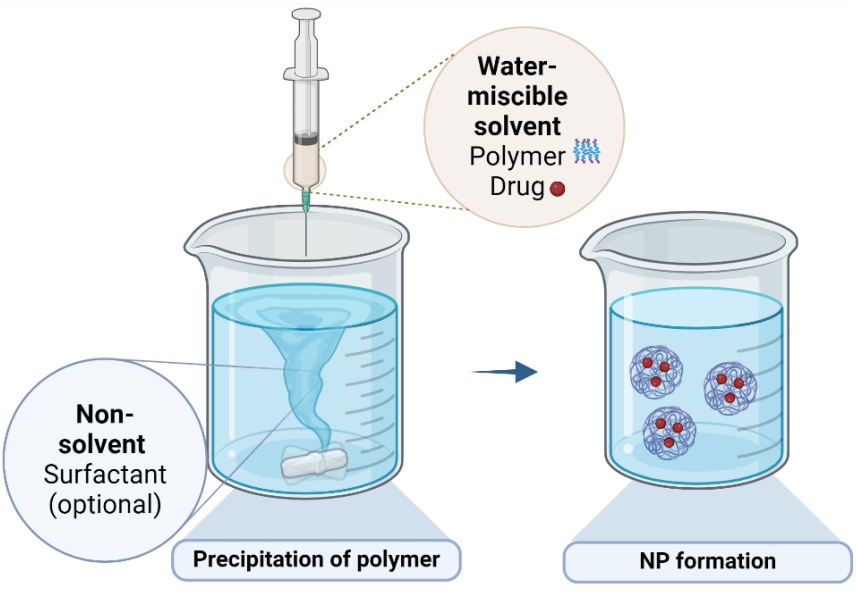

Figure 8. Nanoprecipitation method. The figure is modified from [108].

While simple, several factors were addressed in the literature as an essential step to prepare polymeric NPs with this method and the optimization of the NPs prepared by the nanoprecipitation method may require consideration of several factors. For instance, Draheim et al. conducted a design of experiment (DoE) study to determine the critical factors in preparation of PLGA NPs by the nanoprecipitation method. They showed that the polymer concentration dominantly controls particle size and the polydispersity of the prepared NPs [125]. Furthermore, Krishnamoorthy et al. proposed a multi-criteria decision-making approach for developing camptothecin-loaded polymeric NPs to identify the best possible method to prepare these particles according to several criteria based on instrument (*e.g.*, ease of operation), process (*e.g.*, yield, minimum number of excipients, minimum average particle size and PDI), and cost. The study showed that nanoprecipitation would be the most suitable method to prepare these NPs [126].

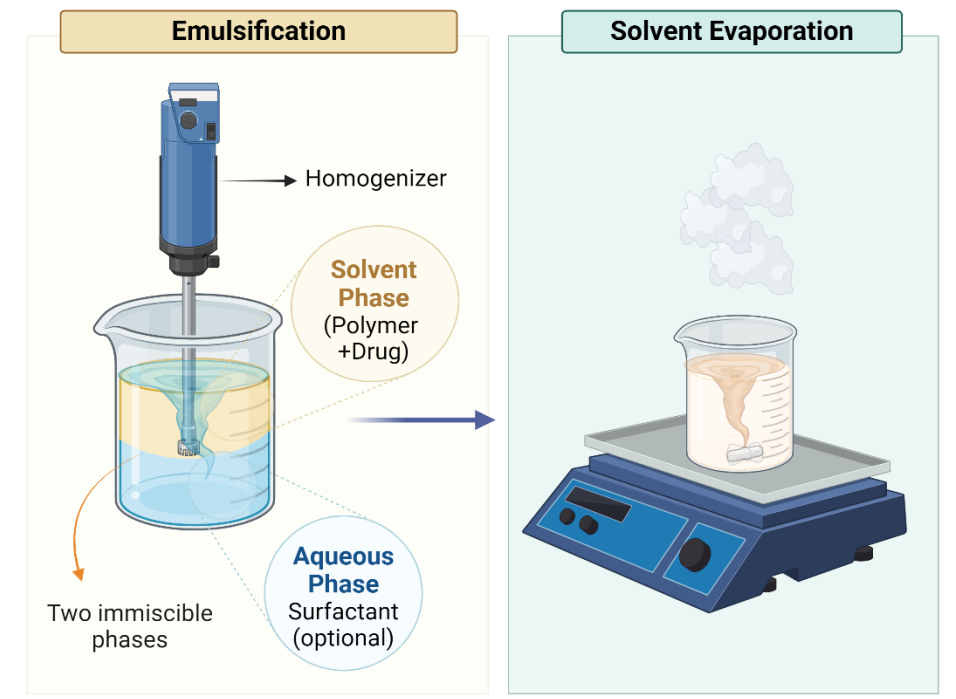

Figure 9. Emulsification/solvent evaporation method. The figure is modified from [108].

Solvent evaporation is another technique widely used for preparing polymeric NPs. In this technique, the polymer is dissolved in a volatile organic solvent and emulsified with an aqueous phase in presence of external high-shear force. The volatile organic solvent evaporates upon emulsification, and the polymer solidifies to form the NPs (Figure 9) [127]. This method can be used for preparing single or double emulsions. In double emulsion method, the primary emulsion is dispersed into another liquid phase and emulsified in presence of an external force to form the NPs [128]. While single emulsion technique is considered more suitable for encapsulating hydrophobic drugs, double emulsion method (water-in-oil-in-water, W/O/W) serves for encapsulating hydrophilic drugs [129]. A detailed discussion on solvent evaporation/emulsification method to form the double emulsions is discussed in techniques of interest/emulsification solvent evaporation (double emulsion) section.

In a study by Hernández-Giottonini et al., polymeric NPs prepared by nanoprecipitation and emulsification-solvent evaporation methods were studied to evaluate the factors

affecting particle size and polydispersity. They showed that high velocities of agitation in solvent evaporation decreased the particle size in both techniques. While in the nanoprecipitation technique, particle size was controllable with polymer and surfactant concentration, in the emulsification-solvent evaporation technique, these could be controllable by organic solvent fractions [130].

Another technique to prepare polymeric NPs is the emulsification/solvent diffusion method, where the polymer is dissolved in an organic solvent phase, which is saturated by the excess water. As in the emulsification/solvent evaporation method, this phase is emulsified by an external high-shear force in an aqueous phase to form the NPs. The addition of extra water is necessary to dilute the solvent phase and, therefore, enhance diffusion and subsequent polymer precipitation, a critical step to form the NPs [131].

Salting-out is also a variation of a solvent diffusion method widely used for developing polymeric NPs where the polymer is dissolved in a water-miscible organic solvent. The polymer-containing-organic solvent phase is added to the aqueous phase with a salting-out agent in the salting-out method (Figure 10). The process does not require high energy, and nucleation occurs when the addition of the excess water leads to diffusing into the organic solvent [132]. Magnesium sulfate, sodium chloride, calcium chloride, and calcium sulfate are the most used salting-out agents [131]. While it is an easy and efficient way to prepare polymer NPs, extensive purification processes are required due to the presence of salting-out agents.

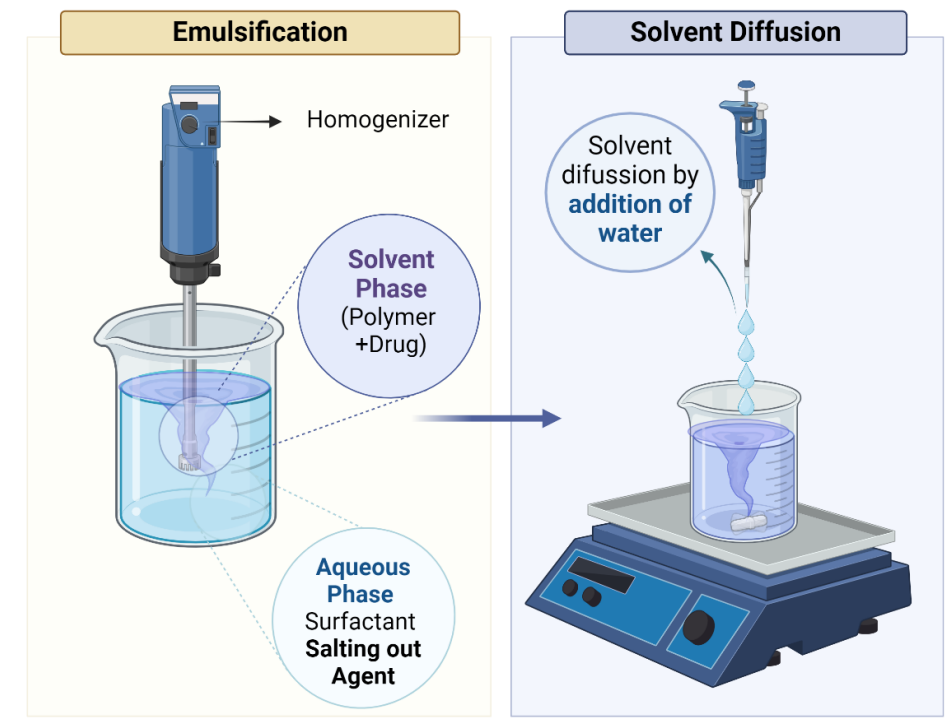

Figure 10. Salting-out method. The figure is modified from [108].

1.1.5.2. Scalability of NP Production Methods

As presented, different traditional nanoparticle manufacturing methods represent different advantages and disadvantages in developing NPs. For instance, nanoprecipitation method is simple and easy to operate, but the particle growth control is limited. The salting-out method requires extensive purification cycles and is considered time-consuming, while high-pressure homogenization is not suitable for thermosensitive drugs due to the heat that the production process requires as well, as removing the solvent used could be problematic [133,134]. While no single production technique fits in producing different types of NPs, developing nanomedicines that can translate from bench side to bedside relies on consideration of the material, process, and regulatory aspects. From a materials perspective, the materials that have been chosen could be biocompatible and regarded as safe to minimize any further biological intolerance. The material's particle size, shape, and degradability are also essential parameters to consider [106]. In terms of processes, as mentioned, there is not a single

process that fits the production of all kinds of NPs. Indeed, the top-down methods are considered more for large-scale industrial production due to ease of operation and control of the final product. Still, there is a need to develop continuous manufacturing technologies that can fill the gap from the lab-scale production to the industrial scale. These technologies offer control over the process parameters, and well-defined parameters enable easier transition in scale-up practices. Therefore, the following section focuses on the different innovative manufacturing technologies and techniques to shorten this gap with examples of brain delivery applications.

1.1.5.3. Innovative Manufacturing Methods

Different innovative methods and technologies such as flash nanoprecipitation and microfluidics are used to prepare NPs with fine physicochemical properties with continuous flow synthesis methods [135].

Flash nanoprecipitation is an innovative milli-fluidic industry-friendly approach like T-junction mixing to produce polymeric NPs [136]. This method uses nanoprecipitation to stimulate the supersaturation through a jet mixer. The process takes place in milliseconds; therefore, this flash mixing induces instant precipitation [137]. One of the limitations of this technique is encapsulation of hydrophilic substances. To overcome this, Massella et al. developed caffeine-loaded poly-ε-caprolactone (PCL)-based polymeric NPs by a confined impinging jet mixer using acetone as the solvent and water as the non-solvent. Their study showed that while caffeine-loaded PCL NPs successfully prepared to entrapment of the substance as well as modifying the release profile, the solvent-drug interactions and the structure of the drug chosen played a vital role in NP production. In another study, Caggiano et al. presented a proof-of-concept study as an extension of the flash nanoprecipitation called the Sequential Flash Nanoprecipitation (SNaP) technique. They showed that using two connected FNP

mixers, core-shell NPs could be prepared at higher core loading and total mass concentration than the traditional single-step procedure with up to 90% core loading [138]. In a different study, researchers encapsulated ibuprofen, which showed potential in treating Alzheimer's disease. The polymeric NPs were prepared under optimized conditions using a four-stream multi-inlet vortex mixer (MIVM) with poly(ethylene glycol)-poly(lactic acid) (PEG-PLA) diblock copolymer as a stabilizer. Notably, *in vivo* studies with mice demonstrated that polysorbate-80 (PS-80)-coated NPs resulted in greater drug uptake into the brain compared to the drug solution itself, highlighting the impact of the PS-80 coating on enhancing drug delivery. [139].

There are also many microfluidic approaches for NP production that can be suitable for large-scale production. Microfluidics offers advantages in NP productions such as being high-throughout, cost-effective, controllable, eco-friendly and due to their easy-to-operate characteristics [140]. In fact, several studies have been conducted to produce DDS for efficient CNS delivery using microfluidics [141]. As an example of these efforts, for instance, Wang et al. developed a microfluidic platform to enhance the delivery of miRNAs through intranasal delivery for glioblastoma therapy. Their microfluidic platform demonstrated that it could efficiently encapsulate therapeutic miRNAs and drugs into size-controllable extracellular vehicles (EVs) using a pressure-based disruption and reconstitution procedure. Their neural stem cell (NSC)-derived EVs loaded with miRNA and labeled with CXCR4 (a G-protein-coupled chemokine receptor) successfully target glioblastoma and enhanced tumor cell apoptosis when combined with temozolomide (TMZ) in their *in vivo* mice studies [142].

In a different study, Samaridou et al. investigated N2B delivery by focusing on delivering RNA via encapsulation into nanocomplexes enveloped with different protective polymeric by traditional and microfluidics methods. They reported that their

microfluidic method yielded fine particle size distribution with tunable mean particle size, protected the RNA from degradation, and prevented premature RNA release in the release media. Furthermore, the *in vivo* studies with mice models of Alzheimer's disease confirmed an increase in miRNA in the hippocampus after intranasal administration [143].

In addition to these efforts, Mohebichamkhorami et al. prepared a novel microfluidic approach to prepare ultra-small and monodispersed chitosan/graphene quantum dot hybrid NPs to prepare optimal NPs for intranasal delivery. Upon intranasal administration, the hybrid ultra-small NPs could penetrate the cytoplasm of C6 glioma cells and showed cell viability depending on exposure and time [144]. Furthermore, Martins et al. developed a microfluidic method to prepare PLGA NPs loaded with an anti-HIV drug to enhance its delivery to the brain. Microfluidic production yielded smaller particle sizes, higher drug association degrees, and higher encapsulation efficiency compared to the conventional method [145].

1.1.6. GMP-compliant Downstreaming Methods

1.1.6.1. Purification

Industrialization and scalability of the NPs would be possible in reasonable compliance in downstream methods for purification, concentration, and storage. For instance, Operti et al. investigated industry-friendly production and downstreaming of PLGA NPs suitable for continuous operation. They manufactured NPs using a scalable inline sonication method. To purify the particles continuously, they employed cross-flow filtration (CFF) and reported that the technique was suitable for sufficient purification of the NPs. Moreover, the choice of enclosed systems made sterilization possible for GMP-compliance manufacturing [146].

The purification of the NPs is an essential step during the particle development process. Sufficient cleaning is necessary to remove any excess substances and impurities that might lead to incompatibility and biological intolerance in future studies. The laboratory-scale purification processes generally involve centrifugation, extraction, dialysis, and filtration-based techniques [147]. While these techniques might suit small-scale laboratory-based production, large-scale NP production requires compliant and automatized methods to achieve sufficient cleaning procedures. One of the industrial-friendly purification techniques is known as CFF (Figure 11) which is an industry-friendly technique that purifies the NPs and removes excess substances. Unlike dead-end filtration methods where the solute goes through to the membrane perpendicularly, which could result in membrane caking and a decrease in the flux, during the CFF procedure the fluid passes through a filter tangentially [148].

In the CFF process, the NPs are passed through a hollow fiber membrane with a specific size cut-off. The hollow fiber membrane is chosen according to the particle size of the prepared nanoparticle, the molecular weight (Mw) of the substance encapsulated, and the required time to perform the purification process. During the CFF, the NPs cannot cross the membrane, so they are collected in the retentate and circulated back to the sample reservoir. Due to their smaller molecular weights, non-encapsulated drugs, excess of surfactant and free polymer chains could pass through the hollow fiber membrane and collected at the filtrate. The CFF system can be used to concentrate the sample, or the initial sample concentration can be kept constant by adding continuous aqueous medium by addition at the same flow rate as the filtrate flow rate.

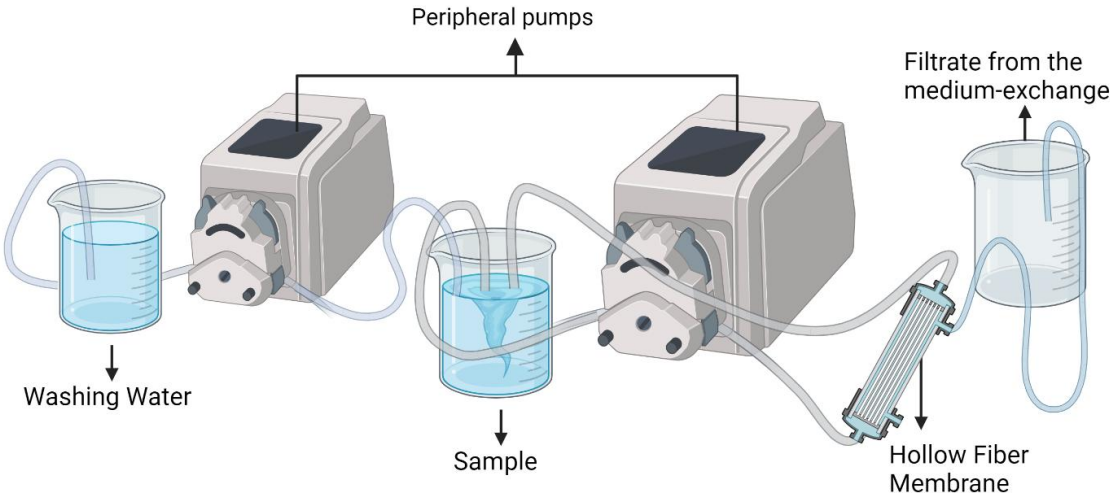

Figure 11. Illustration of a simple cross-flow filtration setup

For instance, in a study by Dalwadi et al., researchers compared diafiltration and the CFF procedure. The study showed that the CFF, with a concentration mode at trans-membrane pressure (TMP) of 10 psi, could efficiently remove the excess polyvinyl alcohol (PVA) in 2.8 h in large batches, unlike the diafiltration and dialysis methods. Moreover, this purification process had less impact on the physicochemical properties of NPs than the ultracentrifugation [149]. Additionally, Lombardo et al. compared the traditional dialysis method with the innovative NanoDis device which relies on the sample and separate technique using the CFF hollow fiber membranes to assess the release profiles of the PLGA nanocapsules loaded with retinoic acid. They showed that while the innovative method could accurately demonstrate the high burst release of retinoic acid from the nanocapsules, the dialysis method could not efficiently demonstrate this effect, underlining the superiority of the NanoDis device.

1.1.6.2. Lyophilization

Lyophilization, also known as freeze-drying, is a dehydration process to improve formulations' (such as NP suspensions) stability, extend their shelf-life, and ease their storage [150]. Including lyophilization is a critical step in the scale-up transfer of NPs.

Developing a design space for lyophilization processes is essential for successful scale-up and technology-transfer processes and should be a focal point of in-process control strategies [151]. Important factors to be considered for the lyophilization of the NPs could be the appropriate choice of the cryoprotectant, cryoprotectant/surfactant ratio, and extensive comparison of the physicochemical properties of NPs before and after lyophilization. For instance, Amis et al. investigated different cryoprotectants for developing lyophilized SLNs. Their study showed that the appropriate choice of cryoprotectant and defining the suitable concentrations were critical, as optimal trehalose concentration prevented significant particle growth after lyophilization [152].

1.2. Techniques of Interests

1.2.1. Emulsification/Solvent Evaporation (Double Emulsion) Method

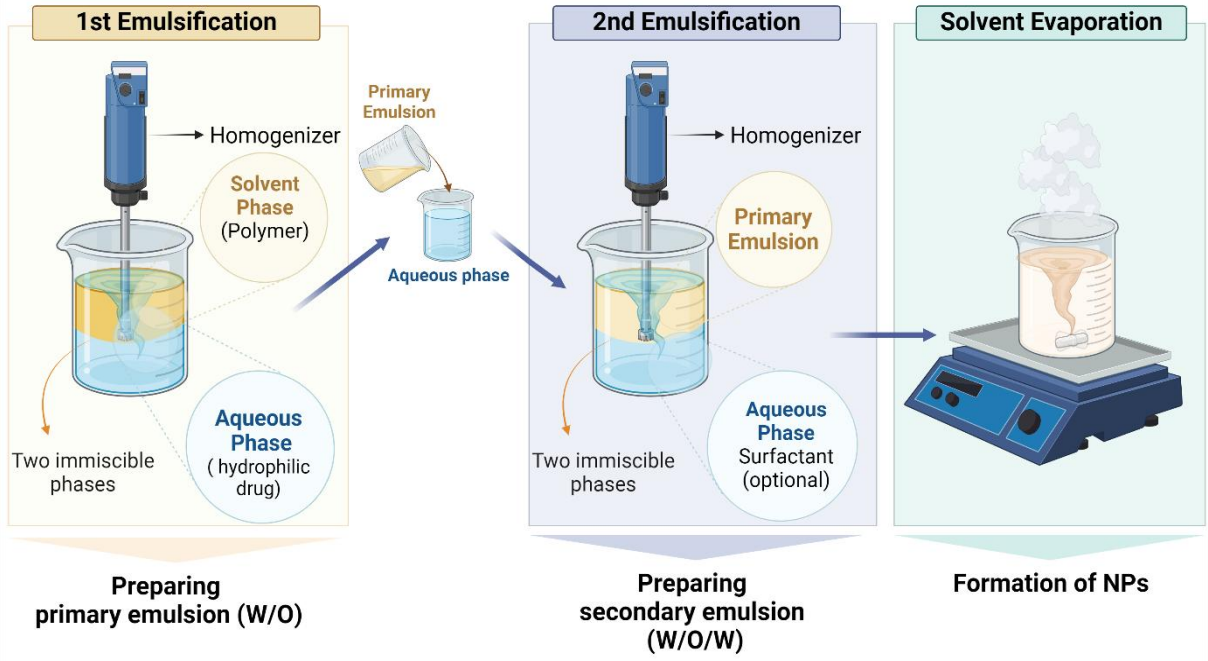

Figure 12. Preparation of polymeric NPs by double emulsion method

Emulsions of emulsions or double emulsions can be prepared by dispersing the droplets of a primary emulsion into another liquid phase. Water-in-oil-in-water (w/o/w) double emulsions can be formulated to encapsulate hydrophilic molecules in its

aqueous core successfully and could provide prolonged release profiles [153]. Unlike the nanoprecipitation method, which is mostly suitable for hydrophobic substances, and the salting-out method, which requires excessive purification processes for purifications, the double emulsions method offers higher encapsulation efficiencies for hydrophilic molecules[154].

In this method, two subsequent emulsifications are performed. Firstly, as in the single emulsion method, the drug is dissolved in the aqueous phase and emulsified with the polymer-containing organic solvent phase to form the primary emulsion. To perform secondary emulsification, the prepared primary emulsion is emulsified with another aqueous phase, generally with a larger volume than the inner (first) aqueous phase. The subsequent evaporation after the emulsification leads to the polymer's solidification and the NPs' formation (Figure 12) [155]. While homogenizers are commonly used in the first step of emulsification for preparing primary emulsion, for secondary emulsification, high-pressure homogenizers [156] or microfluidics [157] have also been used. However, efforts such as microfluidics could also lead to the formation of microparticles rather than NPs.

Multiple critical factors have been identified in polymeric NP preparation using the double emulsion method. For instance, Lamprecht et al. showed that preparation of albumin-loaded polymeric NP encapsulation with regard to particle size and PDI was influenced by the homogenization time, as well as polymer and surfactant concentration in the outer aqueous phase [158]. In another study, Zambaux et al. also showed that high surfactant concentration (3% or more) led to smaller particle size (around 200 nm) [159]. Therefore, while preparing NPs in addition to the homogenization time, the concentration of the polymer and surfactant, as well as phase ratios, should be also considered.

In fact, double emulsions can be used in brain delivery, especially in intranasal drug delivery. For instance, Deepika et al. developed polymeric NPs prepared using the double emulsion method to successfully deliver the frovatriptan succinate to the brain through N2B delivery. The double emulsion method was reportedly chosen to increase the encapsulation efficiency of the hydrophilic drug. As a result, the polymeric NPs prepared by the double emulsion method with a mean particle size of 264 nm showed three times more enhanced permeation across goat nasal mucosa compared to the drug solution [160]. In another study, carboplatin-loaded PCL-based polymeric NPs were developed using the double emulsion method to increase the brain delivery of the anticancer drug by the N2B delivery. As a result, *in situ* nasal perfusion studies with Wistar rats showed higher nasal absorption was achieved by the NP formulation compared to the drug solution [161]. Moreover, the double emulsion method has been used to successfully encapsulate biopharmaceuticals such as bovine serum albumin (BSA) [162,163], human serum albumin (HSA) [159], peptides, [164], insulin [165], oligonucleotides [166], antigens [167] for sustained and controlled release purposes, as well as achieving high encapsulation efficiency for encapsulating biopharmaceuticals [168].

These efforts in encapsulating both small Mw drugs and biopharmaceuticals, as well as their success in N2B delivery indicate that polymeric NPs prepared by the double emulsion method can be a choice for DDS to study N2B delivery of biopharmaceuticals. On the other hand, the scale-up of the double emulsion is considered difficult [154] mainly due to the use of homogenizers in both emulsification steps. While microfluidic efforts have been made to produce double emulsions with scale-up friendly processes, these efforts generally yielded micron-sized particles, and low flow rates and high-pressure drops in the micro-channels make further scalable

practices challenging to perform [169]. Therefore, to promote the bench side transition of polymeric NPs prepared by the double emulsion method, there is a need for efficient continuous manufacturing technologies to promote scalability of this technique. Thus, the following sections focus on possible continuous manufacturing techniques (*e.g.*, MSR-system and SDS for preparing polymeric NPs not only by the nanoprecipitation method for small Mw hydrophobic drugs but also by double emulsion method to encapsulate small Mw hydrophilic drugs and biopharmaceuticals for their possible applications in N2B delivery.

1.2.2. Spinning Disc System

The spinning disc is a device that is designed for automated and continuous production. The systems are designed to provide a continuous flow process where the liquid is fed generally to the center of a rotating disc and spread on the surface of the spinning disc due to centrifugal forces. The process eventually led to a thin film formation on the disc surface, yielding a large surface-to-volume ratio for the fed liquid. One of the advantages of the SDS is that it can be combined with single or multiple feeding jets to micromix different liquids to prepare NPs. In the literature, the preparation of NPs by a spinning disc reactor with titanium oxide [170], silver [171], zinc oxide [172], and beta-carotene [173] has been reported. In addition to these efforts, the adaption of a spinning disc reactor into a spinning disc photocatalytic reactor has been performed where the liquid was fed onto a ceramic disc through a pump, and blue LED lamps were combined with a glass disc for the light illumination purposes for the photocatalytic process [174,175]. A further study enabled the deposition of a yolk-shell nanostructure on the ceramic disc surface for coating and induced photocatalytic degradation of amoxicillin pollutants [176], showing broad application range of spinning disc technology.

In terms of NP preparation techniques, uniform and rapid mixing of liquids on the spinning disc surface enables the application of the nanoprecipitation method in NP production. As a method, nanoprecipitation is based on polymer precipitation by adding the non-solvent (NS) to the solvent (S) solution that contains polymer and involves four main mechanisms: supersaturation, nucleation, crystal growth (a diffusion phenomenon), and coagulation, which leads to NP formation. This uniform mixing of the SDS offers control over the supersaturation, providing control over the following steps, such as nucleation and growth [177]. Thanks to this process, which also influences the spread of the fed liquid on the surface of the disc, in-process control of physicochemical properties of NPs, such as particle size and polydispersity, is possible by controlling different parameters such as disc rotating speed. A study by Mohammadi et al. [170] highlighted that by increasing the disc rotation speeds, it was possible to decrease particle size, which can be attributed to increased shear forces. Another study by Sana et al. also observed the same phenomenon and underlined that an increase in non-solvent to solvent (NS to S) ratio led to reduced particle size due to reduced solubility which promotes higher nucleation and supersaturation. These results also show the possibility of the application of the SDS on preparing polymeric NPs. In addition to the possibility of controlled synthesis of polymeric NPs, post-synthesis purification procedures can be minimized due to the subsequent removal of organic solvents during the production of the NPs by the SDS thanks to the high surface-to-volume ratio the disc surface offers.

Therefore, in this thesis, possibilities of preparing polymeric NPs by nanoprecipitation and double emulsion methods have been investigated by establishing different lab-scale prototypes that enable the assessment of NP formation and subsequently possible process parameters that can influence NP formation for optimizing the NP

production protocols. Unlike the traditional nanoprecipitation method, the modified-nanoprecipitation method, which is also investigated by Zander [178], involves the initial mixing of NS and S phases and, therefore, enables a single starting solution and subsequent evaporation on the disc surface. This potentially reduces NP production time and steps—as illustrated in figure 13.

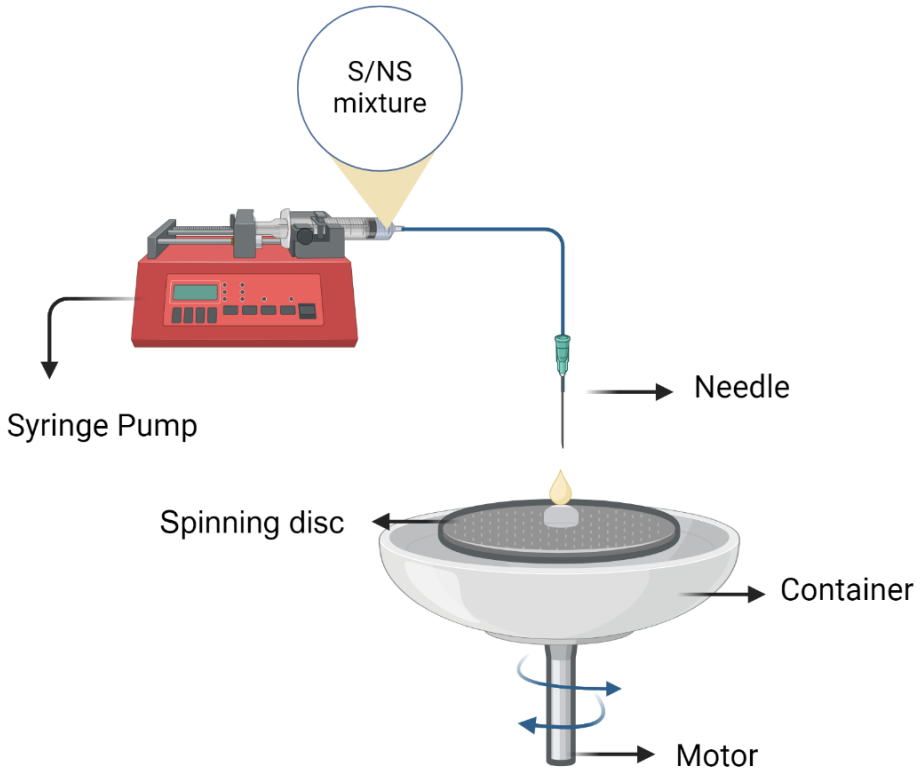

Figure 13. Illustration of SDS set-up. A syringe pump feeds the S/NS mixture through a needle placed on the center of a spinning disc rotated by a motor. The samples are collected directly from a container placed under the disc.

As discussed in previous sections, preparing polymeric NPs by the double emulsion method could also offer high encapsulation efficiencies to hydrophilic substances such as biopharmaceuticals, and these could offer innovative therapeutic options for the treatment of CNS diseases when combined with the N2B delivery. Therefore, in scope of this thesis, polymeric NP production using the double emulsion method with SDS was also investigated to promote scalable polymeric NP manufacturing practices. Previously, a spinning disc reactor has been investigated for encapsulating a flavonoid

with a double emulsion method: yet, this effort yielded emulsions with the size range of 13-15 μm [179] and was limited to the application of the process into brain delivery where optimal particle size was reported around 200 nm [180]. Therefore, in the scope of this thesis, different configurations of SDS set-up have also been investigated to prepare polymeric NPs by the double emulsion method.

1.2.3. Micro-spray-reactor System

Microreactor technology has gained attention for the scale-up of NP production. The technology usually relies on a mixing chamber of defined size and configuration and on the collision of jet streams in the mixing chamber leading highly turbulent processes where the “S” and “NS” phases are mixing and resulting in nanoprecipitation process to form NPs [181]. As an example of microreactor technologies, Günday-Türeli developed ciprofloxacin complex loaded PLGA NPs by the microreactor system for pulmonary treatment of cystic fibrosis infections and evaluated the effect of process parameters on NP quality by the DoE approach. Overall, the production of NPs by continuous manufacturing technology yielded fine particle size and PDI values [182]. In another study, Lombardo and Moya et al. focused on preparing surfactant-coated (PS80 or P188) polymeric NPs by the same technology for delivery to the brain through the BBB. Their study demonstrated the interaction of the NPs with human brain-like endothelial cells (BLECs) by *in vitro* coculture human BBB models, and surfactant-coated NPs were internalized by the cells and showed biocompatibility [183]. These promising results indicate that microreactor technologies can be used for brain delivery applications.

To bring an innovative approach for preparing polymeric NPs with microreactor technologies, in scope of the thesis, MSR-system has been investigated. As an microreactor, the MSR-system relies on the solvent and the non-solvent mixing

through the spray movement through the nozzles enabling the interaction in each droplet and providing control over the fine particle productions as illustrated in figure 14. A third opening placed in MSR-system offers ease collection of the NPs. As a system, it gives a chance to prepare NPs with different formulations by adjusting phase ratios basically by arranging the flow rates of each phase introduced through the nozzles or choosing differing mixing chamber sizes.

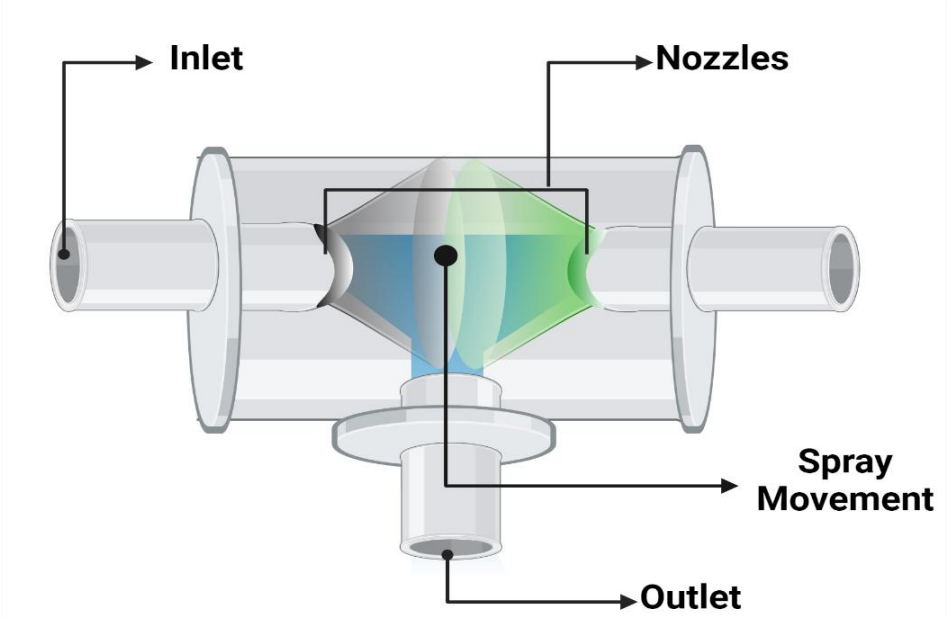

Figure 14. Illustration of MSR-system

In addition to this, it provides chances with interchangeable geometry and adjustable distance and enables methods not only limited to nanoprecipitation but also methods such as coating and micronization by looping the NPs through the nozzles with repeated cycles of looping. Moreover, as a continuous manufacturing system, it allows large-scale production of NPs, offers high quality manufacturing of NPs which leads to homogeneous emulsions and drug encapsulation processes.

2. Aim and Scope of the Dissertation

This doctoral project aims to prepare polymeric NPs to deliver hydrophilic substances for N2B delivery applications for advancing treatments for CNS diseases. The NP formulation should not be internalized by the nasal cells so could be delivered to the olfactory region to bypass the BBB. So that it can deliver therapeutics to the brain with the non-invasive approach. Another aim of the doctoral project is to prepare polymeric NPs for N2B delivery with scalable methods to enhance their potential for the transition from bench side to bedside. Therefore, the focus is given to designing and investigating different continuous manufacturing processes and technologies to identify the effect of possible process and formulation parameters on preparing these NPs by these systems, enabling their scalability. As mentioned previously, to fulfill this goal and prepare scalable polymeric NPs, SDS and MSR-system have been investigated and re-purposed to prepare polymeric substances as blank NPs, as loaded with small Mw hydrophilic and hydrophobic substances, and as loaded with large Mw substances. Especially the latter could increase the potential of these polymeric NPs to deliver innovative hydrophilic molecules like mAbs in the future while providing fine physicochemical characteristics to NPs. To compare these systems and understand their potential, the NPs would be prepared by both traditional bench top methods and continuous manufacturing techniques. Moreover, different methods for preparing polymeric NPs could be beneficial for loading small and large Mw hydrophilic and hydrophobic substances. Thus, different methods, such as nanoprecipitation, its derivative modified-nanoprecipitation, and double emulsion methods, have been studied.

Moreover, as the main goal is to prepare NPs for the N2B delivery for CNS diseases, and this requires biocompatible formulations, a special consideration is given to choosing biocompatible formulation components. These NPs were prepared using

regulatory-approved polymers such as PLGA, ensuring their safety and reliability. Their compatibility was then assessed with well-known cell viability assays, and internalization profile has been assessed with the imaging technologies.

Also, NP formulations should not be affected by the burst release profile and should deliver the drugs with sustained release to unlock their potential of delivering the advanced therapeutics with longer intervals while increasing their bioavailability at the site of action, potentially the brain. Therefore, *in vitro* release profiles of these formulations were assessed with traditional methods as well as with imaging techniques to assess and confirm sustained release, a crucial factor in the effectiveness of these formulations.

3. Formulating and Manufacturing Scalable Polymeric NPs

The experimental work for encapsulation of curcumin into PLGA NPs and optimization by the DoE was performed by Shehneela Jamil during her master thesis project where I, Selin Akpinar Adscheid, supervised and co-performed the experiments and the thesis project.

The experimental work represented for preparing double emulsions by the SDS setup was completed with Mohamed Saqawa during his internship as part of his master program Erasmus Mundus Joint Master's degree BIOPHAM and the experiments were co-performed and supervised by me, Selin Akpinar Adscheid throughout the training.

The Cryo-SEM imaging was performed at Contipro a.s. in Dolní Dobrouč, Czechia as part of collaboration within Bio2Brain project.

The figures in this chapter have been created with Biorender.com in scope of the student licensing plan.

3.1. Introduction

Polymeric NPs can deliver drugs to the site of action while PLGA being biodegradable and biocompatible [127,184]. One class of polymeric NPs, PLGA NPs, has been studied in the literature to overcome the challenges of different pathologies from lung to brain [182,183]. Even PLGA is an FDA-approved polymer for medical use over a decade, only limited products based on the PLGA microspheres have been approved [185], and there is no PLGA NP based drug available on the market. This is since producing PLGA NPs while meeting high-quality continuous manufacturing remains a challenge [186]. On the other hand, studies show that innovative large molecules (*e.g.*, monoclonal antibodies) could enhance therapeutic options for complex therapeutic challenges such as in the case of CNS diseases when encapsulated to drug delivery systems such as PLGA NPs [40,98]. Thus, there is a need for developing and optimizing continuous manufacturing systems to produce PLGA NPs, that can also be loaded with innovative molecules to tackle complex therapeutic challenges.

To tackle this issue, the following chapter represents design, screening, optimization and the characterization of the PLGA NPs produced by two continuous manufacturing systems: SDS and the MSR-system. Moreover, to successfully encapsulate the innovative large hydrophilic molecules such as biopharmaceuticals to PLGA NPs with high encapsulation efficiencies, the production of the PLGA NPs by the double emulsion method with these continuous manufacturing systems was evaluated. Briefly, while the SDS offers a platform to produce PLGA NPs by evaporation-triggered modified nanoprecipitation, the MSR-system relies on the S and the NS mixing through spraying of the two phases and provides control over the fine particle production. The systems offer interchangeable geometry and adjustable distances while enabling methods such as precipitation and coating.

In this chapter, the following steps evaluate the advantages and limitations of both continuous manufacturing systems to produce PLGA NPs loaded with small and large Mw hydrophobic and hydrophilic substances.

1. Preparation of the PLGA NPs with the SDS by the modified-nanoprecipitation method and assessment of process parameters.
2. Preparation of the curcumin-loaded PLGA NPs by the SDS by the modified-nanoprecipitation method and optimizing the process parameters by the DoE approach.
3. Preparation of the PLGA NPs with the emulsification/solvent evaporation (double emulsion) method. This part focuses on the preparation of the PLGA NPs as double emulsions by the traditional homogenization methods to enable the successful encapsulation of hydrophilic substances.
4. Design of the prototype and screening for the possible process parameters to produce PLGA NPs as double emulsions with the SDS.
5. Investigation of the MSR-system for preparing PLGA NPs as double emulsions. This part also underlines preparing PLGA NPs loaded with small and large Mw hydrophilic substances by the MSR-system.

3.2. Materials and Method

3.2.1. SDS Design and Functionality: Prototype I

To evaluate the SDS set-up and prepare PLGA NPs with the modified-nanoprecipitation method, the prototypes established by Zander [178] was re-established. This set-up is then used for assessing possible process parameters (*e.g.* disc rotation steep, droplet size, disc material type) that could have an influence on physicochemical properties of NPs such as particle size and polydispersity. The discs

used in the SDS were prepared from 3D-printed polyamide or polypropylene discs and placed on a motor (RND Lab DC Power Supply RND 320 – KD3005D, Nikon, Switzerland) located inside of a plastic container. The plastic sample container enabled easy collection and cleaning during and after sample preparation. The power supply provided control over the disc rotation speed of the disc. The conversion of the voltage value to the revolutions per minute (rpm) was performed by a tachometer (Voltcraft DT – 10L Laser Speed meter, Hirschau, Germany). The flow rate was kept constant during the procedure by using a syringe pump. The needle was connected to the syringe pump with a plastic tubing to adjust the placement of the needle and the dropping distance of the sample to the disc surface. After the preparation of the sample, the samples were collected directly from the plastic container.

3.2.2. Preparation of PLGA NPs with the SDS by the modified nanoprecipitation method

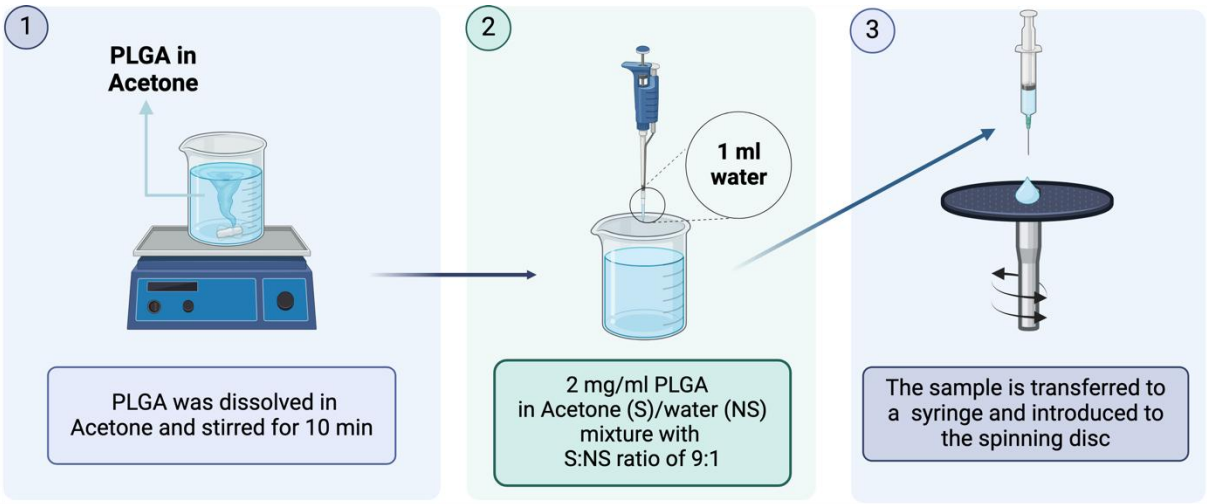

Figure 15. Preparation of the PLGA NPs by the SDS with the modified nanoprecipitation method

The NPs were prepared (Figure 15) with a solvent (S) containing 20.0 mg of Resomer® RG 503H (50:50, acid terminated, Mw: 24.000-38.000, Evonik, Essen, Germany)

dissolved in acetone (HiPerSolv CHROMANORM for HPLC, VWR, Darmstadt, Germany). After stirring the solution for 10 min, distilled water is added to the initial solution with a S/NS ratio of 9:1. Finally, the S/NS was introduced to the center of a spinning disc with a flow rate of 0.5 ml/min and the sample was collected from the collector located under the spinning disc.

3.2.2.1. Screening of possible process parameters to produce PLGA NPs with the SDS by the modified nanoprecipitation method.

To produce PLGA NPs by the SDS with modified-nanoprecipitation method, disc type, disc rotation speed, and the droplet size were screened to evaluate the effect of these parameters on the PLGA NP production (Table 1).

Table 1. Screened process parameters for the PLGA NPs prepared by the SDS

Parameters	Disc Type	Disc Voltage	Needle
Disc Type / Material	**PA-**1/-2/-3/-4/-5/-6/-7/-8/-9, **PP**-1/-2, **CA**-1/-2/-3	3.00 V	0.90 x 40 mm
Disc Rotation Speed	**PP**-1	2.20 V, 2.50 V, 2.80 V, 3.00 V, 3.50 V, 3.93 V	0.90 x 40 mm
Droplet Size	**PP**-1	3.00 V	0.90 x 40 mm, 0.80 x 120 mm, 0.60 mm x 80 mm
Repeatability	**PP**-1	3.00 V	0.90x 40 mm

PA: polyamide, PP: polypropylene, CA: concave shape polypropylene discs

3.2.2.2. Screening of the effect of different disc types on PLGA NP production

To screen the effect of different disc materials and disc surface patterns on evaporation, thus the production of the PLGA NPs, polypropylene (PP) and polyamide (PA) or concave shape polypropylene (CA) discs were 3D-printed. The discs were named according to their different shapes and material (PA-1/-2/-3/-4/-5/-6/-7/-8/-9, PP-1/-2 and CA-1/-2/-3 (Figure 16). To prepare these polymeric NPs, the S/NS was introduced to the center of the disc by a needle (0.90 x 40 mm) with a flow rate of 0.5 ml/min. The disc rotation speed was set to 1314 rpm.

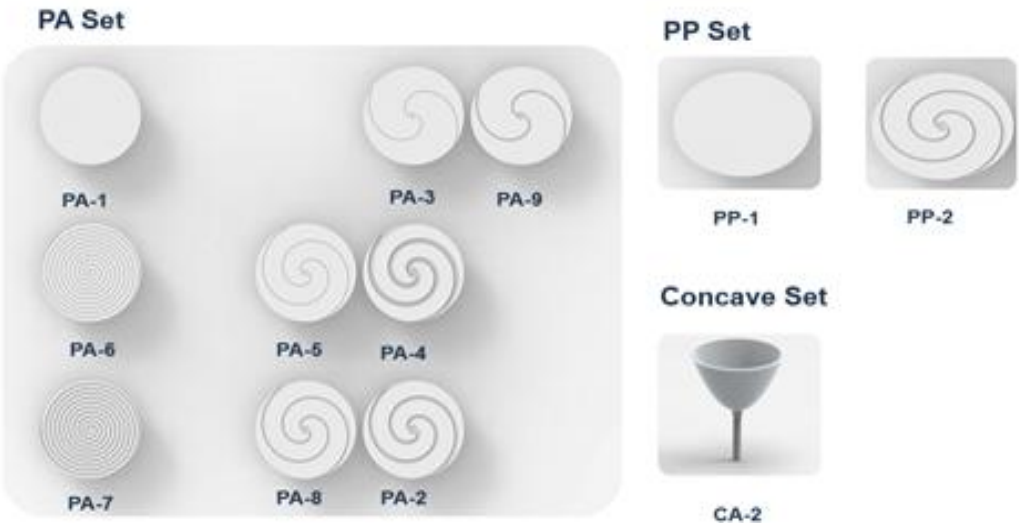

Figure 16. Different disc materials and surface structures for polyamide (PA), polypropylene (PP), and concave shaped polypropylene (CA) discs

3.2.2.3. Screening of the effect of different disc rotation speeds on PLGA NP production

To screen the effect of different disc rotation speeds on preparing PLGA NPs by the SDS, different disc rotation speeds were screened. The conversion of the voltage values to rpm was performed by a tachometer and the following disc rotation speeds were screened: 2.20 V (~ 311 rpm), 2.50 V (~ 688 rpm), 2.80 V: (~ 1090 rpm), 3.00 V

(~ 1314 rpm), 3.50 V (~ 1930 rpm), 3.93 V (~ 2550 rpm). To produce NPs, the S/NS was introduced to the center of the polypropylene disc (PP-1) by a needle (0.90 x 40 mm) with a continuous flow rate of 0.5 ml/min.

3.2.2.4. Screening of the effect of needle types (droplet size) on PLGA NP production

To evaluate the effect of different droplet sizes on producing PLGA NPs, syringe needles with different droplet sizes (0.90 x 40 mm, 0.80 x 120 mm, and 0.60 x 80 mm) were used. To produce NPs, the S/NS was introduced to the center of the disc rotation speed of 1314 rpm with a flow rate of 0.5 ml/min.

3.2.2.5. Repeatability of the PLGA NP production with the SDS

To assess the repeatability of producing PLGA NPs with the SDS, the S/NS (solvent/non-solvent) mixture was introduced to the center of a polypropylene disc (PP-1) by a needle (0.90 x 40 mm) with a flow rate of 0.5 ml/min. The disc rotation voltage and speed were set to 3.00 V (~ 1314 rpm). The results were obtained as triplicates and the experimental procedure were performed during the same day.

3.2.3. Preparing Curcumin-loaded PLGA NPs by SDS

A DoE has been performed to prepare and optimize curcumin-loaded PLGA NPs, where curcumin is chosen as a small Mw hydrophobic model substance for the encapsulation process. Factors were chosen according to the possible process parameters screening performed with the blank-PLGA NPs prepared by the SDS using the modified-nanoprecipitation method. For preparing the curcumin-loaded PLGA NPs

by the SDS with the modified-nanoprecipitation method, the following experimental procedure was followed:

The NPs were prepared (Figure 17) with a solvent containing 20.0 mg of Resomer® RG 503H (50:50, acid terminated, Mw: 24.000-38.000, Evonik, Essen, Germany) dissolved in acetone (HiPerSolv CHROMANORM for HPLC, VWR, Darmstadt, Germany). After stirring the solution for 10 min, distilled water was added to the initial solution with an S/NS ratio of 9:1. Finally, the S/NS was introduced to the center of a spinning disc and the sample was collected from the collector located under the SDS (Figure 17)

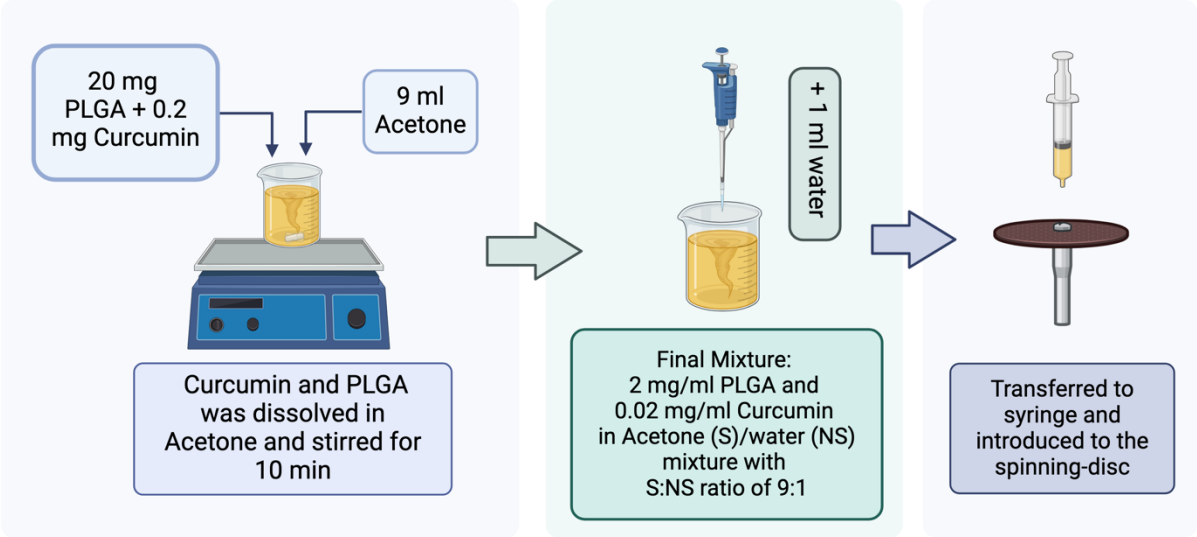

Figure 17. Preparing curcumin-loaded PLGA NPs by the SDS

The physicochemical characteristics of the NPs were then assessed using DLS and the quantification of EE% of curcumin in PLGA was performed using a fluorometer due to curcumin's distinct fluorescence, with a calibration curve linear in the range of 0.1-4.1 μg/ml.

The encapsulation efficiency was then assessed by centrifugating the obtained NPs at for 30 min at 24,610 rcf to obtain the supernatant. Then, the supernatant is centrifugated at 1950 rcf for 10 min with Nanosep® centrifugal devices (100 kDa

membrane, Pall Laboratory purchased from VWR from Darmstadt, Germany). The obtained filtrate is then read at the calibration curve prepared by a microplate reader with a filter of D400/20 nm excitation and 590 nm emission wavelengths.

3.2.3.1. Design of Experiment

Table 2. Factors in Box-Behnken design space for process optimization of curcumin-loaded PLGA NP formulation

Factor	Name	Units	Lower level (-1)	Upper level (+1)
A	Disc speed	ml/min	600	2100
B	Flow rate	rpm	0.5	2
C	Droplet size (needle diameter size)	mm	0.7	0.9
D	Polymer concentration	mg/ml	1	4

Box-Behnken DoE design has been performed to optimize the preparation of the parameters. Four factors: flow rate, disc rotation speed, droplet size, and polymer concentration were tested at two levels in the design space studied. At the same time, the responses were set as particle size, PDI, and encapsulation efficiency %. As a result, a Box-Behnken design with 29 runs and five center points was analyzed using Design-Expert ver. 7.1.9 (Stat-Ease Inc., Minneapolis, MN, USA) and the results were

analyzed using regression analysis of variance (ANOVA). Factors studied with their lower and upper level are shown in Table 2 above.

3.2.4. Preparation of PLGA NPs as double emulsions by the emulsification/solvent evaporation method

The PLGA NPs were prepared by the emulsification/solvent evaporation method to obtain W/O/W double emulsion (Figure 18). The experimental procedure was adapted from Spindler et al. [117]. To prepare the primary emulsion, 1% Tween® 80 (Merck, Darmstadt, Germany) in distilled water and 5 mg/ml PLGA Resomer® 503 H (Evonik, Darmstadt, Germany) in 3:1 ethyl acetate (VWR, Darmstadt, Germany): dichloromethane (ACS Reagent, Reag. ISO≥99.9%, GC) (Merck, Darmstadt, Germany) solution were emulsified with a ratio of 1:10 by a homogenizer. The obtained primary emulsion was added to a water phase containing PVA (Mowiol® ,4-98, Mw ~ 27,000, Sigma – Aldrich, Munich, Germany) as a surfactant with ratio of primary emulsion to outer aqueous phase of 1:10. Both emulsification steps were performed at the 13,500 rpm for 1 min with a homogenizer (Witeg, Wise-Tis, Wertheim, Germany). The prepared sample was stirred overnight to evaporate the organic solvent and form the PLGA NPs. To identify the phases clearly, the inner aqueous phase is notated as "W_1" phase, organic solvent phase is notated as "O" phase and outer aqueous phase is notated as "W_2" phase in the next sections when mentioning the phases of the double emulsions prepared.

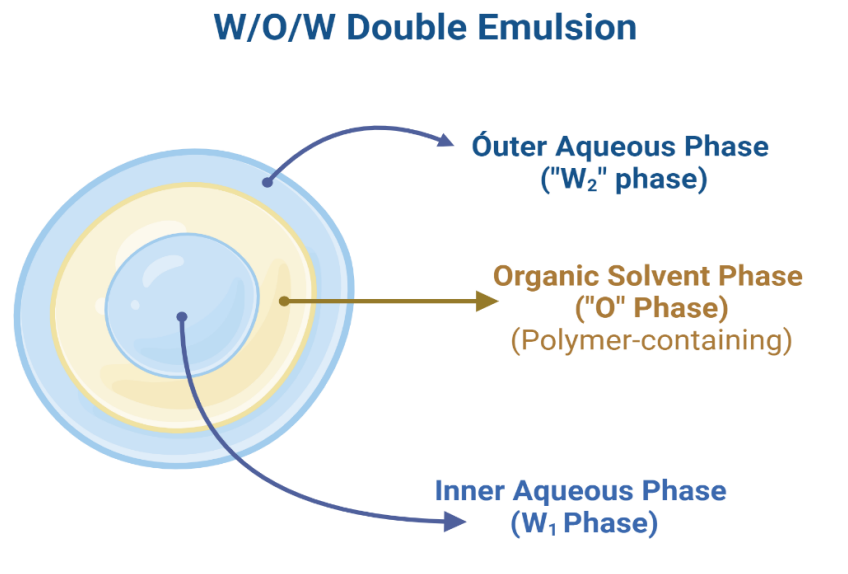

Figure 18. Illustration of the W/O/W Double emulsion structure

3.2.4.1. Optimization of the preparation of PLGA NPs by the double emulsion method

The preparation of the PLGA NPs with this method was further optimized by preparing the samples with different phase ratios (W_1:O:W_2), and surfactant concentrations in both aqueous phases. Two different W_1:O:W_2 phase ratios were tested (1:10:100 and 1:5:100) and for each phase ratio 1%, 2% and 3% PVA concentration in "W_2" phase was prepared. Finally, samples prepared with 3% PVA concentration in their "W_2" phase were further evaluated with the different Tween® 80 surfactant concentration as well as with different primary emulsification times (30 s and 60 s) as explained in figure 19. This enabled further assessment of the stability of the double emulsions. During the method optimization, all preparations were evaluated in terms of particle size, as well as polydispersity.

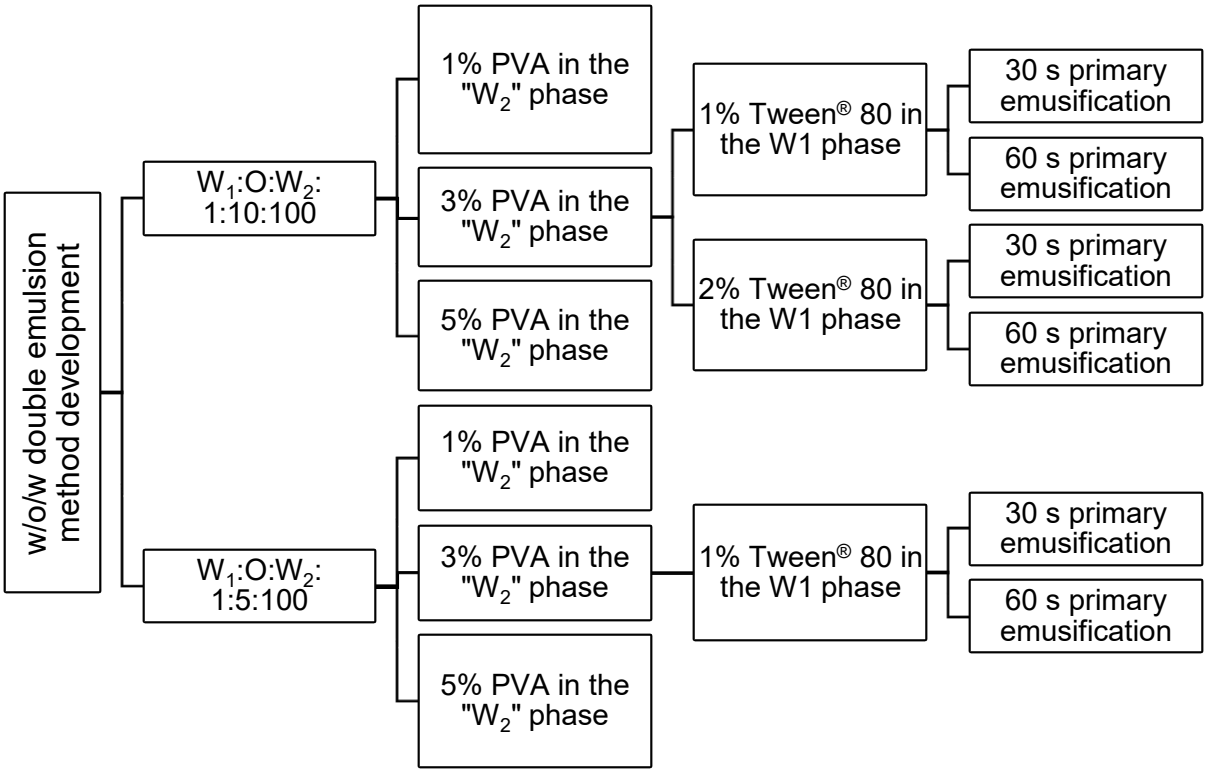

Figure 19. Further method development for preparation of PLGA NPs with the double emulsion method

3.2.4.2. Final preparation of the PLGA NPs by the double emulsion method

For the final preparation of the blank PLGA NPs by double emulsion method (W_1:O:W_2, 1:10:100) (Figure 20), the primary emulsion was prepared by the addition of the "W_1" phase with 1% Tween 80 to polymer containing phase consisted of 5 mg/ml PLGA (RESOMER® RG 503 H) dissolved in EA:DCM (3:1). Immediately after the addition, emulsification with a homogenizer at 13,500 rpm for 30s was performed to form the primary emulsion. Then, the primary emulsion was transferred into "W_2" phase consisting of 3% PVA, and the emulsification at 20,200 rpm for 60s was performed with the homogenizer IKA Ultra-turrax® (Staufen, Germany). The double emulsion was

evaporated overnight and characterized later in terms of their particle size and PDI values.

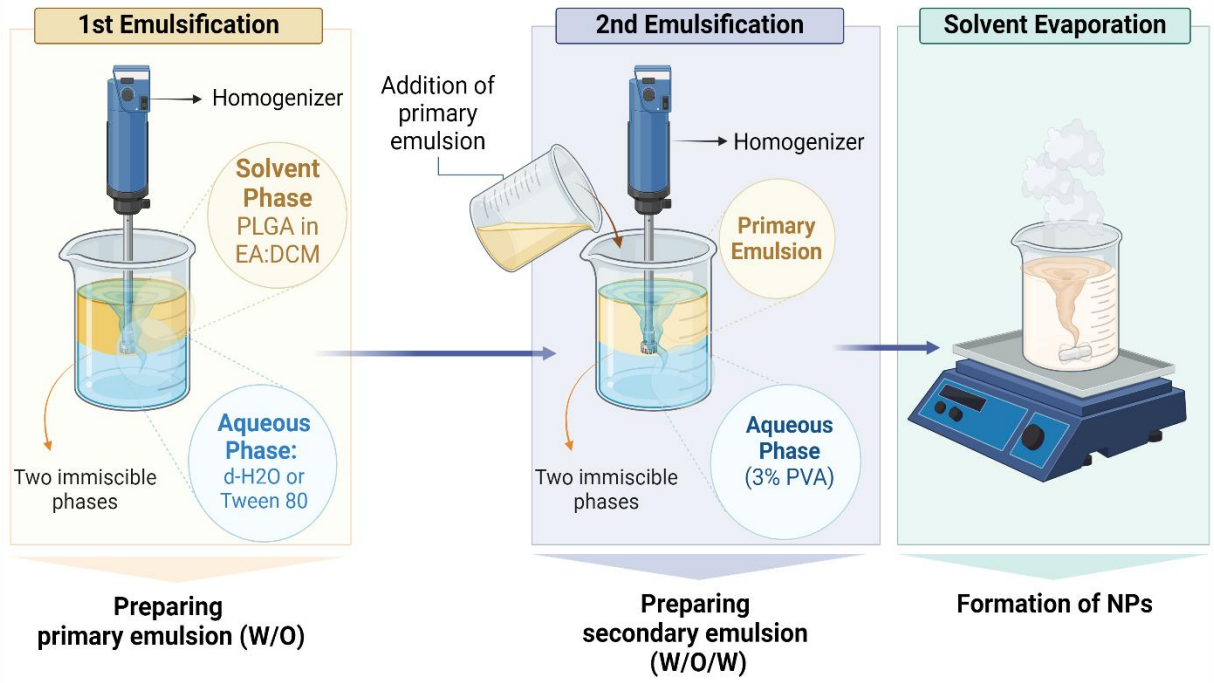

Figure 20. Final preparation of the PLGA NPs by the double emulsion method

3.2.5. Screening of possible process parameters to produce PLGA NPs with the double emulsion method by the SDS.

In this section, possible applications of the SDS on preparing PLGA NPs as W/O/W double emulsions to encapsulate hydrophilic substances were investigated and influence on different possible process parameters were screened. The results were compared to bench top PLGA NPs prepared by the double emulsion method in terms of particle size and polydispersity.

3.2.5.1. Second SDS prototype for preparing PLGA NPs as double emulsions by the SDS

To investigate the application of the SDS as a single-step tool to directly prepare the PLGA NPs as double emulsions, another set-up was built (Illustrated in Figure 21).

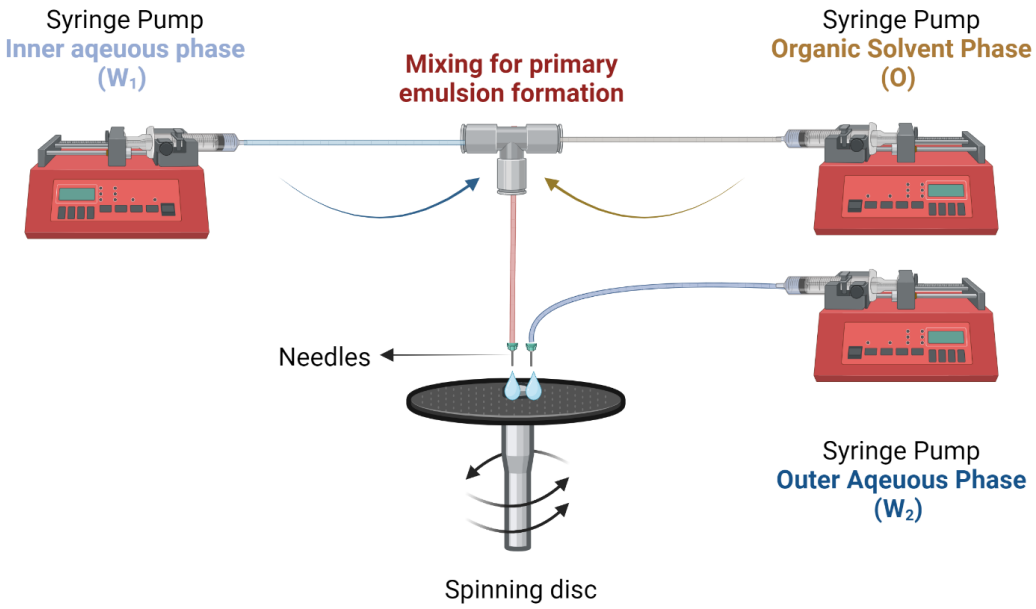

Figure 21. Second SDS Prototype for preparing PLGA NPs by the double emulsion method

In this set-up, both the primary emulsion and the secondary emulsion were aimed to be prepared through the SDS and introduced on the rotating disc. During the process, the "W_1" and the "O" phases were pumped from two separate syringe pumps. Both phases were mixed through a connector to maximize the mixing between these phases and to directly prepare primary emulsion. Meanwhile, "W_2" phase was also ejected on the surface of a spinning disc from another syringe pump. Due to centrifugal forces, all phases were spread through the disc surface and thus mixed on the disc surface. Finally, the final samples were collected from the collector. Overall, the prototype offered easy-to-control adjustments for screening different possible formulation and process parameters. In the next sections the prepared "W_1" phase contains 1%

Tween© 80, and the "O" phase was prepared with 5 mg/mL PLGA (Resomer© 503 H) in 3:1 Ethyl acetate: DCM, and "W_2" phase was prepared with 3% PVA.

3.2.5.2. Screening of different disc types

Screening of the different disc materials and disc surface patterns was performed by using 10 different disc conformations made from polyamide or polypropylene. During the screening, for all the disc types, the rotational speed was kept constant at 688 rpm and a Y-shaped connector was used to combine the "W_1" and "O" phases.

Table 3. Screening of effect of different disc types to prepare PLGA NPs by the double emulsion method with the SDS

Parameter	Fixed / Screened	Value(s)
Disc type	Screened	Polyamide (PA) and Polypropylene (PP) discs
Connector type	Fixed	Y-shaped connector
Disc rotation speed	Fixed	688 rpm
W_2 phase concentration and flow rate	Fixed	3% PVA in water Flow rate: 100 ml/min
"O" phase concentration	Fixed	5 mg/ml PLGA Resomer© in Ethyl acetate: DCM (3:1)
W_1 concentration	Fixed	1% Tween© 80 in water
W_1: O	Fixed	1:10
Flow rates for the W_1 and O phases	Fixed	W_1: 1 ml/min O: 10 ml/min

The phases were introduced to the disc for 10 seconds and the samples were collected directly from the collector and filtrated with 1 µm glass syringe filter. Other parameters such as droplet distance to the disc (3 mm), and concentration of the formulation parameters were kept constant as stated in Table 3 above.

3.2.5.3. Screening of different disc rotation speeds

To screen the effect of different disc rotation speeds on preparing PLGA NPs, four different rotational speeds have been studied as shown in the Table 4.

Table 4. Screening of effect of different disc rotation speeds to prepare PLGA NPs by the double emulsion method with the SDS

Parameter	Fixed / Screened	Value(s)
Disc type	Fixed	PA-1
Connector type	Fixed	Wide-T-shaped connector
Disc rotation speed	Screened	300, 688, 1314 and 2550 rpm
W_2 phase concentration and flow rate	Fixed	3% PVA in water Flow rate: 100 ml/min
"O" phase concentration	Fixed	5 mg/mL PLGA Resomer© in Ethyl acetate: DCM (3:1)
W_1 concentration	Fixed	1% Tween© 80 in water
W_1: O	Fixed	1:10
Flow rates for the W_1 and O phases	Fixed	W_1: 1 ml/min O: 10 ml/min

The conversion of the measured voltage to rpm was performed by a tachometer. For all screened disc rotation speeds, the disc type was fixed to the PA-1, flow rate of W_2 phase was fixed to 40 ml/min, and the ratio between "W_1" phase and the "O" phase was set to 1:10. Other parameters such as droplet distance to the disc (3 mm above the disc) and the concentration of phases in the formulation were kept constant. All samples were filtrated with 1 µm glass syringe filter.

3.2.5.4. Screening of different primary-emulsion-to-W_2 phase ratios

To screen the effect of different primary emulsion-to-W_2-phase ratios for preparing PLGA NPs, two different ratios of primary emulsion-to-W_2: 1:5 and 1:10 were evaluated. To set these ratios, the flow rate of the "W_2" was changed while keeping the flow rates of other phases constant. The phases were introduced on the disc for 10 s and the samples were collected directly from the collector and then filtrated with a 1 µm glass syringe filter. During the experiments, the influence of the flow rates of the phases on mixing properties was also considered. The flow rates of each phase have a direct influence on the total flow rate passing through the connector. This is since the phase with a higher flow rate has a driving force on the phase with a slower flow rate and affects the mixing through the connector. Moreover, it should be noted that the formation of the primary emulsion depended on the ratios of the "W_1" and "O" phases, and their corresponding flow rates. Thus, while maintaining the same W_1:O phase ratio (1:10), two different flow rates for "W_1" phase (1 and 0.5 ml/min) "O" phase (10 and 5 ml/min) were also studied. Other parameters like disc type, disc rotation speed, and the concentration of the formulation parameters were kept constant and listed in Table 5 below.

Table 5. Screening of effect on different primary emulsion-to-W_2 phase ratios to prepare PLGA NPs as double emulsions by the SDS

Parameter	Fixed / Screened	Value(s)
Disc type	Fixed	PA-1
Connector type	Fixed	Wide-T-shaped connector
Disc rotation speed	Screened	300, 688, 1314 and 2550 rpm
W_2 phase flow rate	Screened	50 ml/min, and 100 ml/min
O" phase concentration	Fixed	5 mg/ml PLGA Resomer© in Ethyl acetate: DCM (3:1)
W_1 concentration	Fixed	1% Tween© 80 in water
W_1: O	Fixed	1:10
Flow rates for the W_1 and O	Screened	W_1: 0.5 and 1 ml/min O: 5 and 10 ml/min

3.2.5.5. Screening of different connector types

The connector is the part of the setup responsible for mixing the W_1 and the organic solvent containing phase (O) before ejecting them on the rotating disc. To identify whether the connector type was affecting the formation of the PLGA NPs as double emulsions, three different connector configurations was designed and studied (Table 6) as following: Y-shaped connector, narrow T-shaped connector, and the wide T-shaped connector. The structure of each connector is shown in Figure 22.

Table 6. Screening of effect on different connector types to prepare PLGA NPs as double emulsions by SDS

Parameter	Fixed / Screened	Value(s)
Disc type	Fixed	PA-1
Connector type	Screened	Y-shaped, narrow T-shaped, and wide T-shaped
Disc rotation speed	fixed	688 rpm
W_2 flow rate and concentration	Fixed	3% PVA in water Flow rate: 50 ml/min
Organic solvent containing phase (O) concentration	Fixed	5 mg/mL PLGA Resomer© in Ethyl acetate: DCM (3:1)
W_1 concentration	Fixed	1% Tween © 80 in water
W_1: O	Fixed	1:10
Flow rates for t he W_1 and O	Fixed	W_1: 1 ml/min O: 10 ml/min

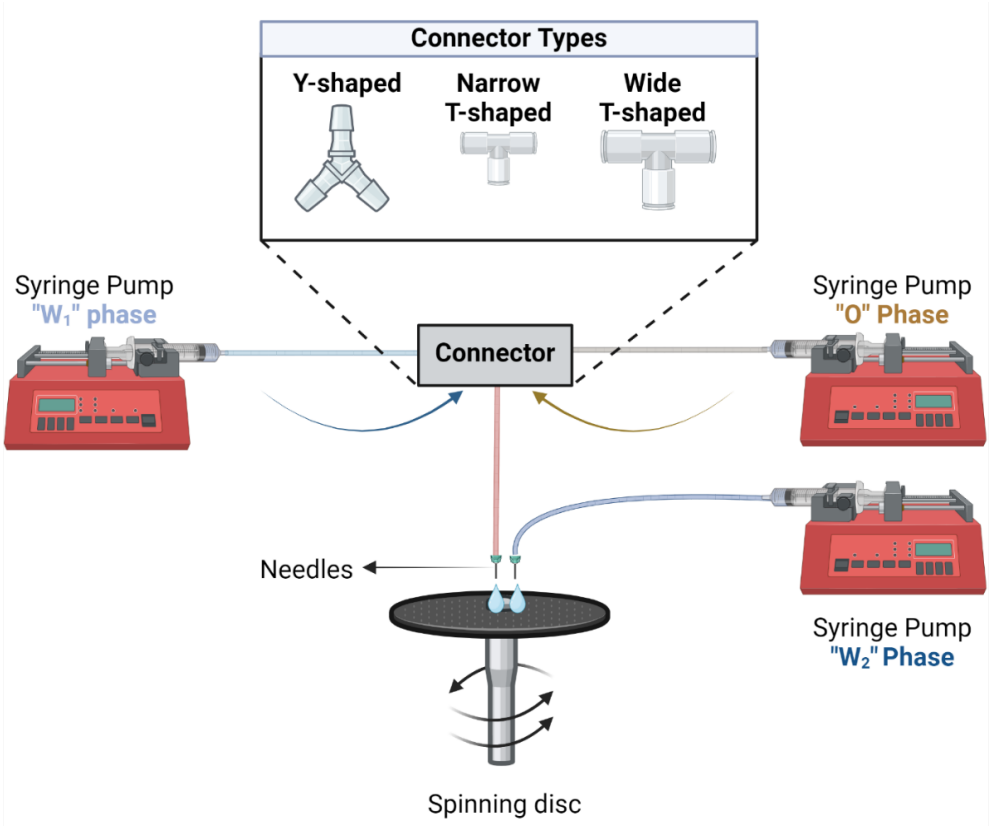

Figure 22. Representation of different connector types for the SDS

3.2.6. Preparation of PLGA NPs by the MSR-system

After the results of preparing PLGA NPs with double emulsion method by the SDS another potential continuous manufacturing system, the MSR-system was investigated to prepare PLGA NPs. As mentioned in the previous sections, the preparation of the PLGA NPs with the double emulsion method involves a two-step process, the preparation of the primary emulsion and the preparation of the secondary emulsion. In this scope, the MSR-system was investigated to prepare both primary emulsion and the secondary emulsion within the system (Figure 23). The experimental design and the use of the system was optimized to prepare PLGA NPs loaded with small and large Mw hydrophilic substances such as Ciprofloxacin HCl and albumin. The NPs were characterized in terms of their particle size and PDI values, as well as morphology.

The free drug concentration after the encapsulation was characterized by HPLC-UV and a fluorometer. The PLGA NPs were further purified by CFF to wash out the excess amount of the non-encapsulated substances as well as excess surfactants and polymer chains.

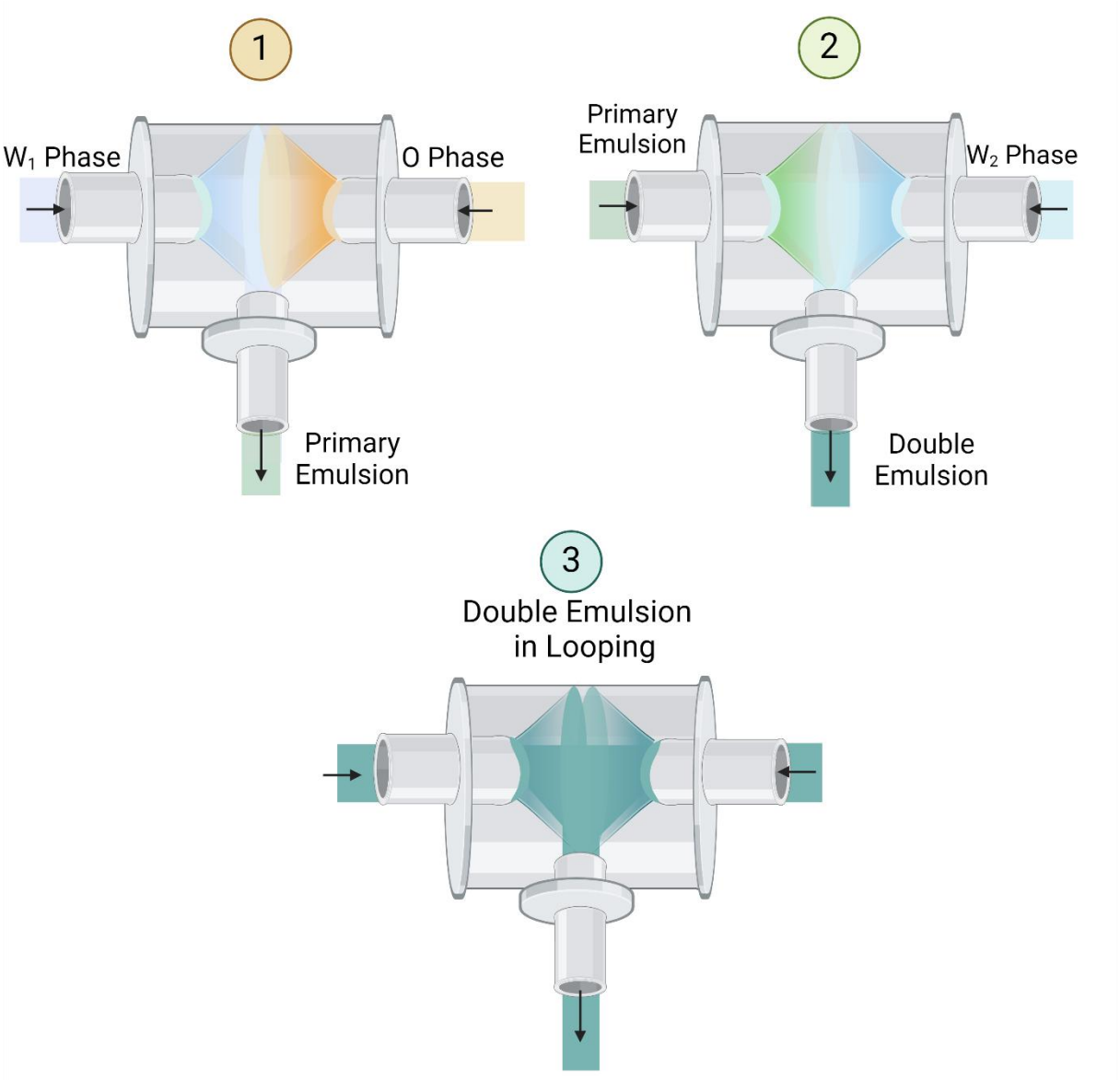

Figure 23. Preparing PLGA NPs by the MSR system

3.2.6.1. Establishing experimental protocols to prepare Ciprofloxacin HCl-loaded PLGA NPs by the double emulsion method with the MSR-system

For the preparation of PLGA NPs with the reactor system by the double emulsion method and to test the preparation of both primary and secondary emulsification steps through the MSR-system, 35.7 mg/ml Ciprofloxacin HCl was dissolved in water, and added into 5 mg or 10 mg/ml PLGA Resomer 503H dissolved in EA:DCM (3:1) while vigorously stirring. The primary emulsion looped for 15 min at the highest flow rate through a MSR-system with a spray nozzle size of 300 µm. Then the collected primary emulsion was added into the 3% PVA solution with a ratio of 1:25 also while vigorously stirring. After a second looping of 200 ml/min, the sample was stirred overnight under the hood to evaporate the organic solvent and form the particles.

3.2.6.2. Optimized experimental protocol to prepare Ciprofloxacin HCl-loaded PLGA NPs by the MSR-system with the double emulsion method

The optimal method for preparing Ciprofloxacin HCl-loaded PLGA NPs by the MSR-system with the double emulsion method (Figure 24) relies on preparing the primary emulsion by a high-shear force homogenizer, and secondary emulsion by the MSR-system to ensure the stability of the primary emulsion. For this, 35.7 mg/ml Ciprofloxacin HCl (Ph. Eur. pure, pharma grade from PanReac AppliChem, ITW Reagents, Darmstadt, Germany) was dissolved in distilled water, and added into 10 mg/ml PLGA Resomer 503H (Evonik, Darmstadt, Germany) dissolved in 3:1 EA (VWR,

Darmstadt, Germany): DCM (ACS Reagent, Reag. ISO. ≥99.9% (GC)) (Merck, Darmstadt, Germany) solution. The emulsification took place at 13,500 rpm for 5 min. The primary emulsion looped at 200 ml/min flow rate through the MSR-system with a spray nozzle size of 300 µm. Then the collected primary emulsion was added to 3% PVA (Mowiol®,4-98, Mw ~ 27,000 from Sigma – Aldrich, Munich, Germany) solution with primary emulsion-to-W_2 ratio of 1:25 while vigorously stirring and looped through the MSR-system with a flow rate of 200 ml/min. Subsequently, the sample was stirred overnight under the hood to evaporate the organic solvent and solidify the polymer to form the polymeric NPs. The obtained NPs were purified by the CFF with a 100 kDa MicroKros© mPES (modified polyether sulfone) hollow fiber membrane (Repligen, Waltham, United States) with a surface area of 155 cm^2.

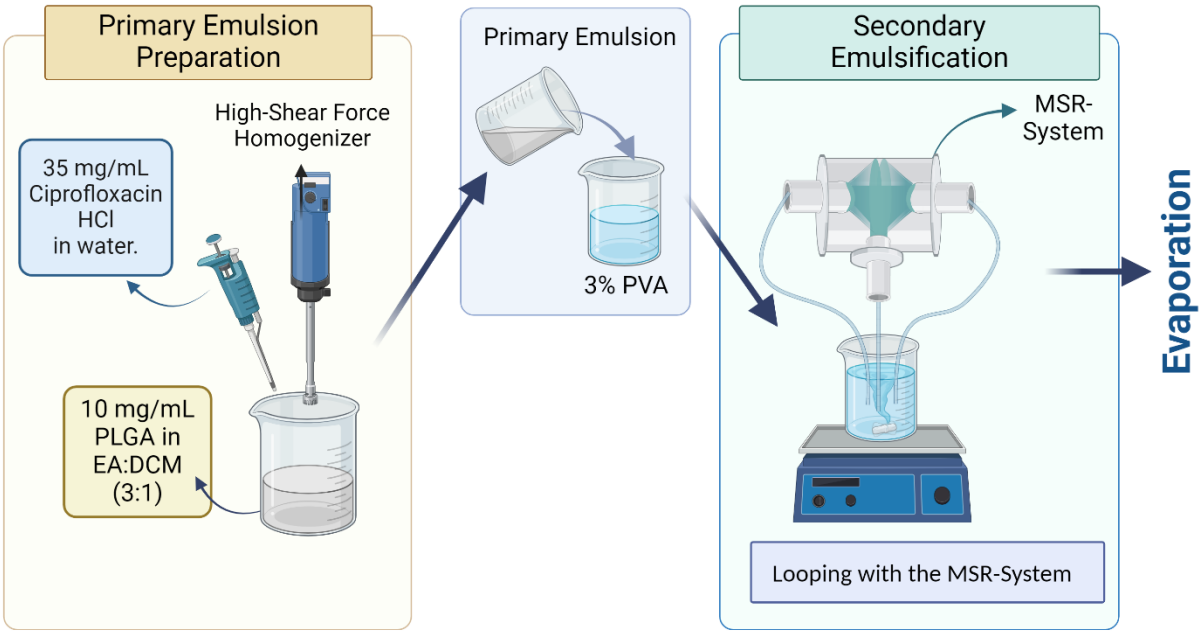

Figure 24. Final preparation protocol for PLGA NPs by the MSR-system by the double emulsion method

3.2.6.3. Determination of the total and free Ciprofloxacin HCl concentration in PLGA NPs

To determine concentration of the Ciprofloxacin HCl in the PLGA NPs, the sample was dissolved in dimethyl sulfoxide (DMSO) and analyzed directly by the HPLC-UV with the HPLC Method explained in detail (Table 7). To determine the concentration of the non-encapsulated (free) drug concentration in the PLGA NPs, the supernatant was separated from the sample by using Nanosep® centrifugal devices with Omega™ membrane (mPES) (Pall Laboratory purchased from VWR, Darmstadt, Germany) (Figure 25). Nanosep® centrifugal devices offer rapid and convenient concentration, fractionation, salt removal, and purification purposes and their molecular weight cut-off varies from 3 kDa to 300 kDa.

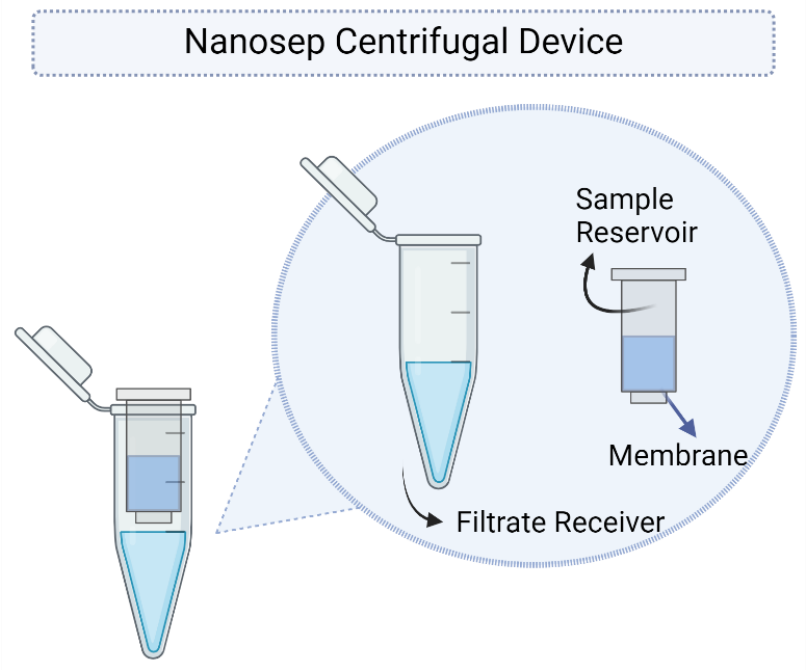

Figure 25. Illustration of the Nanosep® centrifugal devices

The samples were centrifuged with the Nanosep® (10K cut off) at 1950 rcf for 15 min. The concentration in the supernatant as well as in the assay samples was determined

by the HPLC-UV (Hitachi Elite LaChrom® equipped with Chromaster 5410 UV Detector, VWR, Darmstadt Germany).

Table 7. HPLC-UV Method, Ciprofloxacin HCl

HPLC-UV Method, Ciprofloxacin HCl

System	Hitachi 5410 UV Detector
Column	Waters Symmetry C18, 3.5µm 75 x 4.6 mm
Mobile Phase	MP A: 0.025M H_3PO_4 pH 3.0 adjusted with TEA:ACN (87:13 v/ v%)
Flow	1.5 ml/min
Mode	Isocratic
Run Time	5 min
Temperature	30 °C (Column), 20 °C (Autosampler)
Injection volume	10 µl
UV detection	278 nm

3.2.6.4. Preparation of Albumin-loaded PLGA NPs with the double emulsion method by the MSR-system

The W_1 phase was prepared by dissolving 4 mg/ml albumin or fluorescent albumin (albumin-fluorescein isothiocyanate (FITC)) (Merck, Darmstadt, Germany) in PBS 7.4 pH. Organic solvent phase prepared by dissolving 20 mg/ml PLGA Resomer® 502H (50:50 acid terminated (7,000-17,000) (Evonik, Darmstadt, Germany) dissolved in

dichloromethane (DCM) (ACS Reagent, Reag. ISO. ≥99.9%, GC from Merck, Darmstadt, Germany) with a "W_1" to "O" phase ratio of 1:10. The first emulsification was performed by Ultra-Turrax®, a high-shear force homogenizer at 13,000 rpm for 60 sec.

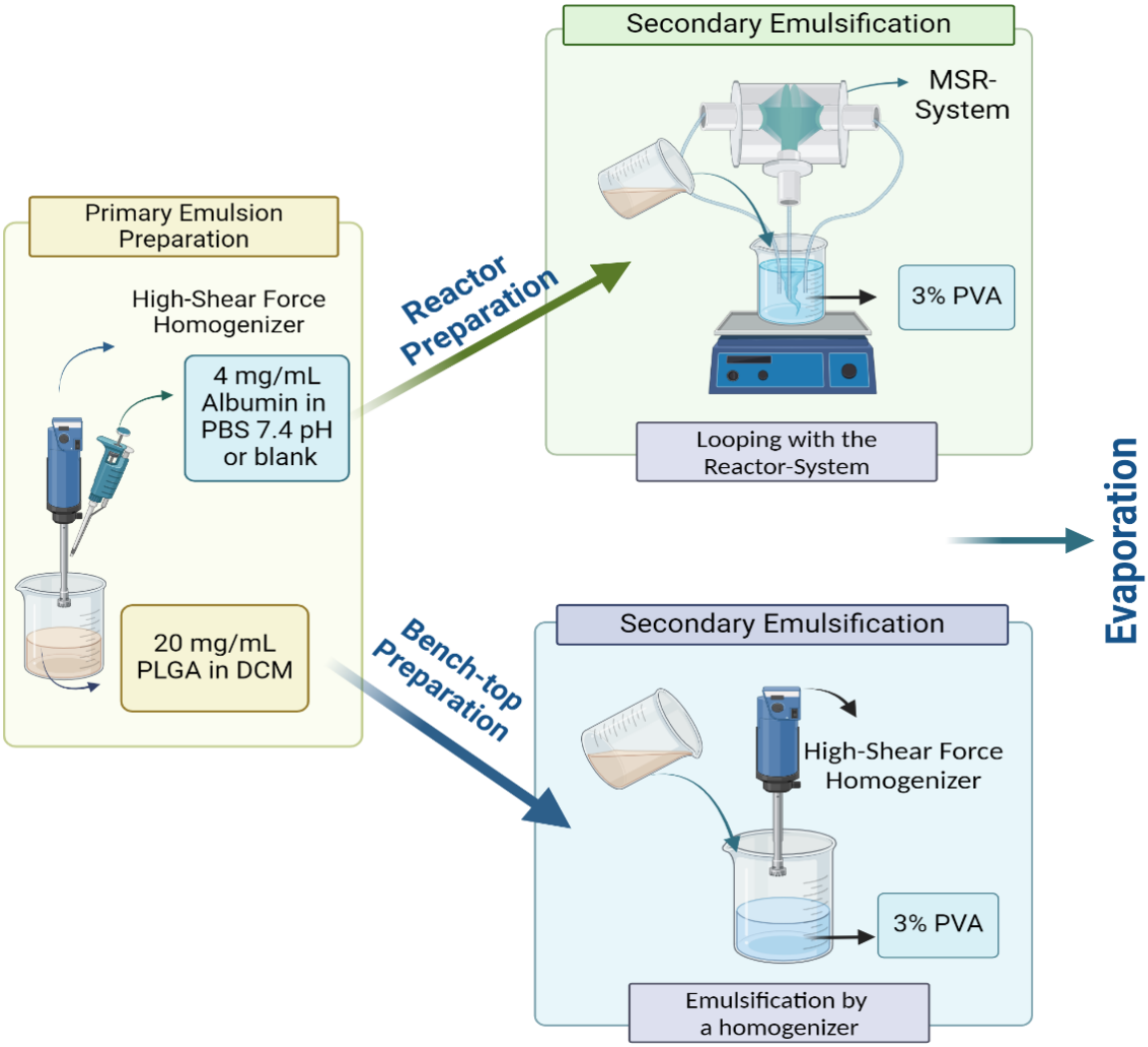

Figure 26. Preparation of albumin-loaded PLGA NPs (reactor and bench top preparations)

Then, the primary emulsion is added into 3% PVA (Mowiol®,4-98; Mw ~ 27,000 from Sigma – Aldrich, Munich, Germany) in water solution with primary-emulsion-to-W_2 ratio of 1:5. The phases continuously looped through a reactor with a spray nozzle size of 300 µm with a flow rate of 200 ml/min. Later, the obtained NP prepared as double emulsion was moderately stirred overnight to remove the organic solvent and form the

PLGA NPs. Finally, the particles were purified by the CFF with MicroKros© mPES (modified polyether sulfone) hollow fiber membrane of 300K filter cut off and the surface area of 235 cm^2 (Repligen, Waltham, USA).

3.2.6.5. Preparation of the Albumin-loaded PLGA NPs with the double emulsion method by the emulsification/solvent evaporation method (bench top / double emulsion method)

For preparing albumin-loaded PLGA NPs by the traditional emulsification/solvent evaporation method (bench top / double emulsion method) (Figure 26), the W_1 phase was prepared by dissolving 4 mg/ml albumin or fluorescent albumin (albumin-FITC) (Merck, Darmstadt, Germany) in PBS pH 7.4. Organic phase prepared by dissolving 20 mg/ml PLGA Resomer® 502H (50:50 acid terminated (7,000-17,000), Evonik, Darmstadt, Germany) dissolved in DCM (ACS Reagent, Reag. ISO, ≥99.9%, GC from Merck, Darmstadt, Germany) "W_1" to "O" phase ratio of 1:10. The first emulsification was performed by Ultra-Turrax®, a high-shear force homogenizer at 13,000 rpm for 60 sec. Then, the primary emulsion is added into the 3% PVA (Mowiol®,4-98; Mw ~ 27,000 from Sigma – Aldrich, Munich, Germany) aqueous solution with primary-emulsion-to-W_2 ratio of 1:5. The final emulsification was performed also by the Ultra-Turrax®, at 13,000 rpm for 2 min. Later, the obtained double emulsion was moderately stirred overnight to remove the organic solvent and subsequently form the PLGA NPs. Finally, the PLGA NPs were purified by the CFF with MicroKros© mPES hollow fiber membrane of 300K filter cut off and the surface area of 235 cm^2 (Repligen, Waltham, USA).

3.2.6.6. Determination of Encapsulation Efficiency of the Albumin-FITC-loaded PLGA NPs

To determine the total concentration of the albumin-FITC in the PLGA NP sample, the sample was diluted in 1M NaOH (1:1) and centrifuged at 24,610 rcf for 10 min. The solution was read at the calibration curve ranging from 4 µg/ml to 100µg/ml by a fluorometer with filters of 485 nm for excitation, and 590 nm for emission. To quantify the free albumin-FITC concentration, the sample was centrifuged at 24,610 rcf for 60 min. The supernatant was read at the same excitation and emission wavelengths to quantify the free albumin-FITC concentration.

3.2.6.7. Cryo-SEM Imaging of PLGA NPs in suspension and lyophilized form

A small drop of the NP formulation (5 µl) was placed on a specialized holder and covered with a second holder, forming a “sandwich-like” configuration, and submerged in liquid nitrogen within a small, evacuated chamber maintained at a temperature of -210 °C. Following this cryo-fixation step, it was transferred to a specialized cryo-preparation station (Leica, Germany) where it was mounted on a cryo-holder and subsequently transferred using the VCT500 shuttle system (Leica, Germany) maintained at -120 °C to the EM ACE600 sputter coater (Leica, Germany). In the sputter coater, the sample underwent three preparatory steps: cutting, etching the surface, and coating. These procedures were conducted at a temperature of -120 °C. After coating, the sample was transferred again using the cold shuttle into the Quattro S electron microscope (Thermo Fisher, Czech Republic). SEM images were made under the following conditions: temperature of -135 °C, working distance of 5 mm, high voltage of 10 kV, spot size of 2.5, and vacuum of 10^{-3} Pa.

3.2.7. Particle Size Measurements

The colloidal characteristics of the prepared NPs were characterized by the Zetasizer (NanoZS90 from Malvern Instruments, Malvern, UK) using dynamic light scattering (DLS). The z-average particle diameter, polydispersity index (PDI), zeta potential, and intensity distribution were checked by diluting the optimal samples with distilled water. The z-average particle diameters were analyzed at a scattering angle of 90° at 25 °C

3.3. Results and Discussion

3.3.1. Screening of possible process parameters to produce PLGA NPs with the SDS by the modified nanoprecipitation method.

3.3.1.1. Screening of the effect of different disc types on PLGA NP production with the SDS

Different disc materials (PP and PA) were used to prepare 3D-printed discs. These discs were also prepared with different disc surface patterns with different surface depths. These efforts offered a possibility to study if the disc surface influences NP formation due to an increased evaporation based on increased surface area. In other words, when S/NS ejected on the disc surface, the longer that the S/NS is in contact with the disc surface, it could trigger enhanced evaporation. As evaporation is an essential step to remove the organic solvent and solidify the polymer in the nanoprecipitation method to form the PLGA NPs, the effect of different disc patterns and their depth is an important factor to be evaluated. The concave discs, on the other hand, could not be used to produce PLGA NPs, as the disc shape was not optimal to collect the PLGA NP droplets inside the 3D-printed concave disc.

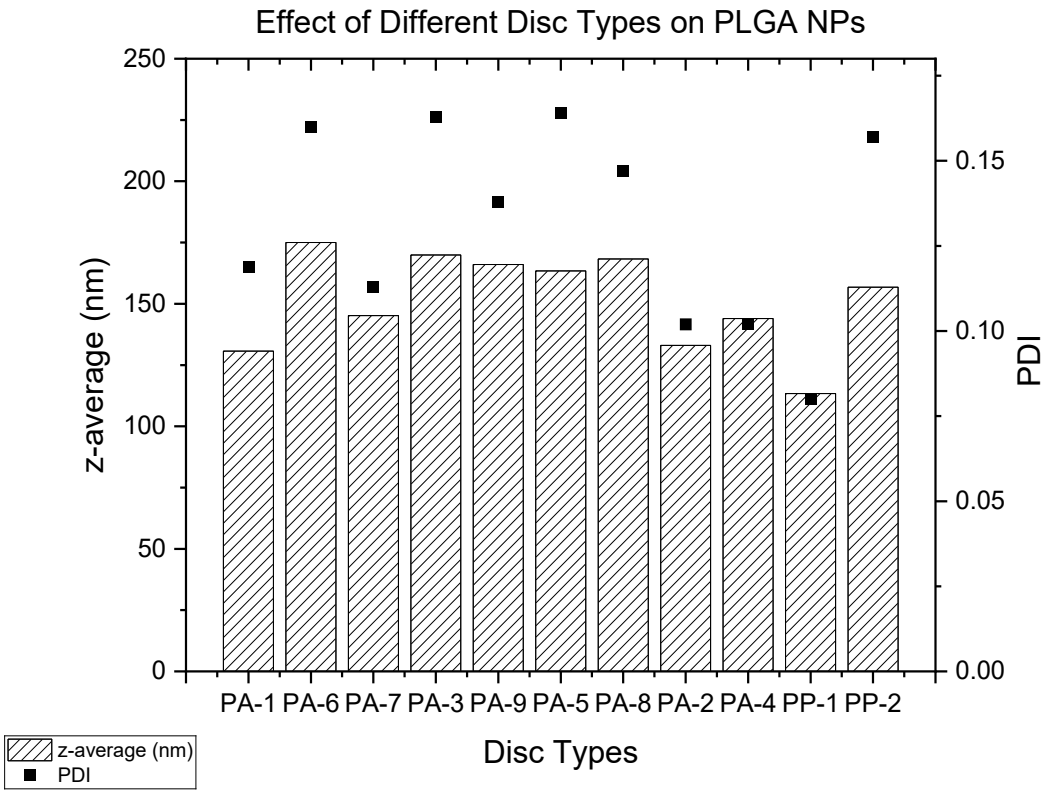

Figure 27. Representation of how different disc types influence the particle size and distribution properties of the PLGA NPs

Thus, the evaluation was performed with the other disc types. As a result of the particle size and PDI measurements performed by DLS, it was seen that the smallest particle size (113 nm) and PDI values (0.080) were achieved by the PLGA NPs produced by PP-1 (polypropylene) (Figure 27). Moreover, when the discs were made of the same material compared with each other in terms of disc surface pattern and their depth, it was observed that the smaller particle size was achieved for the flat disc surface pattern (Figure 28). This could be explained that due to high centrifugal forces of the rotating disc, the droplets from the S/NS mixture could not properly follow the designed path, and the expected evaporation effect could not be achieved properly. Therefore, in the optimization processes followed by the screening studies, the disc types and surfaces were not studied as a factor.

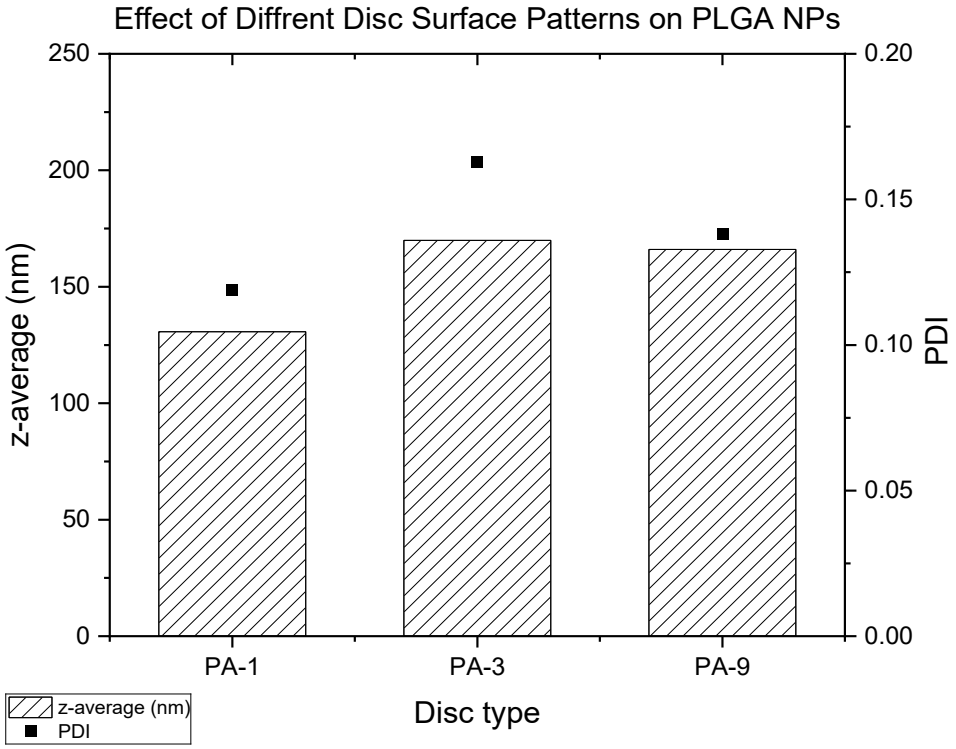

Figure 28. Representation of the effect of different disc surface patterns on PLGA NPs with PA-1 having a flat surface while PA-3 and PA-9 featuring non-flat surface structures.

3.3.1.2. **Screening of the effect of different disc rotation speeds on PLGA NP production with the SDS**

During the screening of different disc rotation speeds, it was observed that an increase in disc rotation speed resulted in a decrease in the particle size (Figure 29). These results are in correlation with the studies in the literature [3,4] where the researchers also reported smaller particle sizes at higher rotation speeds (400-1200 and 500-3000 rpm). These results are expected and attributed to the higher centrifugal forces at the higher rotational speeds which subsequently leads to smaller particle size at higher disc rotational speeds.

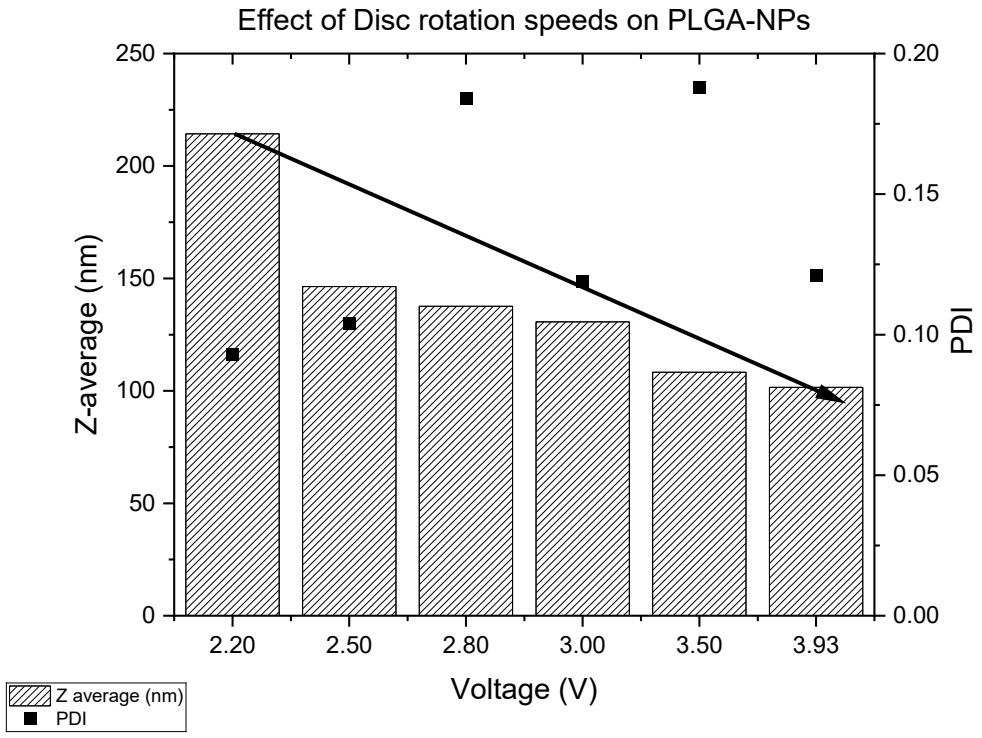

Figure 29. Effect of motor voltage correlated with disc rotation speed on PLGA NPs size and size distribution. The arrow in the figure indicates that the z-average values decrease from 2.20 V to 3.93 V.

3.3.1.3. Screening of the effect of different needle types (droplet sizes) on PLGA NP production with the SDS

To evaluate the effect of different needle types and their corresponding droplet sizes on preparing PLGA NPs, 0.90 x 40 mm (20 G), 0.80 x 120 mm (21 G) and 0.60 x 80 mm (23 G) syringe needles were used. In a study conducted by Tripp et al. [187] on the effect of needle gauge and needle type on the drop volume for sharp needles, they observed that when the gauge size decrease, in another words, when the diameter of the needle hole increases, the corresponding mean drop volume also increased. During the screening, the smallest particle size for preparing the PLGA NPs were achieved by the needle 0.90 x 40 mm (Figure 30), which provides the largest droplet

volume compared to the other needle types studied. This could be attributed to the fact that the larger droplets were influenced by the centrifugal forces more significantly due to their larger weight. On the other hand, this effect was minimal as NPs prepared by using different syringe needles led to similar particle size values. However, the effect of the droplet size could also be observed more clearly for higher rotation speeds due to the higher centrifugal forces on the droplets at higher rotation speeds.

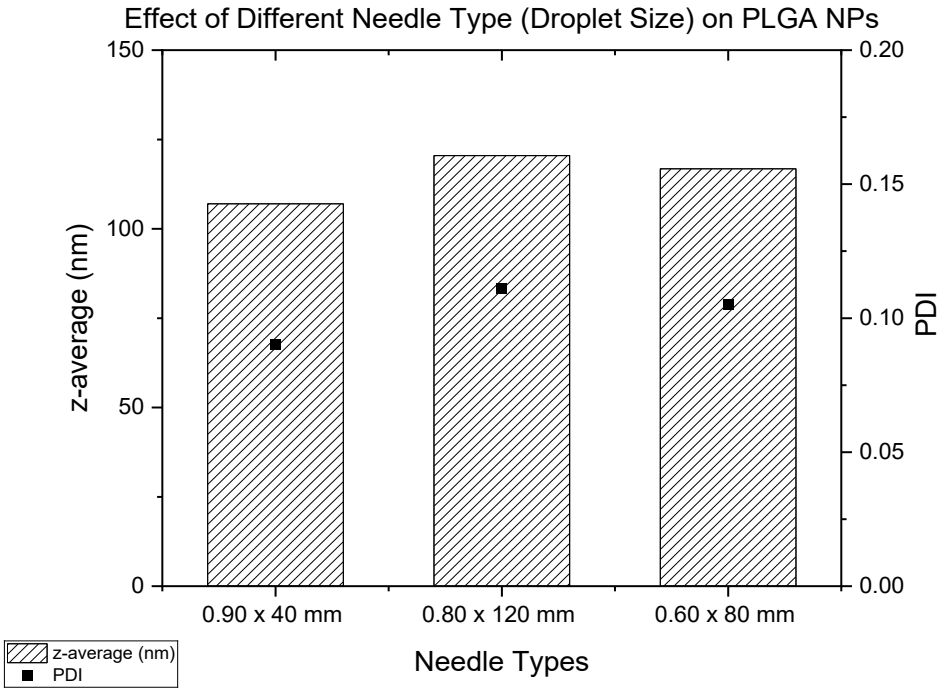

Figure 30. Influence of needle diameter (droplet size) on the properties of PLGA NPs

3.3.1.4. Repeatability of the PLGA NPs prepared by the SDS by the modified-nanoprecipitation method

The repeatability of the PLGA NPs prepared by the SDS by the modified-nanoprecipitation method was tested at the suggested optimal conditions according to the disc type, disc pattern, needle type (droplet size) as well as the disc rotation speed. According to the DLS measurements with the optimal parameters, PLGA NPs with

mean particle size of 106 nm were prepared. This shows the repeatability of the sample and represents that the prototype established produces PLGA NP. While the experimental parameters are not directly comparable, the results are also in alignment with the particle size results of the NPs produced with the SDS-prototype used by Zander where the NP particle sizes measured <200 nm [178].

3.3.2. Preparing and Optimizing Curcumin-loaded PLGA NPs: a DoE study

Table 8. Box-Behnken design coefficient table for the NPs**,** p-values <0.05 indicating the data is statistically significant.

	Inter-cept	*Disc Speed (A)*	*Flow Rate (B)*	*Droplet Size (C)*	*PLGA Conc. (D)*	*AB*	*AC*	*AD*	*BC*	*BD*	*DC*
Size	+212,80	***-31.44***	***+29.89***	+0.1250	***+42.37***						
p-values		***<0.0001***	***< 0.0001***	0.9770	***<0.0001***						
PDI	+0,0456	-0.0073	-0.0073	+0.0048	***+0.0124***	-0.0022	+0.0133	***+0.0283***	***+0.0177***	+0.0020	+0.0112
p-values		0.1796	***0.0098***	0.4746	***0.0265***	0.7319	0.2601	**0.0078**	**0.0211**	0.7605	0.3342
EE%	+99.09	***+0.4960***	***-0.3712***	-0.0130	***-0.1125***	***+0.4901***	+0.0254	-0.1216	-0.0085	***-0.1770***	***-0.2273***
p-values		***<0.0001***	***< 0.0001***	0.6220	***<0.0001***	**<0.0001**	0.5412	0.0936	0.8372	**0.0013**	**0.0013**

For optimizing the PLGA NPs loaded with curcumin prepared by the SDS, Box Behnken DoE design has been performed to analyze the effect of factors such as disc speed, flow rate, droplet size, and polymer concentration on experimental outcomes/responses such as particle size, PDI, and the encapsulation efficiency. For this purpose, 29 runs with five center points were performed. The results showed that particle sizes of the obtained NPs were between 138 and 289 nm, and the PDI values were between 0.026 and 0.1, indicating narrow size distribution. Moreover, for all the NPs prepared, the encapsulation efficiency was calculated as more than 99%, showing the success of the process and encapsulation of the small Mw hydrophobic substances into PLGA NPs.

For optimization, the responses were fitted on models, which was also confirmed by ANOVA, and showed reliability. R^2 values of 0.8765, 0.9345 and 0.9889 for particle size (nm), PDI, and EE%, respectively, showed that the models are consistent and reliable for predicting highly accurate responses. For particle size (nm), a linear model, for PDI, and EE% quadratic models were chosen, as the coefficients were shown in Table 8, where a positive sign implies the positive direct relations. In contrast, the negative sign of the coefficient implies the indirect relation between dependent and independent variables. The boldly written coefficients imply that values are significant.

As a result, it was shown with the *p*-values that droplet size did not show any significance for any response studied. For particle size value, disc speed, flow rate, and polymer concentration chosen were affected significantly. Flow rate and the PLGA concentration significantly affected the PDI response, while droplet size and disc speed showed no significant effect. Lastly, for EE%, all factors except droplet size were found to be significant.

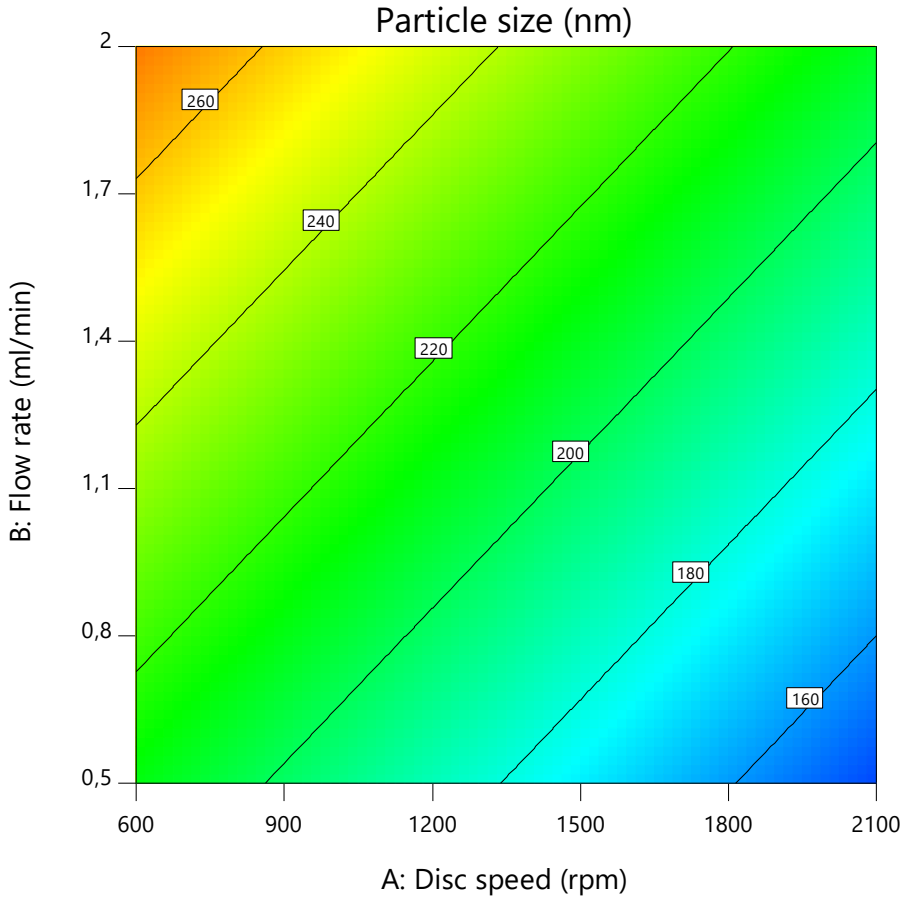

Figure 31. Contour plot for effect of disc speed and flow rate on particle size

It was suggested and shown in the contour plot (Figure 31) that increasing the disc rotation speed decreased the particle size while decreasing the flow rate also decreased the particle size. The contour plot result showed that a slower flow rate and faster disc speed resulted in smaller NPs overall covering sizes from 160 nm to 260 nm (blue and green regions). This can be predicted as higher rotation speeds result in higher centrifugal forces. Moreover, it was observed that increasing the polymer concentration resulted in increasing the particle size. Dao et al. observed a similar effect of increasing the polymer concentration on increased particle size [188]. They attributed this to increased viscosity in the phase, which leads to larger droplet formation and, consequently, larger particle sizes. For the nanoprecipitation technique,

higher polymer concentration could also lead to faster supersaturation; therefore, precipitation can occur faster.

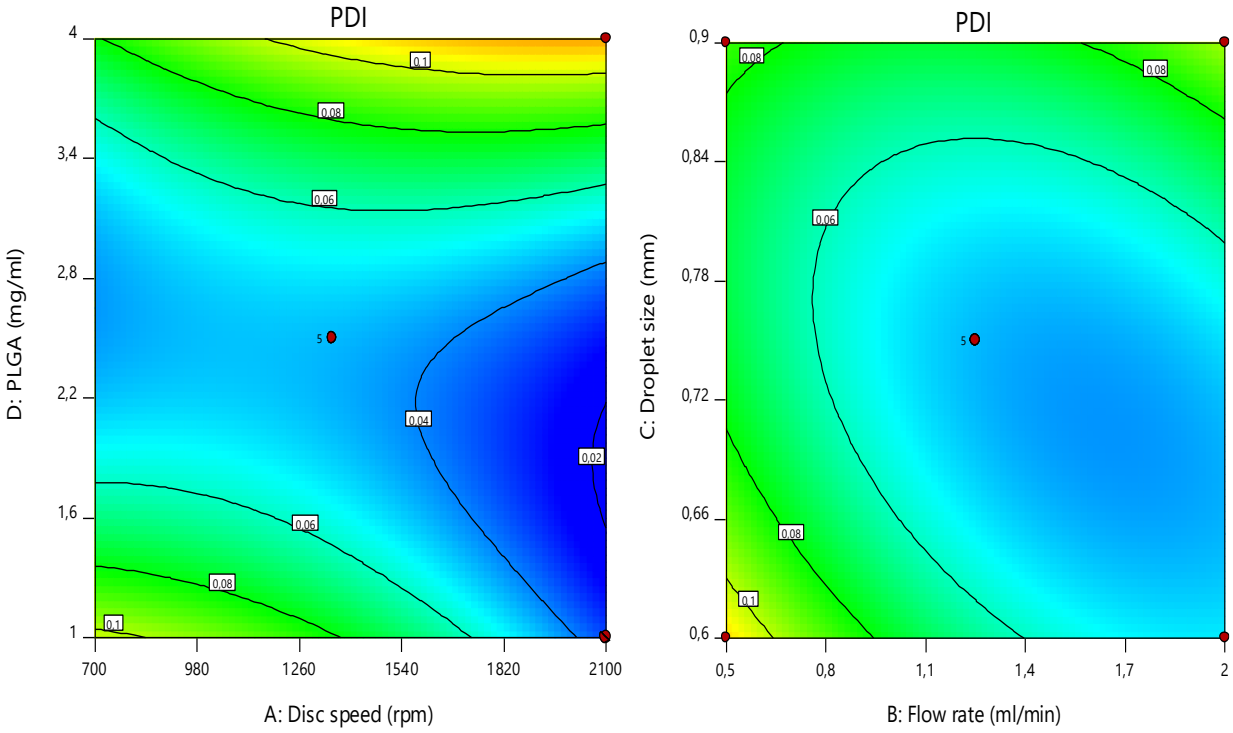

Figure 32. Contour plots for the effect of disc speed and polymer concentration on PDI as well as effect of droplet size and flow rate on PDI

For the PDI value, flow rate and polymer concentration both showed (Figure 32) that increasing these factors decrease the PDI value. For preparing NPs with PDI values less than 0.06, a lower polymer concentration, and faster flow rate value, moderate level of disc speed and low to moderate droplet size should be chosen.

For EE%, it was shown (Figure 33) that increasing the disc rotation speed increases the EE% while faster flow rates decrease the EE%. For polymer concentration, higher polymer concentration decreased the encapsulation efficiency. It was reported in the literature that increasing polymer concentration, where the drug loading was constant (*e.g.*,increase in polymer:drug ratio), should also lead to increased encapsulation efficiency [189]. Therefore, drug and polymer interactions for preparing PLGA NPs with

this method could be further investigated to understand this phenomenon. Regardless, for all NPs prepared, EE% > 99% has been achieved, showing the success of the encapsulation.

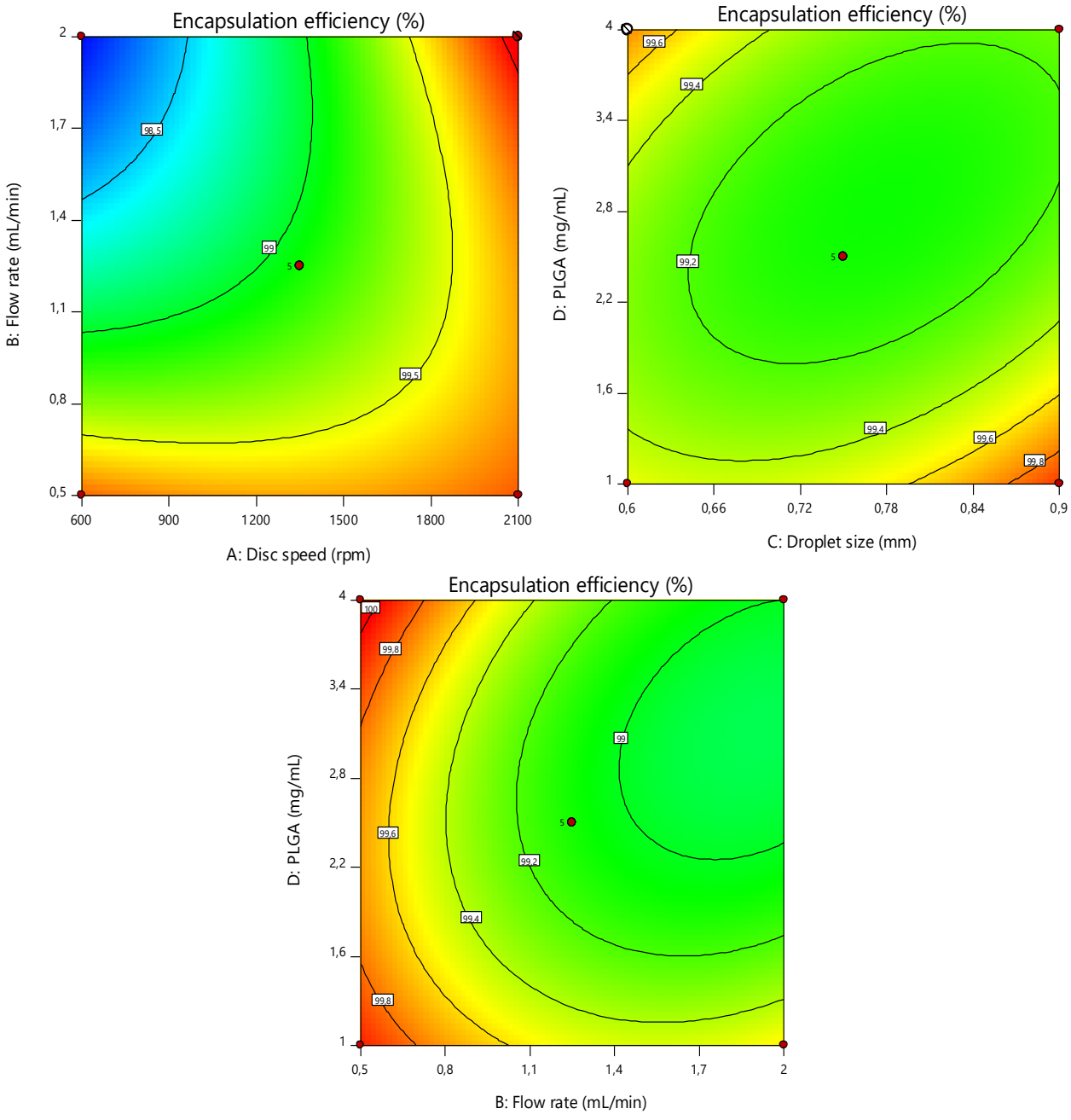

Figure 33. Contour plots for the effect of disc speed and flow rate, droplet size and polymer concentration, and the flow rate and polymer concentration on the EE%

3.3.3. Preparation of PLGA NPs as double emulsions by the emulsification/solvent evaporation method

3.3.3.1. Optimization of the preparation of PLGA NPs by the double emulsion method

The blank PLGA NPs as double emulsions were prepared according to Spindler et al., [117]. The formulation described in the study was initially designed with W_1:O:W_2 of 1:10:100, and 1% Tween® 80. To see the effect of surfactant content and concentration, the "W_1" phase was firstly prepared with distilled water and then 0.5% and 1.0% Tween® 80. For the emulsions prepared with only distilled water, repeatability in particle size and PDI values could not be achieved. This could indicate that there was a need for further stabilization. While the particle size for the PLGA NPs with 0.5% Tween® 80 in "W_1" phase yielded smaller particle size than the double emulsions prepared with 1% Tween 80, the PDI values measured were around 0.35, which was above the threshold of 0.20, an indicator for acceptable polydispersity range for the polymeric NPs [190]. This indicated possible problems for the encapsulation of the model substances to the PLGA NPs double emulsions in the future formulation development as the encapsulation of the drug itself also would lead to a possible increase in particle size values and could affect the polydispersity. A comparison between the different W_1:O:W_2 ratios for the double emulsions prepared highlighted that 1:5:50 and 1:10:50 phase ratios resulted in lower PDI values and smaller particle sizes.

To achieve a higher stability in the development of the PLGA NPs, the method optimization continued by increasing the PVA concentration in the "W_2" phase as suggested by Zambaux et al. [159]. According to the results, when the concentration

of PVA was increased in the "W_2" phase, the particle size and PDI values for both NP formulation with 1:10:100 and 1:5:100 phase ratios decreased as expected (Figure 34). The particle size results were found to be similar between 3% and 5% PVA concentrations for both 1:10:100 and 1:5:100 W_1:O:W_2 ratios. To reduce the concentration of the surfactant, 3% PVA concentration was chosen as an optimal surfactant concentration for "W_2" phase.

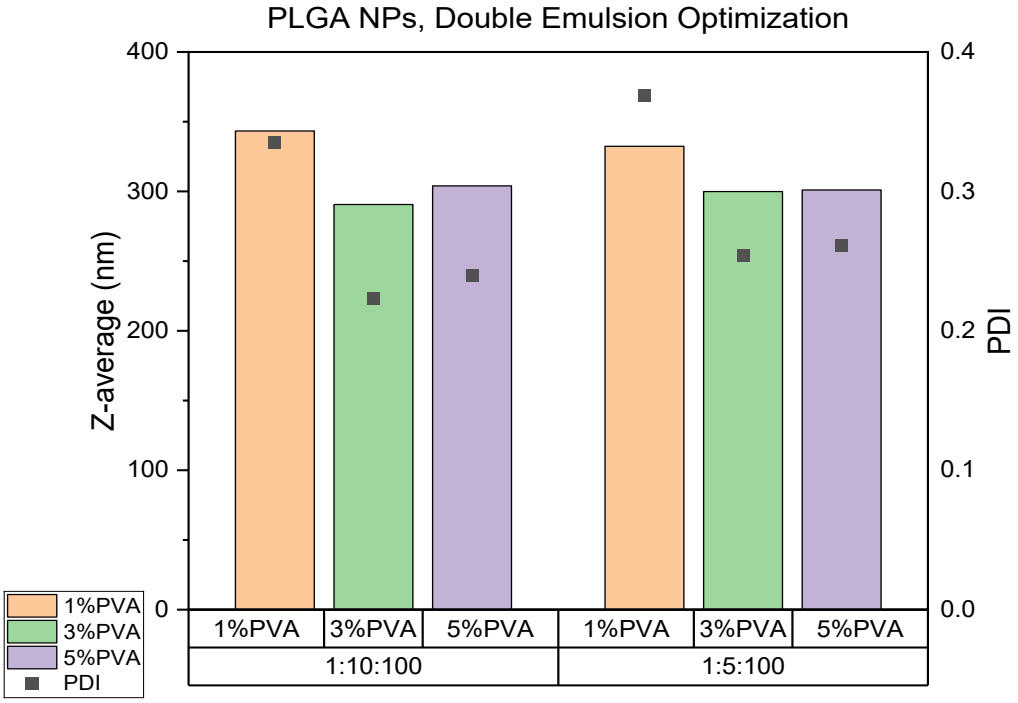

Figure 34. PLGA NPs, double emulsion optimization, influence of W:O:W ratio and surfactant concentration

To observe the influence of surfactant concentration in the "W_1" phase and the primary emulsion homogenization time on the physicochemical characteristics of the double emulsions, the surfactant concentration in the "W_1" phase was increased from 1% to 2% Tween® 80 (Figure 35). In addition to this, NP formulations with both 1.10:100 and 1:5:100 phase ratios were further prepared and evaluated. It was observed that particle size results were similar between the blank-PLGA NPs prepared with 1% Tween® 80

or 2% Tween® 80 concentrations. Increasing the primary emulsification time also did not affect the final particle size and PDI results. So, the optimal preparation for this step was chosen as the "W_1" phase with 1% Tween® 80 concentration with 30 s primary homogenization time for 1:10:100 W_1:O:W_2 phase ratio to minimize the time and the surfactant concentration used. Although PLGA NPs prepared with 1% Tween® 80 and 30 s primary emulsification time showed similar particle size values for both 1:10:100 and 1:5:100 phase ratios, to observe solvent evaporation on the SDS easier, the PLGA NPs prepared with the larger volume of the organic phase were chosen for the final preparation.

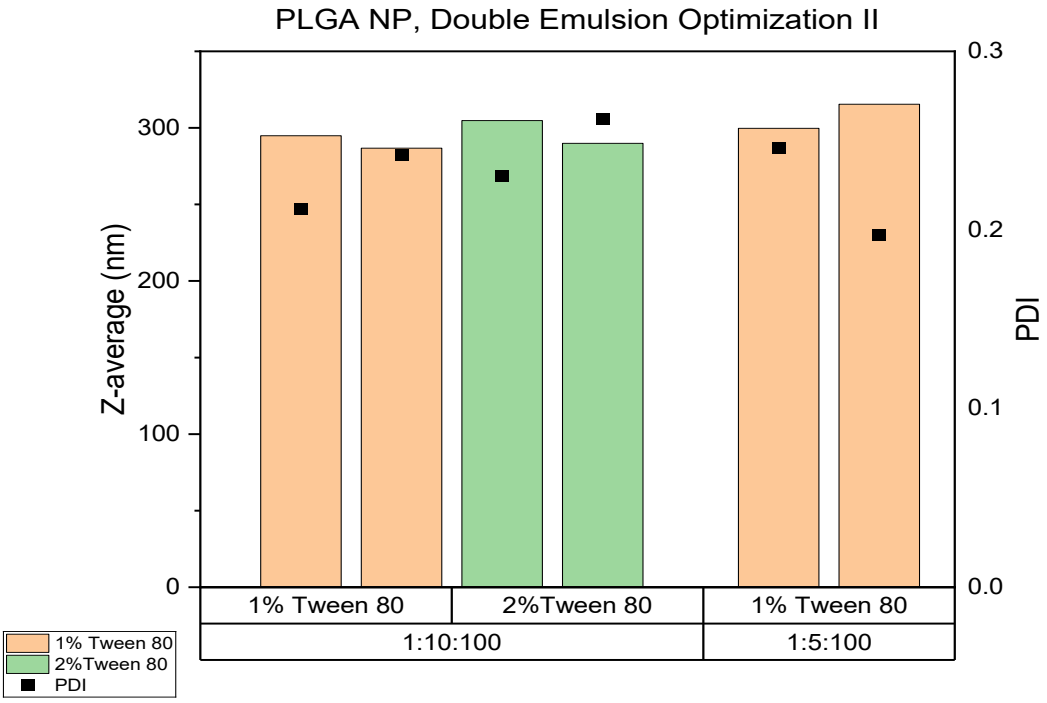

Figure 35. PLGA NP as double emulsion method development optimization: the effect of W:O:W ratio and surfactant concentrations in the outer phase

3.3.4. Screening of the SDS to prepare PLGA NPs as double emulsions.

In the conventional double emulsion preparations, the mixing is performed by high-power homogenizers. These homogenizers apply high shear force needed to overcome the free energy at the interface between the phases, thus overcoming the surface tension and consequently forming the emulsion. On the other hand, in the SDS there are no homogenizers involved in the procedure to produce the particle systems. The process of mixing takes place in the connector as well as on the surface of the disc. In this section, the SDS mixing process has been studied by screening different possible parameters to prepare PLGA NPs. During the screening, the effect of each parameter to achieve better mixing of phases to form double emulsions was analyzed. After the screening trials, the particle size results and the PDI values were compared to the bench top preparations to understand the performance and the limits of the SDS on the direct production of PLGA NPs.

3.3.4.1. Screening of the different disc types

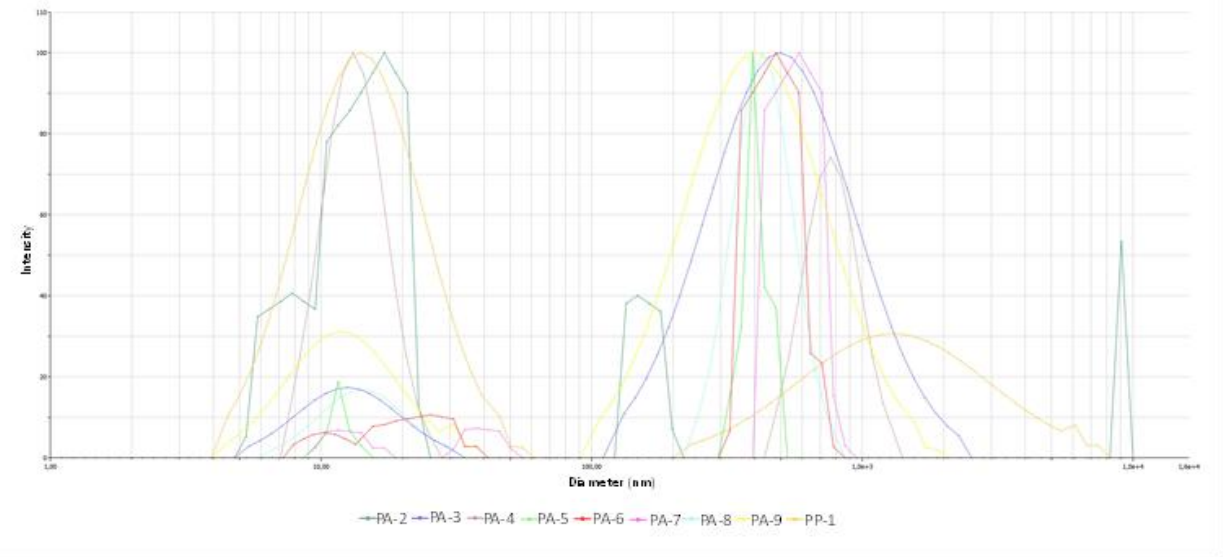

Figure 36. DLS measurements for particles produced with different disc types. In the figure x-axis: the intensity (minimum 0, max 120, increase of 20), y-axis: the diameter (nm).

During the screening of the different disc types, none of the discs that were used for screening yielded a monodisperse nanoparticle formation, and each disc type resulted in multimodal distributions in the corresponding DLS measurements. Moreover, for each disc screened, at least one peak in the DLS results appeared in the micrometer range as shown in Figure 36. This indicates that under these experimental circumstances, changing the disc type did not result in a better mixing of the primary emulsion with the outer aqueous phase on the spinning disc surface to produce NPs. One of the reasons for that could be the lack of sufficient mixing of the inner aqueous phase and the organic phase to form the primary emulsion. The component responsible for this process was the connector. To evaluate this, different connector types were also used in the screening process. In addition to the process parameters, the PLGA NP formulation parameters also could lead to microparticle formation. To screen this, formulations with larger volumes of "W_2" phase were also prepared. In other words, different W_2 ratios were screened. To provide better characterization of the highly diluted samples, DLS measurements were performed in the backscattering mode (172.5°) by the Nanobrook Omni from Bookhaven Instruments (Holtsville, United States). In this mode, the measurement is less dependent on the dilution of the samples than the 90-degree measurements.

3.3.4.2. Screening of the different disc rotation speeds

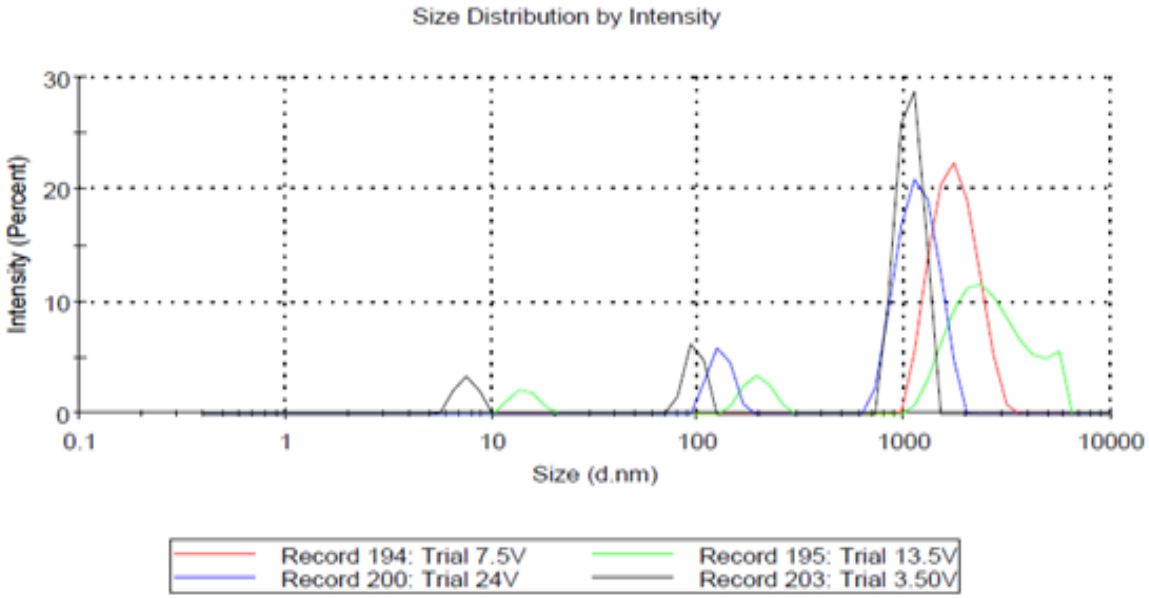

Figure 37. DLS measurements for different disc rotation speeds. The legends were labelled with different colors corresponding to different disc rotation speeds.

According to the screening of the disc rotation speeds and the corresponding DLS measurements, only one sample prepared at 688 rpm resulted in a narrow peak indicating monodisperse microparticles. During this experiment, the W_1 flow rate was 1 ml/min, and the organic solvent containing phase (O) flow rate was 10 ml/min. A comparison between the particles prepared with different disc rotation speeds is shown in Figure 37 As a result, most of the samples showed multimodal distribution in the DLS measurements, which indicates a non-homogeneous mixing of the system as mentioned in the screening of different disc types. On the other hand, a narrow peak was obtained at the second lowest rotation speed: 688 rpm. This could be due to better mixing at the lower rpm and better evaporation due to increased contact time between the disc and phases of the double emulsion at the lower rpm. However, for the slowest disc rotation speed screened (300 rpm), the particles also resulted in multimodal

distribution. This could be explained by the fact that 300 rpm was too slow to provide sufficient forces on the surface of the disc to overcome the surface free energy. Thus, it can be concluded that the optimal rotational speed should be slow enough to let the organic phase evaporate and fast enough to provide sufficient mixing. Consequently, the rotation speeds between 300 and 688 rpm should be further studied to reach the optimal speed. Moreover, the non-uniform mixing could be contributed to the use of T-shaped connector.

3.3.4.3. Screening of the different connectors

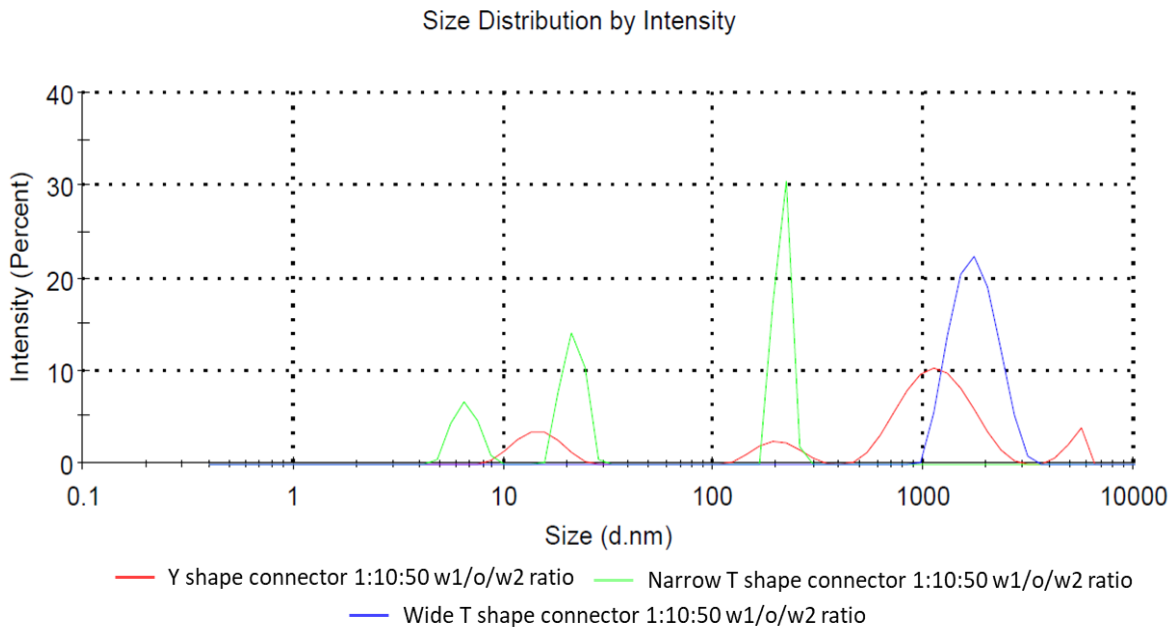

Figure 38. DLS measurement obtained for different connector types. Different connectors were used to mix the "W_1" and "O" phases to form primary emulsion. Three connector types were Y-shaped, narrow T-shaped and wide T-shaped connectors.

To assess the effect of connector type on the PLGA NP formation as double emulsion by the SDS, the screening was performed at 688 rpm. In this rotation speed previous results showed that monodisperse particles in the microparticle range could be produced with the T-shaped connector. On the other hand, the DLS results of the other connectors (Y-shaped and the narrow T-shape connectors) did not result in the same

trend and highly disperse multimodal distributions were observed for the other connector types (Figure 38). However, during some of the following experiments such as primary emulsion-to-W_2 phase ratios, the Y-shaped connector was used. The geometry of the Y-shaped connector could exert greater pressure and direct the mixed phases towards the outlet compared to the T-shaped connector, potentially enhancing the primary emulsion formation on the disc surface.

3.3.4.4. Screening of the primary emulsion to outer aqueous phase ratio

During this screening, W_1:O was kept constant at 1:10, while screening the flow rate of all three phases. This enabled us to observe different primary emulsion-to-W_2 phase ratios. In addition to this, screening different flow rates could change the pressure of the W_1 onto the O. This could directly affect the ratio of the phases while mixing in the connector. To evaluate this, the same W_1-to-O ratio was also tested with higher (10 ml/min) and lower (5 ml/min) primary emulsion injection flow rate. Furthermore, two different disc rotation speeds were studied to expand the screening range. Results showed none of the screened particles led to the production of monodisperse PLGA NPs.

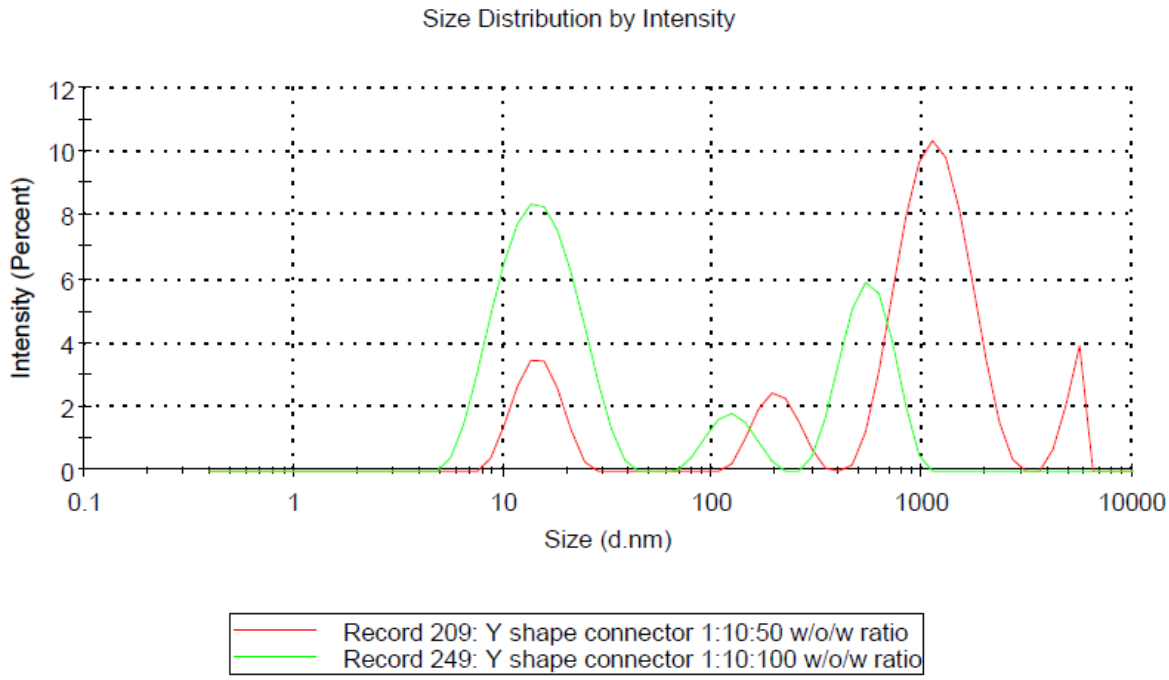

Figure 39. DLS measurement for different phase ratios

Another screening was performed with two different W_2 flow rates (50 and 100 ml/min), while keeping W_1 and O flow rates constant at 1 and 10 ml/min, respectively. This could allow us to study 1:10:50 and 1:10:100 W_1:O:W_2 ratios. Results depicted in figure 39 show that both samples led multimodal distribution in the DLS measurement, where at least one of these peaks was in the micrometer range. This indicated that changing the ratios of W_2 to the primary emulsion did not improve the polydispersity of the PLGA particles under these experimental conditions and this SDS prototype. Moreover, the results indicate that different primary emulsion-to-W_2 phase ratios did not yield monodisperse PLGA NPs. The major contributor for the formation of the double emulsions could be the formulation parameters of the primary emulsion and the stability of the primary emulsion. Based on this, further studies on the mixing of the W_1 and O phases are recommended.

3.3.5. Preparation of PLGA NPs by the MSR

As the particle production with the SDS yielded microparticles, another potential continuous manufacturing system, the micro-spray reactor was investigated to prepare PLGA NPs. The MSR-system, which is a bottom-up method, relies on the solvent and the non-solvent mixing through the spray movement providing control over fine particle production. The system offers interchangeable geometry and adjustable distance while enabling methods such as precipitation and coating. As mentioned in the previous sections, the preparation of the PLGA NPs with the double emulsion method involves a two-step process, which includes the preparation of the primary emulsion and the preparation of the secondary emulsion to form the double emulsion. In this scope, the MSR-system was initially evaluated to prepare both primary and secondary emulsions phases within the reactor system.

To evaluate particle production with the MSR, Ciprofloxacin HCl was chosen as a small hydrophilic model-substance and 35 mg/ml Ciprofloxacin HCl (385.8 g/mol) was added into the organic solvent phase. After that, the primary emulsion was looped through the MSR-system at the highest flow rate to mimic the high-shear force of a traditional homogenizer. While conducting experiments on preparing the primary emulsion with the reactor system, it was observed that the quantification of the loaded model-substance concentration with the MSR was limited. The reason is that W_1-to-O phase ratio depends on the flow rate of each inlet and their respective volumes. When phases are introduced to the system through the pumps with different flow rates to ensure the corresponding phase ratio in the formulation, the phase with the higher flow rate applies an additional driving force on the phase with a slower flow rate. This results in a loss of an amount of loaded-substance during the mixing through the reactor-system,

and results in unstable primary emulsion. This phenomenon yielded repeatability issues in each batch, as well as problems in the quantification of the loaded substance.

To have precise control over the preparation of the "W_1", "O" phases and their ratio to the "W_2" phases, the primary emulsion was prepared with the traditional homogenizer and later combined with the "W_2" within the MSR system with looping. To evaluate this preparation method and test if the looping step with the MSR disturbs the double emulsion structure and turning it into a single emulsion, the primary emulsion was prepared with Ciprofloxacin HCl. The primary emulsion was prepared with a homogenizer and combined with the outer aqueous phase (3% PVA) through the MSR. As the primary emulsion was stable without any surfactant use, it was directly prepared by the addition of 35.7 mg/ml Ciprofloxacin HCl in water to 20 mg/ml PLGA Resomer 503H in DCM with a traditional homogenization method. Then, these two immiscible phases, the primary emulsion and W_2 phases, looped through a reactor with a nozzle size of 300 µm at the highest flow rate to form the PLGA NPs with the double emulsion method. The process followed by the evaporation under the hood overnight to ensure the evaporation of the organic solvent and to form the particles.

3.3.5.1. Characterization of the Ciprofloxacin HCl-loaded PLGA NPs by the MSR-system with the double emulsion method.

The mean particle size of the Ciprofloxacin HCl-loaded PLGA NPs were measured as 322 nm with a mean PDI value of 0.19. After centrifugation, the concentration of the free Ciprofloxacin HCl concentration in the double emulsion formulation was measured as 0.090 mg/ml. The encapsulation efficiency was calculated as 43.75% Table 9.

Table 9. Characterization of the Ciprofloxacin HCl-loaded PLGA NPs, Before CFF

Characterization of the PLGA NPs loaded with Ciprofloxacin HCl, Before CFF	
Parameter	**Result**
Particle size	322 nm
PDI	0.19
Free Ciprofloxacin HCl concentration in water	0.090 mg/ml
Encapsulated Ciprofloxacin HCl concentration	0.070 mg/ml
Encapsulation efficiency	43.75 %

The process continued with further purification by the cross-flow filtration to remove excess amounts of the surfactant PVA, as well as to wash out the non-encapsulated Ciprofloxacin HCl. After the cross-flow filtration with a 100 kDa mPES membrane, it was measured that the particle size and the PDI values remained similar to the sample obtained before the CFF. It was also shown that the free Ciprofloxacin HCl was also successfully washed out with the CFF as the free Ciprofloxacin HCl concentration decreased from 0.090 mg/ml to 0.003 mg/ml after the process Table 10.

Table 10. Characterization of Ciprofloxacin HCl-loaded PLGA NPs, After CFF

Characterization of the PLGA NPs loaded with Ciprofloxacin HCl, After CFF	
Parameter	**Result**
Particle size	294 nm
PDI	0.16
Free Ciprofloxacin HCl concentration in water	0.003 mg/ml
Encapsulated Ciprofloxacin concentration	0.040 mg/ml

However, the concentration of Ciprofloxacin HCl also decreased from 0.070 mg/ml to 0.040 mg/ml as seen in Table 9 and 10. This could be due to dissolution during the CFF, as CFF can further induce the dissolution process due to the sample flow throughout the CFF as well as continuous stirring during the CFF process. Another explanation for this phenomenon could be the washing out the Ciprofloxacin HCl on the surface of the particles, which could be detected before CFF process but washed out from the PLGA NPs after the CFF. Lastly, it could also be due to an agglomeration of the model-substance on the filter. However, no visible agglomeration was observed during the CFF procedure of the Ciprofloxacin HCl-loaded PLGA NPs.

3.3.5.2. Physicochemical characteristics of the albumin-FITC-loaded PLGA NPs by the MSR-system with the double emulsion method

After successful encapsulation of the Ciprofloxacin HCl as a small-molecular-weight hydrophilic substance to the PLGA NPs with the MSR-system, the focus was also given to the preparation of PLGA NPs loaded with larger molecular weight hydrophilic substances to further ease the encapsulation of biopharmaceuticals such as antibodies. To optimize the formulation for the larger-molecular-weight hydrophilic substance encapsulation, albumin was chosen as a model substance.

Table 11. Particle size measurements: PLGA NPs by bench top vs MSR

Particle Size Measurements		
Sample	**Particle Size**	**PDI**
Blank PLGA NP (bench top)	746 nm	0.05
Blank PLGA NP (MSR)	232 nm	0.09
Albumin-FITC PLGA NP (bench top)	738 nm	0.08
Albumin-FITC PLGA NP	240 nm	0.15

To quantify the free albumin concentration in the PLGA NP formulation, a fluorescently labelled derivative of albumin, albumin-FITC was used due to its instinctive fluorescence with an excitation wavelength of 491 nm. The NPs were also prepared with the traditional homogenization method (bench top) to assess and compare the particle production with the MSR to the traditional homogenization method (Table 11).

According to the particle size comparisons between the bench top and MSR PLGA NPs prepared both as blank (without albumin) or with albumin-FITC, it was clearly seen that PLGA NPs with smaller particle size were achieved by the MSR for the same formulation. This shows an advantage of the MSR system to further tailor the particle size of the particles with the looping step.

Table 12. Assay results of the albumin-FITC-loaded PLGA NPs by the bench top and MSR.

Albumin-FITC PLGA NPs Assay Results		
Parameter	**Bench top**	**MSR**
Free albumin-FITC Concentration	0.004 mg/ml	0.013 mg/ml
Encapsulation efficiency	95 %	82 %

Moreover, free albumin-FITC concentration was calculated through the method established. According to the results, PLGA NPs prepared by both bench top method and by the MSR showed high encapsulation efficiency (95% and 82%). This shows the feasibility of both methods to prepare albumin-FITC loaded PLGA NPs (Table 12).

Table 13. Albumin-FITC PLGA NPs Assay Results

Albumin-FITC Assay Results		
Parameter	**Before CFF**	**After CFF**
Mean Particle Size	216 nm	238 nm
Mean PDI	0.02	0.09
Free Albumin FITC concentration	0.012 mg/ml	0.002 mg/ml

After the CFF with 300 kDa mPES membrane, it was measured that the particle size and the PDI values remained like prior measurement by the DLS before the CFF. During the DLS measurements, the effect of the viscosity of the PVA was also considered. As the samples before CFF contained PVA unlike the samples after CFF. This affected the viscosity of the DLS measurements which are dependent on the viscosity of the media. Thus, the measurements were corrected by PVA to successfully compare the results before and after CFF. As a result, it was also shown that the free albumin-FITC was also successfully washed out with the CFF as the free albumin-FITC concentration decreased from 0.012 mg/ml to 0.002 mg/ml after the process (Table 13)

For another batch of albumin-FITC loaded PLGA NP production (mean particle size of 248 nm), lyophilization was also performed with presence of 5% d-mannitol. The success of the particle formation lyophilization process can be further supported by the Cryo-SEM images obtained from lyophilized sample in the presence of the cryoprotectant, showing that the process yielded particulate structures as shown in the Figure 40. As mannitol was used in the lyophilization process, the mannitol crystals are also expected to be shown in the Cryo-SEM images together with the PLGA NPs.

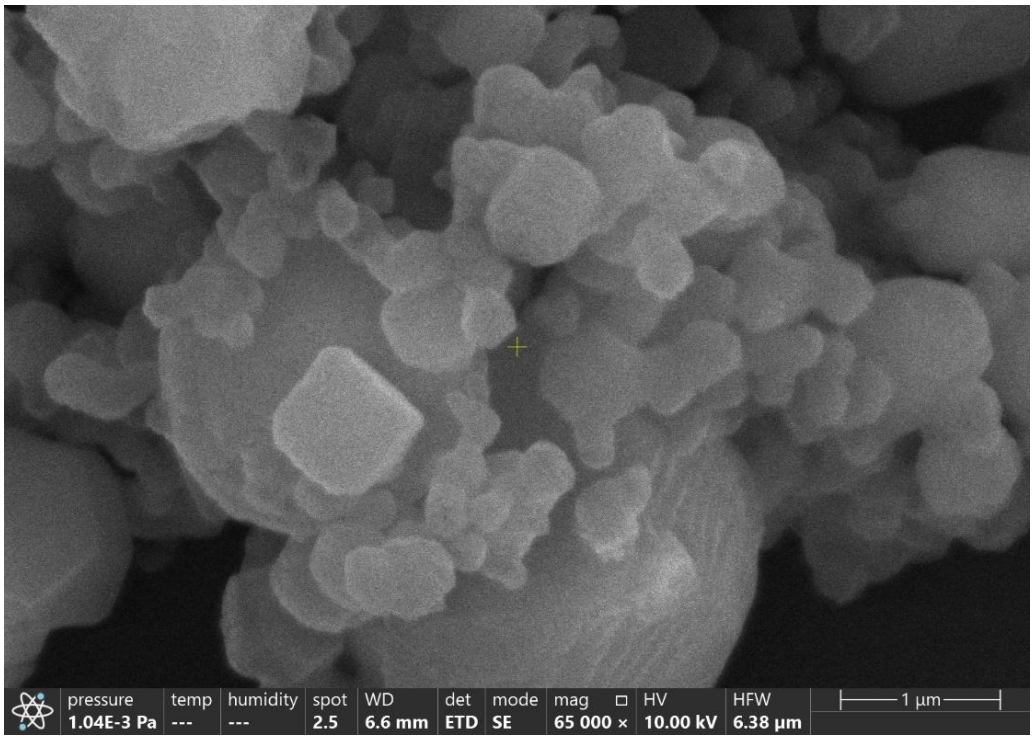

Figure 40. Cryo-SEM image of lyophilized PLGA NPs

3.4. Conclusion

In conclusion, the screening, optimization, and the characterization of the PLGA NPs prepared with different formulation and production protocols were successfully evaluated. The SDS has successfully screened to prepare PLGA NPs by the modified-nanoprecipitation method. The particle size and surface characteristics of the PLGA NPs were comparable to the previously reported PLGA NPs prepared by the same method in the literature, and the design of the system allowed further evaluation of several parameters. This showed the potential of the SDS to be used as a continuous manufacturing system.

Moreover, the system was evaluated in terms of its advantages and limitations to prepare PLGA NPs by the double emulsion method. It was concluded that while PLGA microparticle production was possible with the SDS, the production of the PLGA NPs was not succeeded within the formulation and process parameters studied. To prepare

PLGA NPs by the double emulsion method, another potential continuous manufacturing system MSR was also evaluated. This system enabled the successful encapsulation of small and large molecular weight hydrophilic model substances such as Ciprofloxacin HCl and albumin to PLGA NPs. This also showed that the looping with the MSR system preserved the drug-loaded-primary emulsion, and the overall double emulsion structure.

The Ciprofloxacin HCl-loaded PLGA NPs showed high encapsulation efficiency, in another proof-of-concept study, albumin-FITC was also loaded into PLGA NPs using both traditional homogenization and the MSR system. As a result, both with bench top and with the MSR-system, high encapsulation efficiency was achieved. Additionally, the novel method yielded particles with smaller particle sizes than the traditional homogenization method. Overall, feasibility of the encapsulation of large hydrophilic model substance into the PLGA NPs by the MSR-system was shown. For both studies, the CFF was successfully implemented to wash out the free drug and surfactants. The need for further optimization of the CFF for this sample to avoid a loss in the total amount of the sample was concluded.

4. Scalable PLGA NPs for the potential N2B delivery: The proof-of-concept studies

The following chapter has been published in Pharmaceutics as S. Akpinar Adscheid, M. Rojas Rodríguez, S.M. Abdel-Hafez, F.S. Pavone, M. Schneider, A.E. Türeli, M. Calamai, N. Günday-Türeli, Scalable Manufacturing Method for Model Protein-Loaded PLGA Nanoparticles: Biocompatibility, Trafficking and Release Properties, Pharmaceutics 17 (2025) 87. https://doi.org/10.3390/pharmaceutics17010087.

Some part of the research presented in the following chapter has been performed during the scientific secondment of Selin Akpinar Adscheid at European Laboratory for Non-Linear Spectroscopy located in Florence, Italy in March 2024, in collaboration with Marta Rojas-Rodríguez and principal investigator Dr. Martino Calamai in scope of Horizon 2020 MSCA ITN Bio2Brain project. Live-cell imaging for localization and release studies with the cell line and CLSM analysis were performed by Marta Rojas-Rodríguez.

Preparation of the Rhodamine-labelled-PLGA and RPMI 2650 cell culture studies as well as subsequent cell viability MTT assay were performed by Dr. Salma M. Abdel-Hafez from Saarland University.

The figures used in the following chapter were created with Biorender.com under the student licensing plan.

4.1. Introduction

Although NP formulations offer inevitable advantages to deliver the drug at the site of action, and especially to the brain in non-invasive strategies such as N2B delivery reliable production is still inhibiting translation from lab-scale to the market. There are efforts on scalability of the DDS [110–112,191] but in many cases limitations are encountered.. As explained in the previous chapter, MSR-system, a continuous manufacturing technology, can be used for preparing double emulsions that can serve as a reservoir for hydrophilic substances (*e.g.*, albumin) while providing scale-up opportunities. These NP formulations can also be potentially used for N2B delivery applications, an innovative and non-invasive approach to bypass the BBB as also explained previously. Therefore, this chapter focuses on preparing scalable PLGA NPs by the double emulsion method by the MSR-system and assess the biocompatibility, drug trafficking and release profiles of model-substance-loaded PLGA NPs to assess their compatibility for future N2B delivery approach to target CNS diseases (Figure 41).

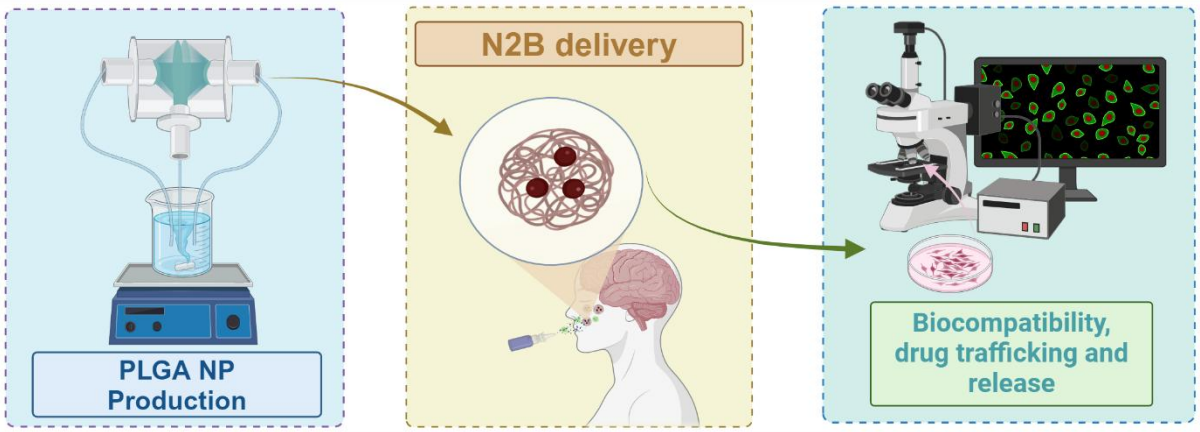

Figure 41. Illustrative summary of aim of the chapter

To test the suitability of PLGA NPs manufactured by the MSR system for possible N2B delivery applications, we prepared fluorescent PLGA NPs. As a large hydrophilic model substance, we chose fluorescent albumin and loaded it into the fluorescent PLGA NPs.

To test the particles' further compatibility with the N2B delivery, we assessed their biocompatibility in different cell lines, evaluated their uptake and trafficking, and determined the release kinetics of the encapsulated fluorescent albumin. Furthermore, we loaded the PLGA NPs with WGA488, a cell membrane marker, to test the functionality of the drug substances after encapsulation and release.

4.2. Materials and Methods

4.2.1. Preparing Scalable Fluorescent PLGA NPs

4.2.1.1. Preparation of the rhodamine-PLGA (Rhod-PLGA)

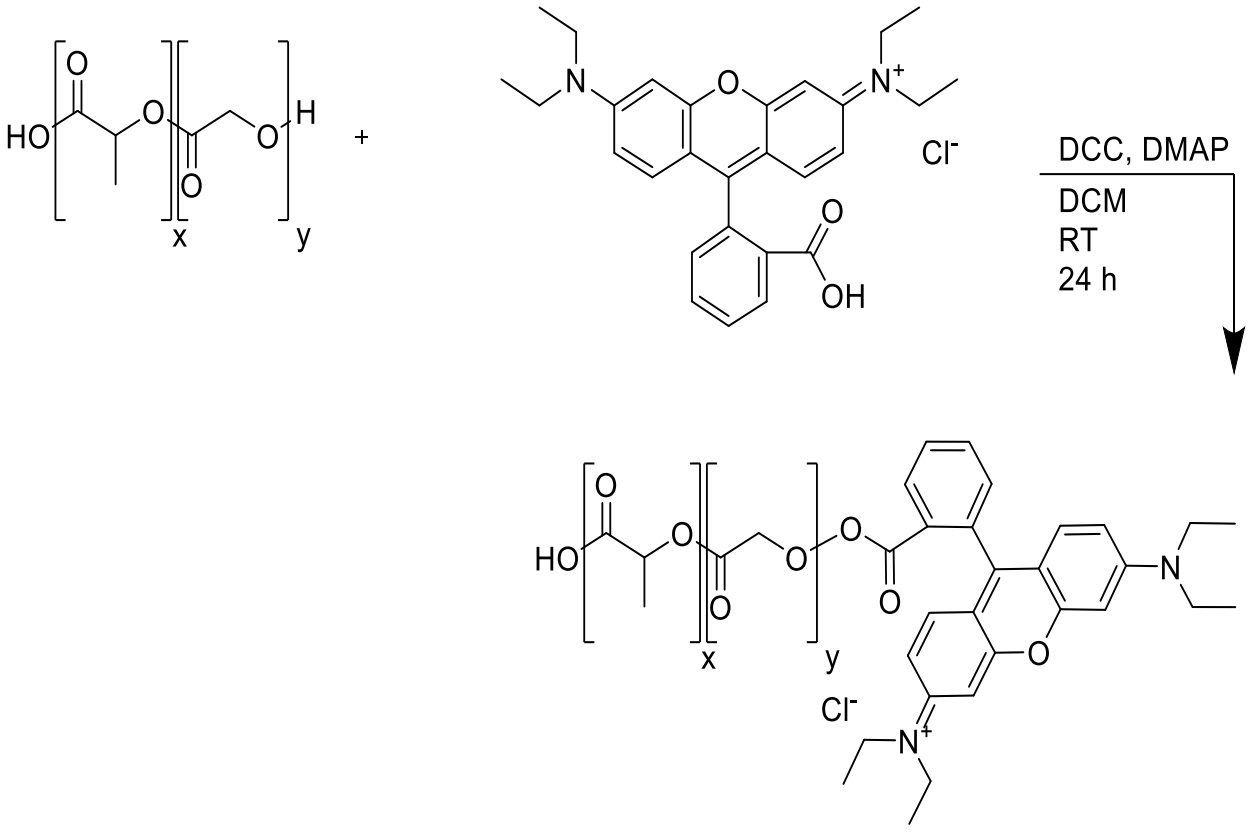

Figure 42. Synthetic Pathway to Rhod-PLGA

PLGA Resomer RG 503 H (molecular weight (Mw): 24,000 - 38,000 g/mol, Evonik Industries, Darmstadt, Germany) was covalently labeled with rhodamine B (Sigma-Aldrich, Steinheim, Germany) (Figure 42) based on the method described by Lababidi et al. [192]. In brief, PLGA (1 molar equivalent (eq), 1 g) and DMAP (Sigma-Aldrich, Steinheim, Germany) (0.1 eq, 0.4 mg) were dissolved in dry DCM (15 ml). Rhodamine B (1.1 eq, 17 mg) and DCC (Sigma-Aldrich, Steinheim, Germany) (1.5 eq, 10 mg) were dissolved in dry DCM (Thermo Fisher Scientific, Darmstadt, Germany) (15 ml). The rhodamine B/DCC solution was added to the PLGA/DMAP solution, followed by stirring for 24 h at room temperature. After 24 h, the reaction was quenched by adding MilliQ water (1 ml). DCM was eliminated using rotary evaporation at 50 ºC under atmospheric pressure. The yielded - Rhod-PLGA was dissolved in acetone (20 ml) using ultrasonic bath and the solution was transferred to centrifugation tubes. The Rhod-PLGA was precipitated by adding equal volume of ethanol (HPLC grade) (Fisher Scientific, Schwerte, Germany), followed by centrifugation at 20,000 g, 20 min, 20 ºC (Multifuge X1R, Thermo Fisher Scientific, Osterode am Harz, Germany) and discarding of the supernatant. The product was redissolved in acetone (HPLC grade) (Fisher Scientific, Schwerte, Germany) and washed 5 additional times (or until a clear supernatant is observed) using the same method. The final pellet obtained after pooling was sonicated for 20 min in a cooled ultrasonic bath, frozen at -80 ºC and lyophilized (Alpha 3-4 LSCbasic, Christ, Osterode am Harz, Germany) for 48 h. The product yield was approximately 88%.

4.2.1.2. Preparation of albumin-loaded and blank Rhod-PLGA NPs

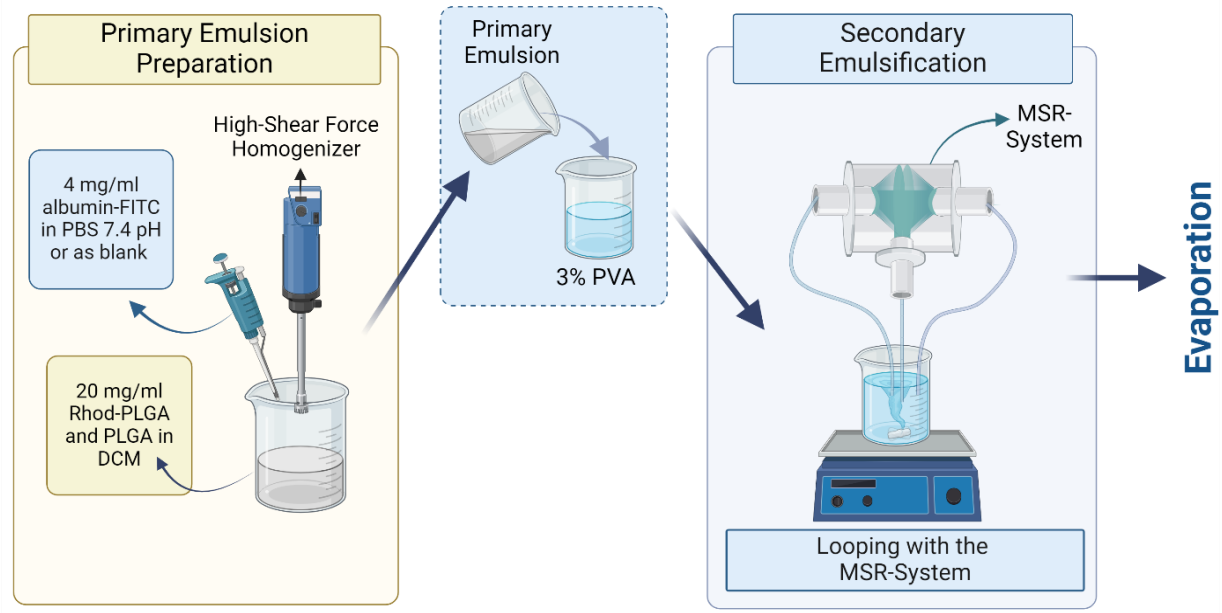

Figure 43. Preparation of the albumin-FITC-loaded Rhod-PLGA NPs

Albumin-FITC-loaded Rhod-PLGA NPs were prepared by the emulsification solvent-evaporation method (double emulsion method) combined with the reactor-system (Figure 43). The primary emulsion was prepared by adding 4 mg/ml albumin-FITC (Bovine Protein) (Sigma-Aldrich, Darmstadt, Germany) in PBS 7.4 pH into 20 mg/ml mixture of Rhod-PLGA and PLGA Resomer 502H (50:50 acid terminated ; Mw: 7,000-17,000, Evonik, Darmstadt, Germany) with a ratio of 1:20. The mixture was then dissolved in dichloromethane (DCM) (ACS Reagent, ISO, ≥99.9% (GC) grade, Merck KGaA, Darmstadt, Germany) with a phase ratio of 1:10. The emulsification was performed by Ultra-Turrax®, a high shear force homogenizer at 13,000 RPM for 60 s. Then, the primary emulsion was added into the 30 mg/mL PVA (Mowiol®,4-98, Mw ~ 27,000, Sigma – Aldrich, Munich, Germany) with 1:5 ratio and continuous looping through a 300 µm reactor were performed for 15 min with a flow rate of 200 ml/min in each pump. Finally, the PLGA double emulsion was stirred overnight to remove the

organic solvent and form the PLGA NPs. For the MTT assay, instead of albumin-FITC, non-fluorescent albumin (Sigma Aldrich, Darmstadt, Germany), and non-fluorescent PLGA from (Evonik, Darmstadt, Germany) were used.

4.2.1.3. Assay Methods

To determine the concentration of the albumin-FITC in NPs the sample was diluted in 1M NaOH (1:1) and centrifuged at 24,610 rcf for 10 min. The solution was analyzed based on the calibration curve by a microplate reader with a filter of 485 nm excitation, and 590 nm emission wavelengths. To quantify the free albumin-FITC concentration, the sample was centrifuged at 24,610 rcf for 60 min. The supernatant was measured at the same excitation and emission wavelengths to quantify the free albumin-FITC concentration. The percentage of encapsulated albumin-FITC concentration was calculated by subtracting the free albumin-FITC concentration from the total albumin-FITC concentration which is divided by the total albumin-FITC concentration, multiplied by 100%.

4.2.1.4. Preparation of the WGA488-loaded PLGA NPs by the bench top method

WGA488-loaded PLGA NPs were prepared by the traditional bench top double emulsion method (Figure 44). The primary emulsion was prepared by adding 1 mg/ml Wheat Germ Agglutinin (WGA) Alexa Fluor 488 (Invitrogen™, Waltham, MA, USA) in PBS 7.4 pH into 20 mg/ml PLGA Resomer 502H (50:50 acid terminated, Mw: 7,000- “W_1” to “O” phase ratio of 1:10. 17,000, Evonik, Darmstadt, Germany) dissolved in DCM with a phase ratio of 1:10. The emulsification was performed by Ultra-Turrax®, a high shear force homogenizer at 13,500 rpm for 60 s. Then, the primary emulsion was added into the 30 mg/ml PVA solution (Mowiol® 4-98, Mw: ~ 27,000, Sigma – Aldrich,

Munich, Germany) with 1:5 ratio. The second emulsification was performed again with the Ultra-Turrax® at the same rpm for 120 s. Finally, the PLGA double emulsion was stirred overnight to remove the organic solvent and form the PLGA NPs.

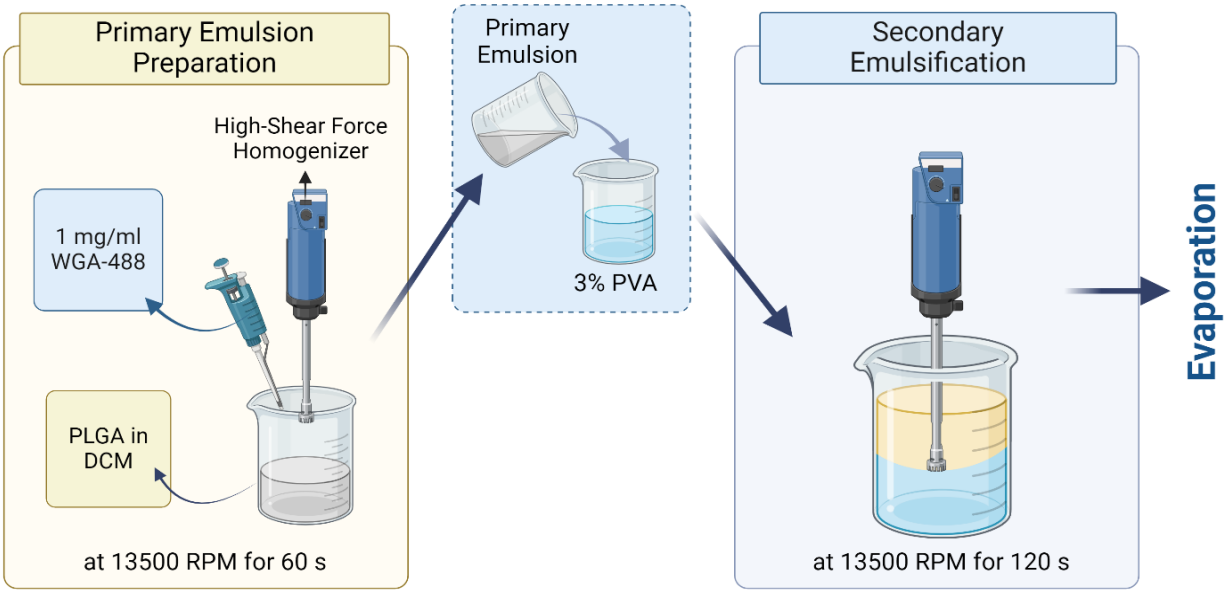

Figure 44. Preparation of the WGA488-loaded PLGA NPs

4.2.1.5. Purification of the NPs by the CFF

The purification was performed by the CFF with 300 kDa MicroKros© mPES (modified polyethersulfone) hollow fiber membranes (Repligen, Waltham, United States) with a surface area of 235 cm^2 to ensure to purify the sample from the free PLGA, surfactant, and albumin.

4.2.1.6. Lyophilization of NPs

For the preparation of lyophilization sample 50 mg/ml of d-mannitol (Sigma-Aldrich, Darmstadt, Germany) was dissolved in nanosuspension and samples were introduced into the lyophilization program with a volume of 2 ml for each vial. To lyophilize the samples, a freezing step at -70 °C for 7 h at 1000 mbar, followed by a two-step-long main drying at -40 °C for 6 h at 0.5 mbar, and at the same temperature at 0.120 mbar

for 19 h was performed. After the main drying, the secondary drying was performed for 20 h at 30 °C, at 0.050 mbar.

4.2.2. Colloidal Characteristics, Biocompatibility and Release Profiles of Fluorescent PLGA NPs

4.2.2.1. Particle Size Measurements

The colloidal characteristics of the prepared NPs were characterized by the Zetasizer (NanoZS90 from Malvern Instruments, Malvern, UK) using dynamic light scattering (DLS). The z-average particle diameter, polydispersity index (PDI), zeta potential, and intensity distribution were checked by diluting the optimal samples with distilled water. The z-average particle diameters were analyzed at a scattering angle of 90° at 25 °C.

4.2.2.2. Evaluating *in vitro* cumulative release profile

The cumulative release studies of albumin-FITC from albumin-FITC-loaded PLGA NPs were performed in PBS at pH 7.4 (n=3). The lyophilized samples were resuspended in 5 ml PBS at pH 7.4 and stirred at 120 rpm. 0.5 ml sample was collected and filtered through syringe filter with 0.02 µm pore size (Whatman®, Anotop®, Maidstone, UK). Filtration, a common technique in release studies, was combined with a fine syringe membrane pore size of 0.02 µm to ensure the successful separation of the NPs and undissolved albumin. This approach aimed at avoiding any misleading high readings in analytical measurements during the release studies [193]. The sampling was performed at time intervals of 1 h, 2 h, 4 h, 24 h and 48 h. The fluorescence intensity at each time interval was measured with a fluorometer with an excitation wavelength of 485 nm, and emission wavelength of 590 nm.

4.2.2.3. RPMI 2650 cell culture Studies

Nasal septum squamous carcinoma cells (RPMI-2650) (Leibniz Institute DSMZ (German Collection of Microorganisms and Cell Cultures GmbH), Braunschweig, Germany) were cultured in Eagle's minimum essential medium (EMEM) (Sigma-Aldrich, Steinheim, Germany) supplemented with 10% fetal bovine serum (FBS) (Thermo Fisher Scientific, Darmstadt, Germany). The cells were sub-cultured once a week and the media was replaced with fresh media every other day. The cultures were maintained at 37 °C in a humidified atmosphere containing 5% CO_2 (BD 260 Standard Incubator, Binder, Tuttlingen, Germany). The cells were used between passages 3 and 10.

4.2.2.4. Cell viability MTT assay

RPMI-2650 cells were seeded (150,000 cells/well) into 96-well plates and grown for 24 h. Afterwards, the cells were washed twice with Hank's Balanced Salt Solution (HBSS) (Thermo Fisher Scientific, Darmstadt, Germany) buffer and non-fluorescent albumin-loaded PLGA NPs suspended in HBSS buffer were added at different concentrations (50, 100, 200, 300, 400 and 500 µg/ml). The samples were tested against negative (HBSS buffer) and positive (2% Triton-X) controls. After 4 h incubation with the formulations and controls, the cells were washed twice with HBSS and incubated with thiazolyl blue tetrazolium bromide (MTT reagent) (Sigma-Aldrich, Steinheim, Germany) for 4 h, followed by aspiration and incubation with DMSO for 20 min. The absorbance of formazan formed by living cells was measured at 550 nm and cell viability was calculated. All experiments were performed in triplicates. The particle size of the NPs was checked in cell culture medium to ensure stability.

4.2.2.5. Neuroblastoma cell culture

Human SH-SY5Y neuroblastoma cells (A. T. C. C. Manassas, VA, USA) were cultured in Dulbecco's Modified Eagle's Medium (DMEM, Thermo Fisher Scientific, Waltham, MA, USA) supplemented with 1% penicillin/streptomycin solution and 10% fetal bovine serum (FBS). Cell cultures were incubated at 37 °C, 5% CO_2 in a humidified atmosphere. The cultures were grown until 90% confluency.

4.2.2.6. Live-cell imaging for localization and release studies with neuroblastoma cells and CLSM analysis

SH-SY5Y cells were plated on 18 mm glass coverslips in 12-well plates at 100,000 cells per well. 24 h after plating, cells were incubated with 100 µg/ml of NPs. The particle size of the particles was checked in cell culture medium to ensure the particles' stability. For the localization experiments, cells were incubated for 4 h with 100 µg/ml of blank Rhod-PLGA NPs in the regular medium. Subsequently, with 5 µg/ml WGA488 for 30 min to specifically label the plasma membrane. 10 min before the time finished, cells were incubated with Hoechst 33342 dye at a concentration of 10 µg/ml in order to stain the cell nuclei. After the incubation cells were washed with phosphate-buffered saline (PBS) and the medium was replaced with Leibovitz's L-15 (Thermo Fisher Scientific) before imaging, a medium designed for supporting cell growth in the absence of CO_2 equilibration.

For the time-course experiments, cells were first incubated for ten minutes with Hoechst, then washed with PBS, mounted on a custom chamber for imaging and the incubation medium was replaced with Leibovitz's L-15. Subsequently the Rhod-PLGA

loaded with albumin-FITC NPs or WGA488-loaded PLGA NPs were added and followed for 60 min in the laser scanning confocal microscope (CLSM).

The analysis of blank Rhod-PLGA NPs and Rhod-PLGA loaded with albumin-FITC NPs was performed after excitation at 561, 488 and 405 nm. The analysis of PLGA NP loaded with WGA488 was performed after excitation at 488 and 405 nm. A Nikon C2 CLSM and a Plan Apo λ 100X 1.45 NA oil immersion objective were used. For each sample, optical sections at median planes of the cells were taken (1024x1024 pixels) using sub-saturation settings and all of them were kept constant for each analysis (laser power, detector gain, and pinhole diameter). Images were processed and analyzed with the Fiji software and Origin(Pro) ("Version 2022b", OriginLab Corporation, Northampton, MA, USA)

To characterize the colocalization degree between the Rhod-PLGA NPS and the plasma membrane, as well as the cargo albumin-FITC and the Rhod-PLGA NPs, the JACoP plugin [194] of Fiji software was used. Specifically, to calculate Pearson's correlation coefficient [195], which estimates the covariance of signal intensities between two images by analyzing them on a pixel-by-pixel basis, and Manders' overlap coefficient [196] which measures the fraction of pixels in image 1 that overlap with those in image 2, and vice versa. The data was analyzed with Origin (Pro).

4.2.2.7. Ratio Measurement Method

To measure the ratio of the fluorescence between two channels, the cargo (albumin-FITC, green channel) and the NPs (Rhod-PLGA, red channel) were used. The images are selected, a strong threshold is applied to the NPs channel (561 excitation wavelength, red channel) and the particles analyzed delimiting the region of interest (ROI). The strong threshold assures that the fluorescence detected is coming from the

NPs alone. These ROIs are selected and saved to be used in the next step. Then applying the Ratio Plus plugin in the Fiji software, a measurement of the ratio between both channels is possible (the cargo from the green channel over the NPs from the red channel) in the ROIs previously selected that are the regions where the NPs are present. Like this, a measurement of how much cargo (albumin-FITC) is present in the NPs (Rhod-PLGA) overtime is obtained (Figure 45).

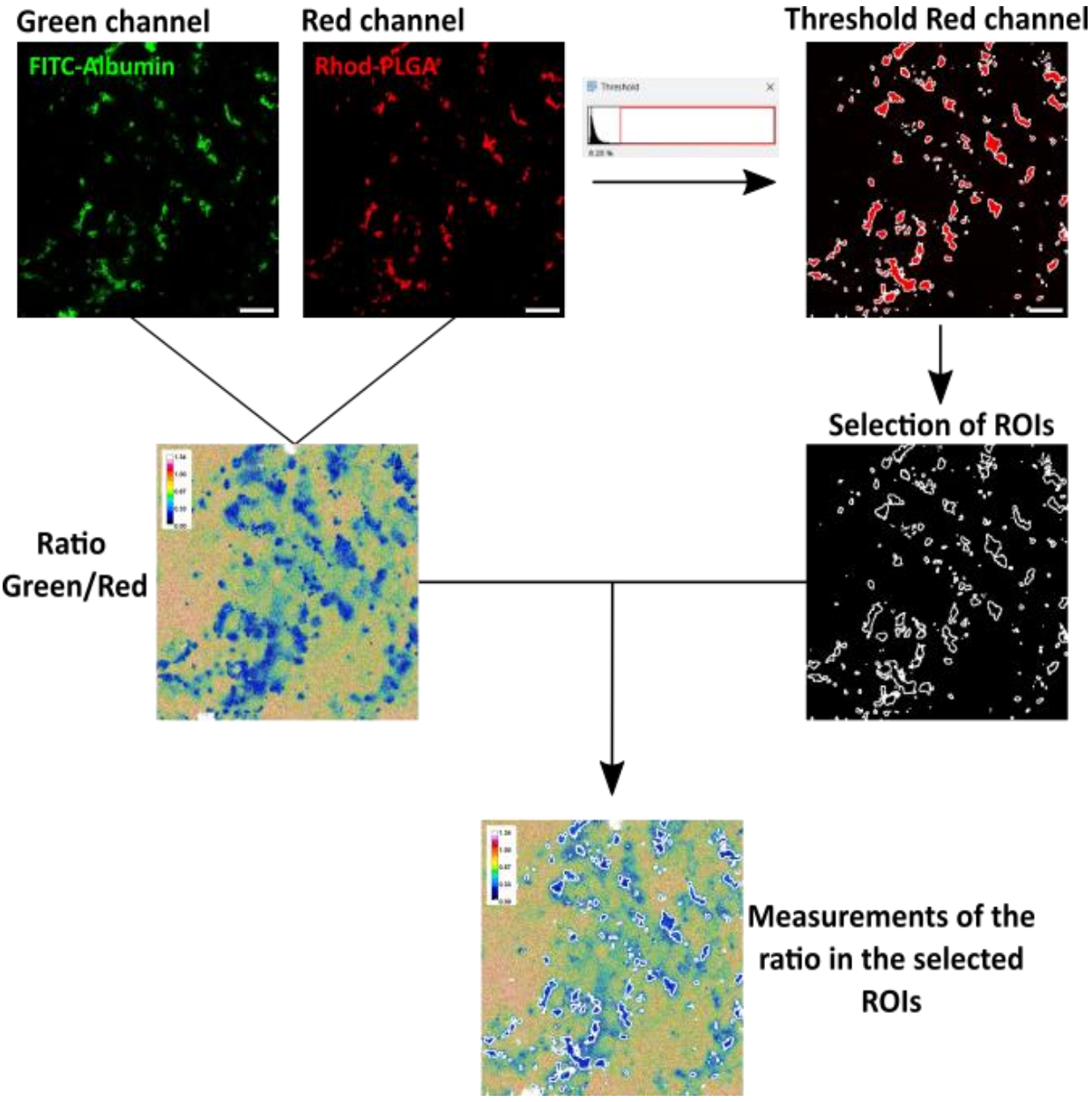

Figure 45. Ratio Measurement

4.3. Results and Discussions

4.3.1. Physicochemical Characteristics of Rhod-PLGA NPs

To quantify the amount of encapsulated albumin in the PLGA NPs and visualize both the PLGA particles and the loaded albumin with confocal microscopy during the incubation with living cells, both albumin and the PLGA were tagged with fluorescent dyes, FITC (fluorescein isothiocyanate) and Rhodamine B (Rhod), respectively. The FITC and the Rhodamine B dyes were chosen according to their distinct excitation and emission profiles. The albumin-FITC-loaded Rhod-PLGA NPs were prepared by combining the traditional homogenization method with the MSR-system. The resulting fluorescent NPs exhibited a mean particle size of 241 nm and a PDI value <0.2, indicating narrow particle size distribution in NP formation. The zeta potential of the NPs was measured as -30 mV after encapsulation. After lyophilization, the mean particle size slightly decreased to 220 nm. A comparison with blank Rhod-PLGA NPs, which had a mean particle size of 222 nm and a zeta potential of -32 mV, revealed that while the encapsulation of albumin-FITC led to a slight increase in particle size, the zeta potential values remained similar. This suggests that albumin-FITC was encapsulated into the NPs and did not alter the surface charge. After the lyophilization the mean particle size of Rhod-PLGA NPs slightly decreased to 206 nm.

The following assay results showed that albumin-FITC-loaded Rhod-PLGA NPs were prepared with an encapsulation efficiency as high as 84% and drug loading capacity of 2% (w/w). Fluorescent NPs were purified by CFF process using a 300 kDa MWCO membrane to sufficiently remove excess amounts of polymer, surfactant, and the free, non-encapsulated albumin-FITC. The hollow fiber membrane with 300 kDa MWCO was chosen as it provides optimal balance between the NP retention and removal of the smaller molecules such as PVA, PLGA and encapsulated substances. Moreover,

Dalwadi et al. previously showed membrane size with a 300 kDa MWCO sufficiently removed the excess PVA in large batches, and demonstrated a better performance than the ultracentrifugation, further supporting the choice of this membrane cut-off [149].

After lyophilization, the mean particle size slightly decreased to 220.9 nm. Overall, the lyophilization processes yielded a homogeneous lyophilization cake. To test NPs´ stability in the cell culture medium for further studies, the particle size measurements in EMEM cell culture medium as well as in water were compared. During the medium stability test for Rhod-PLGA NPs, the mean particle size in EMEM was measured as 188 nm while in water 199 nm. For albumin-FITC-loaded PLGA NPs, the mean particle size and PDI values in EMEM was measured as 167 nm and 0.24 while in water 196 nm and 0.02 were determined. The results showed that despite slight changes in the particle sizes and PDI values the NPs remained stable in the medium.

In order to characterize the co-localization of Albumin-FITC with Rhod-PLGA NPs, we calculated the Pearson's and Manders' coefficient from confocal images. We obtained a Pearson's coefficient value of 0.77 ± 0.016 and Manders' M1=0.84 ± 0.049 and M2=0.74 ± 0.019, where M1 is related to the degree of overlapping of albumin-FITC with the Rhod-PLGA NPs, and M2 the overlapping of Rhod-PLGA NPs to albumin-FITC. These values close to 1 indicate a high degree of co-localization (Figure 46)

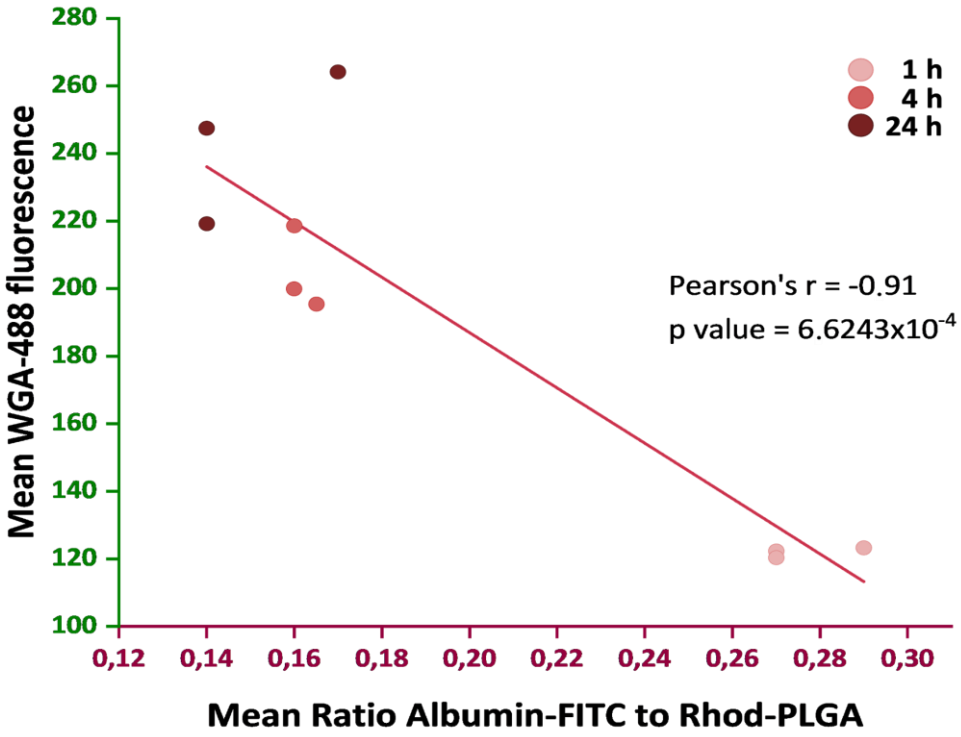

Figure 46. Correlation between the kinetics profiles. Pearson's correlation coefficient calculated between the measurements of the ratio cargo (albumin-FITC) Rhod-PLGA NPs (x axis), and the fluorescence derived from WGA-488 plasma membrane staining due to the cargo release from the NPs (y axis) at 1, 4 and 24 h.

4.3.2. Physicochemical Characteristics of WGA488-loaded PLGA NPs

The WGA488-loaded PLGA NPs were prepared to test the structural integrity of the protein cargo, and its recognition and binding features were retained after encapsulation by the emulsification/solvent procedure. WGA specifically binds N-acetyl-D-glucosamine and sialic acid, and its fluorescent form is commonly used to label the plasma l membrane [197]. The DLS measurements highlighted that the prepared WGA488-loaded PLGA NPs were narrowly distributed with a mean particle size of 441 nm, zeta potential value of -52 mV, and PDI value <0.2. After lyophilization,

the mean particle size slightly decreased to 425 nm. Overall, the lyophilization processes yielded a homogeneous lyophilization cake. The particle sizes were also measured in cell culture medium to ensure stability. During stability in medium studies, the mean particle size in cell culture medium was measured as 395 nm and for the dilution in water as 412 nm indicating particles were stable in the culture medium.

4.3.3. Biocompatibility of Albumin-loaded PLGA NPs

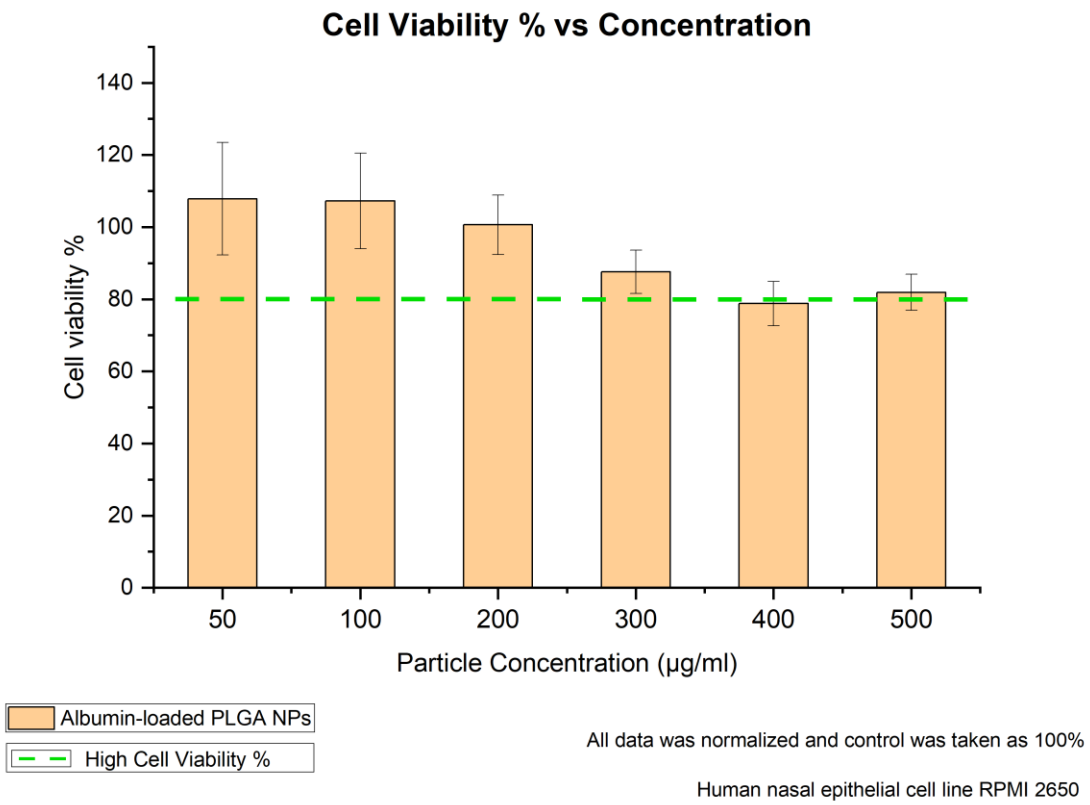

Figure 47. MTT assay results after 4 h of incubation for varying concentrations.

The viability of the treated non-fluorescent albumin-loaded PLGA NPs and untreated cells of the nasal mucosa were investigated using the assay. In literature, a study by Katsikari et al. showed significantly reduced viability above 500 µg/ml particle concentration for albumin-FITC-loaded PLGA NPs prepared with the traditional double emulsion method [198]. Therefore, our 4 h cell viability study further focused on the 50 to 500 µg/ml particle concentration range to evaluate the cellular response over a time

span meaningful for intranasal administration conditions. Figure 47 shows that the RPMI-2650 nasal cells exhibited high cell viability over the studied particle concentrations, indicating their convenience for nasal application. As also explained by Katsikari et al., a further increase in particle concentration could negatively affect cell viability due to several factors, including particle size and surface properties, in addition to polymer degradation products' interaction with the cell functions.

4.3.4. Live-cell imaging for localization and release studies with neuroblastoma cells and CLSM analysis

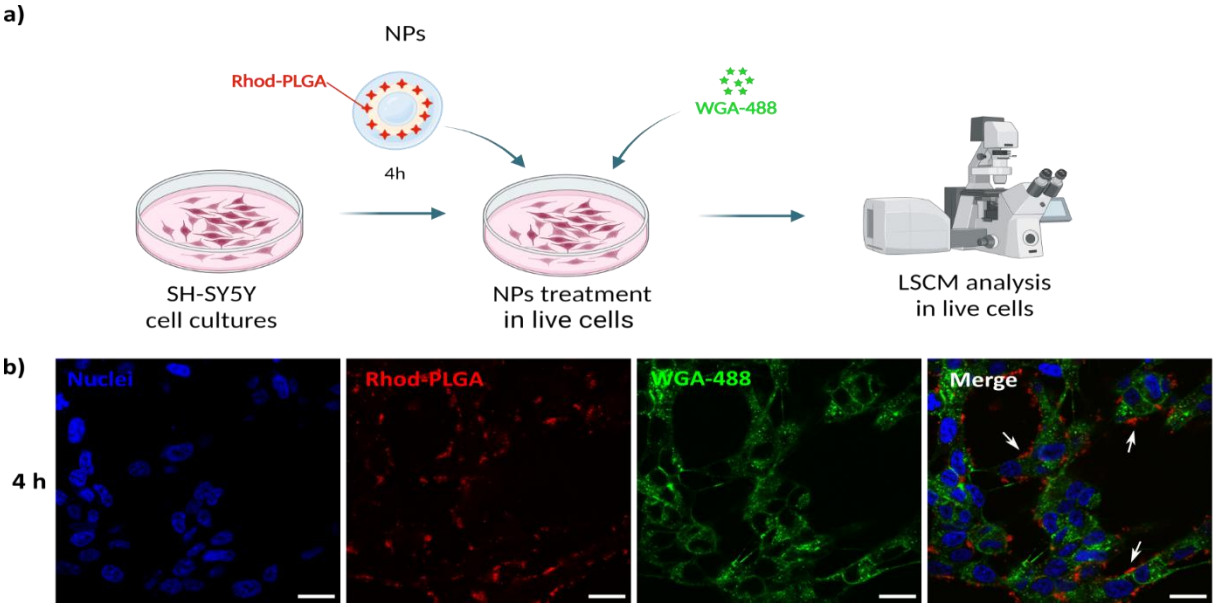

Figure 48. Rhod-PLGA NPs localization after 24 h of incubation. a) Live cells experiment workflow. Created with Biorender.com b) Confocal scanning microscope images of neuroblastoma SH-SY5Y cells incubated for 24 h with 100 µg/ml of NPs. Then with 5 µg/ml WGA-488 for 30 min to specifically label the plasma membrane. Red, Rhod-PLGA; green, WGA-488; blue, Hoechst. White arrows show the NPs` position. Scale bar 20 µm.

To follow the potential uptake of the NPs, human SH-SY5Y neuroblastoma cells were incubated with 100 µg/ml blank Rhod-PLGA NPs for 4 h and subsequently with WGA-488 to label the plasma membrane. The media was then washed and replaced before

image acquisition (Figure 48a). The NPs were present only in the extracellular space, juxtaposed to the cells, without any noticeable internalization taking place (Figure 48b). This result is further corroborated by analyzing the degree of co-localization between the Rhod-PLGA NPs and the staining with WGA-488. The obtained Pearson's coefficient value of 0.14 ± 0.008 and Manders' M1=0.032 ± 0.025 and M2=0.16 ± 0.069 indicate a very low degree of co-localization, supporting the lack of internalization of the Rhod-PLGA NPs.

The fact that these NPs were not internalized by the cells is a desirable characteristic for the possible N2B delivery application. If NPs can get already internalized initially by the cells of the olfactory epithelium, the efficient targeting of distant regions of the CNS would become challenging, especially for low doses of NPs. In some neurodegenerative disorders, the extracellular release is also a desired requirement (for instance, antibodies against Aβ oligomers for Alzheimer's disease, or against anti-remyelinating receptors in the case of multiple sclerosis [199,200]). In addition, the lack of internalization can reduce NPs toxicity and off-target effects, both things of crucial importance when delivering drugs to sensitive regions like the brain, leading to a safer and more focused delivery system for treating neurological disorders.

4.3.5. *In vitro* cumulative release profiles of PLGA NPs

The cumulative drug release studies showed that the percent drug-released increased over the first 4 h, followed by a slight increase up to 24 h. Between 24 h and 48 h, the cumulative release only slightly further increased until approx. 50% released drug, indicating that the release of albumin-FITC from the PLGA NPs continues beyond this time frame (Figure 49).

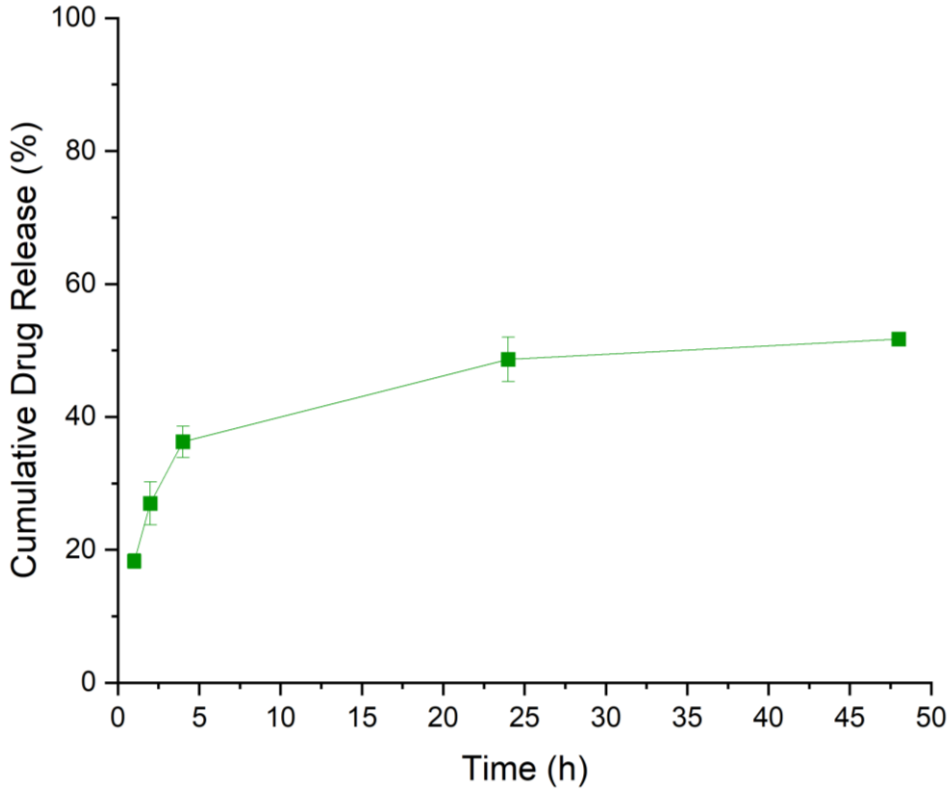

Figure 49. Cumulative release profile from the albumin-FITC loaded PLGA NPs

4.3.6. Release from Albumin-FITC-loaded PLGA NPs by CLSM Imaging

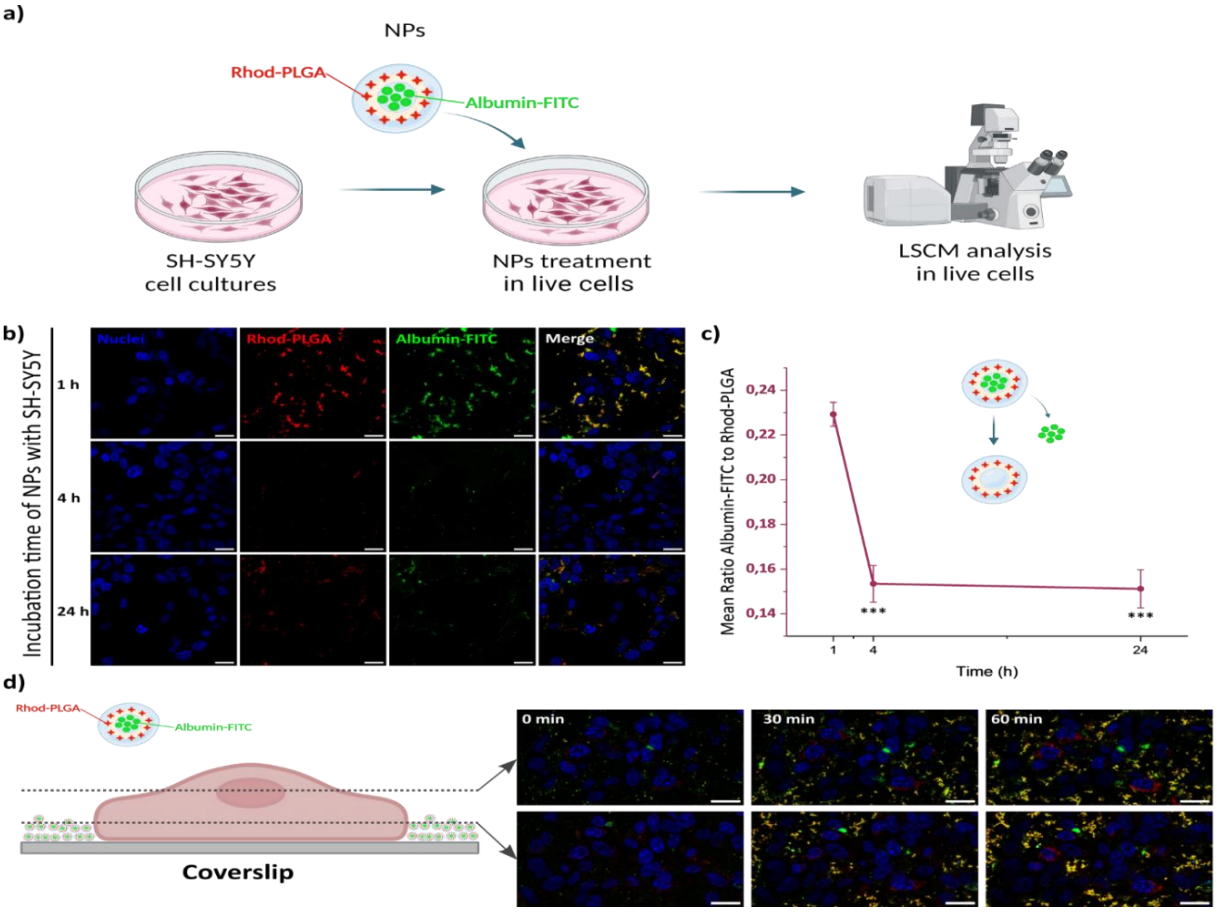

Figure 50. Albumin-FITC loaded Rhod-PLGA NPs localization and release. a) Live cells experiment workflow. Created with Biorender.com b) Confocal laser scanning microscope images of neuroblastoma SH-SY5Y cells incubated for different times with 100 µg/ml of NPs. c) Quantification of the ratio between the albumin-FITC (cargo-green channel) to Rhod-PLGA (NP-red channel) over 24 h. Error bars: SE; asterisks indicate significant differences between the measurements at 1 h using Kruskal-Wallis ANOVA test followed by Dunn's multiple comparison post hoc test (***p<0.001). d) Confocal images of SH-SY5Y cells incubated during 60 min with 100 µg/ml of NPs. Two different planes are shown, one upper plane (first row) and one lower plane closer to the coverslip (second row). The accumulation of NPs at the bottom of the coverslip increases overtime. Red, Rhod-PLGA; green, albumin-FITC; blue, Hoechst. Scale bar 20 µm.

The release kinetics were followed after incubation of neuroblastoma SH-SY5Y cells with 100 µg/ml albumin-FITC-loaded Rhod-PLGA NPs for 1, 4 and 24 h. The release of albumin-FITC from the Rhod-PLGA NPs occurs over 24 h, as indicated by the gradual decrease in the green channel intensity with respect to the red channel (and thus to a shift from yellow towards red in the overlay in Figure 50b and quantified as ratio between the two. While without washing albumin-FITC-loaded Rhod-PLGA NPs were increasingly accumulating with time at the bottom of the coverslip (Figure 50d), the amount of NPs shown in Figure 50b was dependent only on the degree of washing at the end of each incubation time. The ratio between the albumin-FITC and the Rhod-PLGA is however independent of the number of NPs present after the washes.

4.3.7. Effect of Loading on WGA-structure

To verify that the NP's loading procedure was not impairing the properties of the protein cargo, we verified that WGA488 previously loaded in the PLGA NPs could correctly stain the plasma membrane after release. SH-SY5Y cells were incubated with 100 µg/ml WGA488-loaded PLGA NPs for different incubation times. A continuous time-course experiment was performed during the first 60 min after addition of the NPs, acquiring confocal images of the same field of view every 5 min (Figure 51b). The staining of the plasma membrane following the release of WGA488 from the NPs started to be visible as shortly as 5 min from the beginning of the incubation progressive increase in the mean fluorescence intensity of the cell membrane was observed overtime (Figure 51c), in agreement with the release profiles observed *in vitro* and while incubated with cells (Figure 49and 50c).

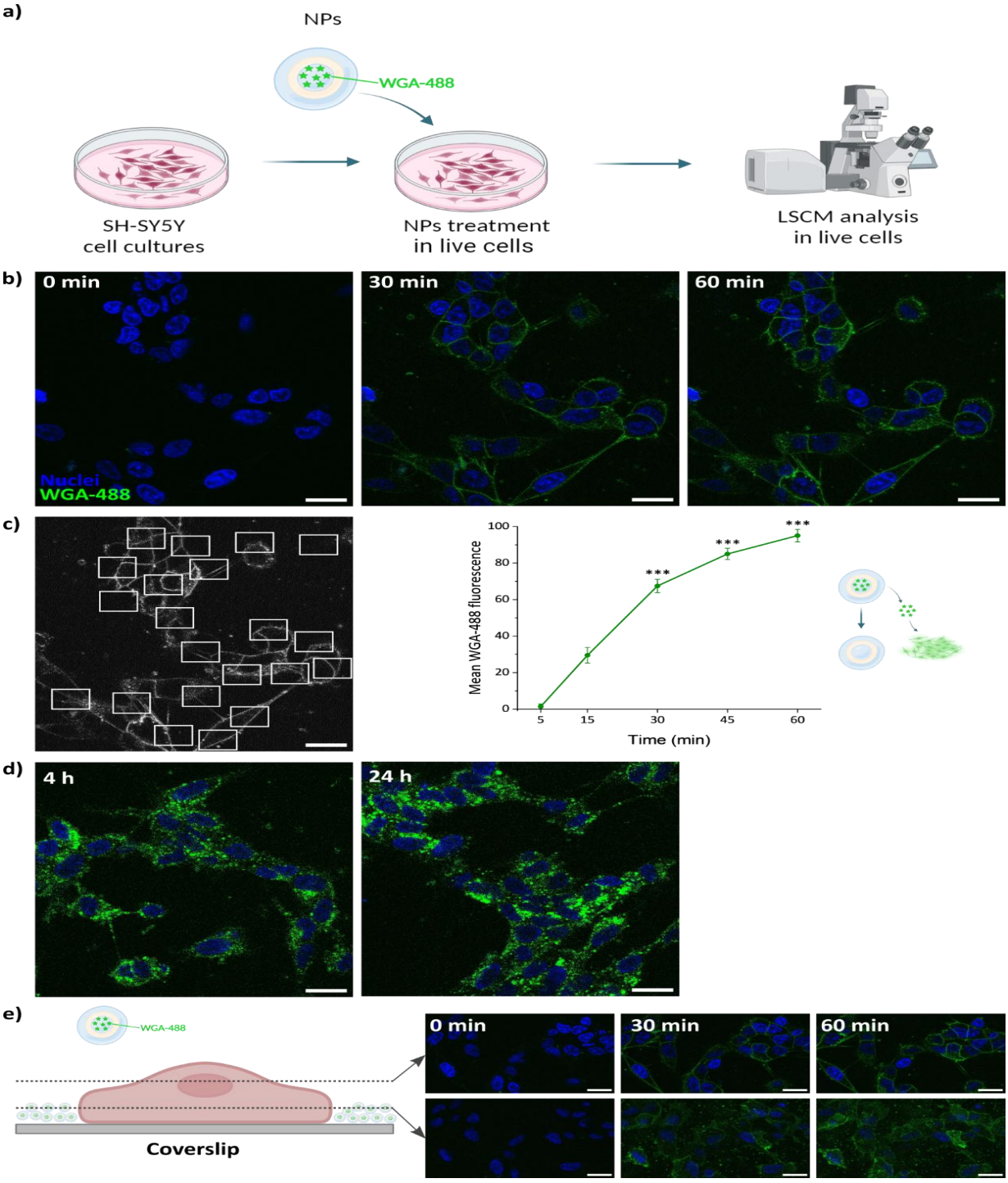

Figure 51. WGA488-loaded PLGA NPs release studies. a) Live cell experiment workflow. Created with Biorender.com b) Representative confocal microscopy images of neuroblastoma SH-SY5Y cells incubated over 60 min with 100 µg/ml of NPs. c) Representative image WGA488-loaded PLGA NPs release studies. a) Live cell experiment workflow. Created with Biorender.com b) Representative confocal microscopy images of neuroblastoma SH-SY5Y cells incubated during 60 min with 100 µg/ml of NPs. c) Representative image showing several

ROIs that were selected to measure mean fluorescence intensity of the WGA488 stained plasma membrane, and subsequent quantification over time; error bars: SE; asterisks indicate significant differences with respect to the measurement at 5 min using Kruskal-Wallis ANOVA test followed by Dunn's multiple comparison post hoc test (***p<0.001). d) Confocal images of SH-SY5Y cells incubated for 4 and 24 h with 100 µg/ml of NPs showing the localization of WGA488 inside the cells. e) Confocal images of SH-SY5Y cells incubated during 60 min with 100 µg/ml of NPs. Two different planes are shown, one median plane (first row) and one lower plane closer to the coverslip (second row). The accumulation of NPs at the bottom of the coverslip increases overtime. Green, WGA488; blue, Hoechst. Scale bar 20 µm.

These results confirm that the structure of the loaded protein was not compromised by the encapsulation process preserving its functionality. The same effect as mentioned before for the albumin-loaded NP can be observed here. The NPs sediment and accumulate on the bottom of the coverslip overtime (Figure 51e). At longer incubation times (4-24 h) internalization of the WGA488 and accumulation in the cytoplasm were observed as a consequence of the natural membrane trafficking and remodeling processes (endocytosis, pinocytosis etc.) occurring in the cells (Figure 51d). The total mean fluorescence intensity per cell kept increasing with time (Figure 52).

4.3.8. Release kinetics of the macromolecular loads

Overall, we used two different approaches to follow the NPs cargo release, one direct and one indirect. First, using the albumin-FITC-loaded Rhod-PLGA NPs, the ratio between albumin-FITC (cargo) and Rhod-PLGA (NPs) fluorescence intensities was measured over 24 h (Figure 51, Figure 52) The ratio decreased significantly over a period of 24 h (red line Figure 52), indicating that the amount of albumin-FITC in the NPs was gradually reduced. Second, using the WGA488 loaded PLGA NPs, the degree of fluorescent labeling of the plasma membrane derived from the WGA488

released from the PLGA NPs was measured. In this case the fluorescence intensity of the labelled membrane increased significantly over time (green line Figure 52). Notably, the kinetic profiles obtained with the two complementary approaches appear inversely correlated.

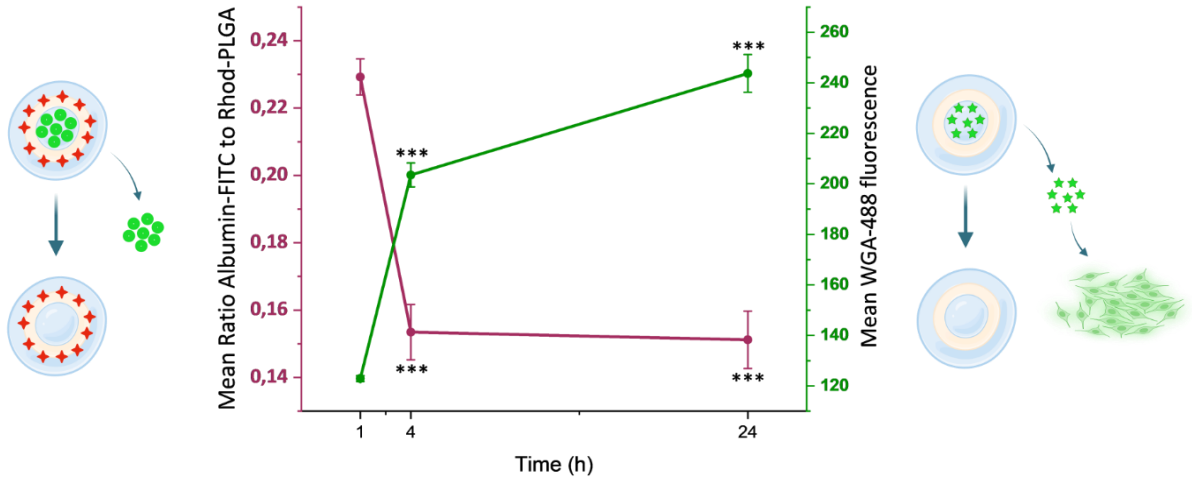

Figure 52. Comparison of the cargo release in 24 h. The plot shows two different measurements related to the cargo released from the NPs. On the left y axis is reported the ratio between albumin-FITC and Rhod-PLGA measured over time. On the right y axis is reported the mean fluorescence intensity values of the WGA488 released from the NPs and staining the cell membrane. Error bars, SE; asterisks indicate significant differences with the measurement at 1h using Kruskal-Wallis ANOVA test followed by Dunn's multiple comparison post hoc test (***p<0.001)

4.4. Conclusions

We have reported a novel continuous manufacturing method to prepare PLGA NPs. Our results showed that albumin-FITC-loaded fluorescent PLGA NPs were successfully prepared with the combination of traditional homogenization and novel continuous manufacturing methods, which offer scalability and robustness to manufacturing. The employment of a continuous manufacturing technology system in the second emulsification step of double emulsion preparation allowed scalability in the mixing of larger volumes of phases during the emulsification. The PLGA NPs prepared by double emulsions demonstrated high encapsulation efficiency and narrow particle size distribution, also indicating the strength of the manufacturing method. The prepared particles showed -sustained release properties, which is confirmed by both *in vitro* release studies. Moreover, the particles showed biocompatibility in two different cell lines, and they were not internalized by the cells, which is a desirable characteristic for N2B delivery. Our studies also showed WGA488 successfully encapsulated into the PLGA NPs by the double emulsion method, where narrow size distribution was also achieved. We demonstrated with WGA488-loaded PLGA NPs that the structure of the protein used as cargo is still functional after encapsulation and release of the NPs and that the release of the cargo is sustained over time in cell culture studies. The release profile of albumin-FITC from the PLGA NPs showed similar characteristics to the release profile of the WGA488. Overall, this study provides some insights into how this production technique can be advantageous for the development of DDS for N2B delivery.

5. Summary and Outlook

Providing effective treatments for CNS diseases is challenging from a pharmaceutical point of view even though there is an immense vascularization within the system, mainly because of the BBB. The BBB, a selective barrier does not allow most of the drugs to reach the brain to exert their therapeutic effect. Intranasal drug delivery, a non-invasive approach to bypass the BBB can be used as an alternative method to provide high patient compliance while delivering advanced therapeutics to the brain with high bioavailability when combined with the DDS. As a type of a DDS, polymeric NPs offer tailorable characteristics and good stability. They can be made of regulatory-approved materials which are proven to be biodegradable and biocompatible. PLGA is one of these FDA-approved polymers for therapeutic use and can be used in preparing polymeric NPs. Polymeric NPs can be prepared by different methods, including but not limited to nanoprecipitation and solvent/evaporation emulsification which can be also employed to prepare them as double emulsions. The double emulsion method especially stands out due to its ability to encapsulate hydrophilic molecules with high encapsulation efficiency.

When combined with advance therapeutics such as mAbs, which are also classified as large Mw hydrophilic substances, they can deliver the drugs to the brain with the N2B delivery. While the potential of polymeric NPs, especially PLGA NPs is obvious there is currently no PLGA NP based therapeutic option available on the market. This is since there is a need for continuous manufacturing technologies that facilitate the transfer of the formulation development of these particles from bench side to bedside.

Hence in this thesis, valuable information on preparing polymeric NPs loaded with different model-substances with bench top and with continuous manufacturing

techniques has been obtained. Later, biocompatibility, trafficking and release profiles of the derivatives of these NPs prepared by a continuous manufacturing technology were assessed to analyze their compatibility for the potential N2B delivery applications.

In a more detailed point of view, in the first chapter of the thesis, the SDS and MSR-systems have been investigated to prepare PLGA NPs as blank and as with loaded with model-substances. For the SDS, valuable information on design of the system for preparing PLGA NPs with different methods such nanoprecipitation and double emulsion techniques have been obtained.

The SDS could prepare blank and hydrophobic small Mw model substance-loaded (curcumin) PLGA NPs by the modified-nanoprecipitation method. To understand the effect of different factors on preparing these NPs, a process screening with blank NPs and a subsequent DoE design have been established. Particle size was affected significantly by the chosen disc speed, flow rate, and polymer concentration. Flow rate and the PLGA concentration also significantly affected the PDI, while droplet size and disc speed showed no significant effect. Moreover, evaluation of how a response of particle size, PDI, and EE% related to two continuous variables (factors) were evaluated with contour plots obtained by the DoE. The results showed that increasing the disc rotation speed decreased the particle size while decreasing the flow rate also decreased the particle size. For the PDI value, flow rate and polymer concentration both showed that increasing these factors decrease the PDI value. For EE%, it was shown that increasing the disc rotation speed increases the EE% while faster flow rates decrease the EE%.

In addition, the obtained NPs prepared with high encapsulation efficiency with this single-step production protocol and the set-up showing the compatibility of SDS for preparing scalable NPs, especially PLGA NPs. As an outlook, for different therapeutic

applications, and especially for CNS diseases, encapsulation of different hydrophobic substances could be incorporated to this strategy and their biocompatibility and uptake profiles with different cell-lines could be studied for biological applications.

The SDS was also investigated for preparing PLGA NPs as double emulsions within the system. During this process, bench top PLGA NPs as double emulsions were prepared, and the formulation was optimized and was compared with the NP productions trials with the SDS. To establish this, different designs of the system as well as configurations of the connectors have been studied to prepare both emulsification steps to prepare primary and double emulsions with the SDS. As a result, within the design space and the factors studied, microparticles were obtained and preparing monodispersed NPs were not successful. In the future, changes in the set-up as well as protocol and the design space could also lead to preparing these NPs as double emulsions by the SDS which could also lead to encapsulation of advanced hydrophilic molecules like mAbs.

To achieve this goal for preparing PLGA NPs as double emulsions for encapsulation small and large Mw hydrophilic substances, a proof-of concept study was established with the MSR-system, another continuous manufacturing technology was studied. After the first trials of preparing both primary emulsion and secondary emulsion within the system, later the focus was given to prepare primary emulsion by a homogenizer and the secondary emulsion by the MSR-system to facilitate the stability of the primary emulsion. This also provided with additional advantages to the scalability as the secondary emulsification step generally involves larger volumes of phases, and therefore a bottleneck in the scalability of the double emulsion production.

Firstly, a small Mw drug, Ciprofloxacin HCl was encapsulated with the MSR-system with high encapsulation efficiency showing the feasibility of the system on

encapsulation such molecule with high encapsulation efficiency which is considered challenging. Later, PLGA NPs loaded with albumin was prepared with the MSR-system and compared with the NPs prepared by the traditional homogenization methods showing that the MSR-system not only provided also high encapsulation efficiency for these NPs but also decreased the NP size. These also provided a chance to study the proof-of concept of potential N2B delivery of large Mw substances prepared by a scalable method. Therefore, fluorescent derivates of these NPs were also prepared and demonstrated high encapsulation efficiency as well as narrow particle size distribution. Moreover, particles were shown to have sustained release profiles. They also showed biocompatibility in different application-relevant cell-lines. In these *in vitro* test systems also an important parameter the uptake into the cell was investigated and no internalization was observed, showing the feasibility of the application to N2B delivery where crossing the cell barrier is the target. The studies were taken one step further, and another functional protein (WGA488) was encapsulated into the PLGA NPs by the double emulsion method demonstrated that the encapsulated WGA488 was functional and showed sustained release. As an outlook, the promising results obtained within the scope of this thesis further be supported by viability studies within different cell-lines. Later, their efficacy and safety could be evaluated within the *in vitro*, *ex vivo* and *in vivo* experimental models. As an example to these, for *in vitro* models, RPMI 2650 cell line, a human cell line used for nasal drug transport studies, a bovine nasal mucosa can be used for nasal permeation and mucoadhesion studies, and *in vivo* studies based on mice can support pharmacokinetics and pharmacodynamics aspects of the delivery of the drug with the DDS.

6. Annexes

6.1. References

[1] H.J. Chiel, R.D. Beer, The brain has a body: adaptive behavior emerges from interactions of nervous system, body and environment, Trends Neurosci. 20 (1997) 553–557. https://doi.org/10.1016/S0166-2236(97)01149-1.

[2] J. Xu, C. Ma, M. Hua, J. Li, Z. Xiang, J. Wu, CNS and CNS diseases in relation to their immune system, Front. Immunol. 13 (2022). https://doi.org/10.3389/fimmu.2022.1063928.

[3] B. Arnone, X. Zhao, Z. Zou, G. Qin, M. Cheng, Chapter 11 - Diagnostic and Prognostic Applications of MicroRNA-Abundant Circulating Exosomes, in: Y. Tang, B. Dawn (Eds.), Mesenchymal Stem Cell Deriv. Exosomes, Academic Press, Boston, 2015: pp. 223–256. https://doi.org/10.1016/B978-0-12-800164-6.00011-3.

[4] T. Chitnis, H.L. Weiner, CNS inflammation and neurodegeneration, J. Clin. Invest. 127 (2017). https://doi.org/10.1172/JCI90609.

[5] B.N. Dugger, D.W. Dickson, Pathology of Neurodegenerative Diseases, Cold Spring Harb. Perspect. Biol. 9 (2017) a028035. https://doi.org/10.1101/cshperspect.a028035.

[6] D.C. Bergen, D. Silberberg, Nervous system disorders: A global epidemic, Arch. Neurol. 59 (2002) 1194–1196. https://doi.org/10.1001/archneur.59.7.1194.

[7] C. Ding, Y. Wu, X. Chen, Y. Chen, Z. Wu, Z. Lin, D. Kang, W. Fang, F. Chen, Global, regional, and national burden and attributable risk factors of neurological disorders: The Global Burden of Disease study 1990–2019, Front. Public Health 10 (2022). https://doi.org/10.3389/fpubh.2022.952161.

[8] M. DiLuca, J. Olesen, The cost of brain diseases: A burden or a challenge?, Neuron 82 (2014) 1205–1208. https://doi.org/10.1016/j.neuron.2014.05.044.

[9] S. Siuly, Y. Zhang, Medical Big Data: Neurological Diseases Diagnosis Through Medical Data Analysis, Data Sci. Eng. 1 (2016) 54–64. https://doi.org/10.1007/s41019-016-0011-3.

[10] M.T. Wallin, W.J. Culpepper, E. Nichols, Z.A. Bhutta, T.T. Gebrehiwot, S.I. Hay, I.A. Khalil, K.J. Krohn, X. Liang, M. Naghavi, A.H. Mokdad, M.R. Nixon, R.C. Reiner, B. Sartorius, M. Smith, R. Topor-Madry, A. Werdecker, T. Vos, V.L. Feigin, C.J.L. Murray, Global, regional, and national burden of multiple sclerosis 1990–2016: a systematic analysis for the Global Burden of Disease Study 2016, Lancet Neurol. 18 (2019) 269–285. https://doi.org/10.1016/S1474-4422(18)30443-5.

[11] S. Bhunia, N. Kolishetti, A. Vashist, A. Yndart Arias, D. Brooks, M. Nair, Drug Delivery to the Brain: Recent Advances and Unmet Challenges, Pharmaceutics 15 (2023) 2658. https://doi.org/10.3390/pharmaceutics15122658.

[12] O.D. Howes, M.A. Mehta, Challenges in CNS drug development and the role of imaging, Psychopharmacology (Berl.) 238 (2021) 1229–1230. https://doi.org/10.1007/s00213-021-05838-3.

[13] J.J. Danon, T.A. Reekie, M. Kassiou, Challenges and Opportunities in Central Nervous System Drug Discovery, Trends Chem. 1 (2019) 612–624. https://doi.org/10.1016/j.trechm.2019.04.009.

[14] A.H. Meyer, T.M. Feldsien, M. Mezler, C. Untucht, R. Venugopalan, D.R. Lefebvre, Novel Developments to Enable Treatment of CNS Diseases with Targeted Drug Delivery, Pharmaceutics 15 (2023) 1100. https://doi.org/10.3390/pharmaceutics15041100.

[15] O. Jung, A. Thomas, S.R. Burks, M.L. Dustin, J.A. Frank, M. Ferrer, E. Stride, Neuroinflammation associated with ultrasound-mediated permeabilization of the blood–brain barrier, Trends Neurosci. 45 (2022) 459–470. https://doi.org/10.1016/j.tins.2022.03.003.
[16] W.A. Banks, From blood-brain barrier to blood-brain interface: New opportunities for CNS drug delivery, Nat. Rev. Drug Discov. 15 (2016) 275–292. https://doi.org/10.1038/nrd.2015.21.
[17] C. Greene, N. Hanley, M. Campbell, Claudin-5: Gatekeeper of neurological function, Fluids Barriers CNS 16 (2019). https://doi.org/10.1186/s12987-019-0123-z.
[18] H.C. Bauer, I.A. Krizbai, H. Bauer, A. Traweger, "You shall not pass"-tight junctions of the blood brain barrier, Front. Neurosci. 8 (2014). https://doi.org/10.3389/fnins.2014.00392.
[19] H. Kadry, B. Noorani, L. Cucullo, A blood–brain barrier overview on structure, function, impairment, and biomarkers of integrity, Fluids Barriers CNS 17 (2020). https://doi.org/10.1186/s12987-020-00230-3.
[20] R. Cabezas, M. Ávila, J. Gonzalez, R.S. El-Bachá, E. Báez, L.M. García-Segura, J.C. Jurado Coronel, F. Capani, G.P. Cardona-Gomez, G.E. Barreto, Astrocytic modulation of blood brain barrier: perspectives on Parkinson's disease, Front. Cell. Neurosci. 8 (2014) 211. https://doi.org/10.3389/fncel.2014.00211.
[21] E.G. Knox, M.R. Aburto, G. Clarke, J.F. Cryan, C.M. O'Driscoll, The blood-brain barrier in aging and neurodegeneration, Mol. Psychiatry 27 (2022) 2659–2673. https://doi.org/10.1038/s41380-022-01511-z.
[22] W.M. Pardridge, The Blood-Brain Barrier: Bottleneck in Brain Drug Development, NeuroRx 2 (2005) 3–14. https://doi.org/10.1602/neurorx.2.1.3.
[23] R.I. Teleanu, M.D. Preda, A.-G. Niculescu, O. Vladâcenco, C.I. Radu, A.M. Grumezescu, D.M. Teleanu, Current Strategies to Enhance Delivery of Drugs across the Blood–Brain Barrier, Pharmaceutics 14 (2022) 987. https://doi.org/10.3390/pharmaceutics14050987.
[24] M.J. Mitchell, M.M. Billingsley, R.M. Haley, M.E. Wechsler, N.A. Peppas, R. Langer, Engineering precision nanoparticles for drug delivery, Nat. Rev. Drug Discov. 20 (2021) 101–124. https://doi.org/10.1038/s41573-020-0090-8.
[25] P. Ghasemiyeh, S. Mohammadi-Samani, Solid lipid nanoparticles and nanostructured lipid carriers as novel drug delivery systems: applications, advantages and disadvantages, Res. Pharm. Sci. 13 (2018) 288–303. https://doi.org/10.4103/1735-5362.235156.
[26] C.-T. Lu, Y.-Z. Zhao, H.L. Wong, J. Cai, L. Peng, X.-Q. Tian, Current approaches to enhance CNS delivery of drugs across the brain barriers, Int. J. Nanomedicine 9 (2014) 2241–2257. https://doi.org/10.2147/IJN.S61288.
[27] M.A. Beach, U. Nayanathara, Y. Gao, C. Zhang, Y. Xiong, Y. Wang, G.K. Such, Polymeric Nanoparticles for Drug Delivery, Chem. Rev. 124 (2024) 5505–5616. https://doi.org/10.1021/acs.chemrev.3c00705.
[28] H.O. Alsaab, F.D. Alharbi, A.S. Alhibs, N.B. Alanazi, B.Y. Alshehri, M.A. Saleh, F.S. Alshehri, M.A. Algarni, T. Almugaiteeb, M.N. Uddin, R.M. Alzhrani, PLGA-Based Nanomedicine: History of Advancement and Development in Clinical Applications of Multiple Diseases, Pharmaceutics 14 (2022) 2728. https://doi.org/10.3390/pharmaceutics14122728.
[29] X. Guo, X. Zuo, Z. Zhou, Y. Gu, H. Zheng, X. Wang, G. Wang, C. Xu, F. Wang, PLGA-Based Micro/Nanoparticles: An Overview of Their Applications in Respiratory Diseases, Int. J. Mol. Sci. 24 (2023) 4333. https://doi.org/10.3390/ijms24054333.

[30] C. Vasile, Chapter 1 - Polymeric Nanomaterials: Recent Developments, Properties and Medical Applications, in: C. Vasile (Ed.), Polym. Nanomater. Nanotherapeutics, Elsevier, 2019: pp. 1–66. https://doi.org/10.1016/B978-0-12-813932-5.00001-7.
[31] F. Wang, C. Li, J. Cheng, Z. Yuan, Recent Advances on Inorganic Nanoparticle-Based Cancer Therapeutic Agents, Int. J. Environ. Res. Public. Health 13 (2016) 1182. https://doi.org/10.3390/ijerph13121182.
[32] G. Sanità, B. Carrese, A. Lamberti, Nanoparticle Surface Functionalization: How to Improve Biocompatibility and Cellular Internalization, Front. Mol. Biosci. 7 (2020) 587012. https://doi.org/10.3389/fmolb.2020.587012.
[33] W.M. Pardridge, A Historical Review of Brain Drug Delivery, Pharmaceutics 14 (2022) 1283. https://doi.org/10.3390/pharmaceutics14061283.
[34] S.M. Lombardo, M. Schneider, A.E. Türeli, N.G. Türeli, Key for crossing the BBB with nanoparticles: The rational design, Beilstein J. Nanotechnol. 11 (2020) 886–883. https://doi.org/10.3762/BJNANO.11.72.
[35] S.K. Niazi, Non-Invasive Drug Delivery across the Blood–Brain Barrier: A Prospective Analysis, Pharmaceutics 15 (2023) 2599. https://doi.org/10.3390/pharmaceutics15112599.
[36] A. Burgess, K. Shah, O. Hough, K. Hynynen, Focused ultrasound-mediated drug delivery through the blood-brain barrier, Expert Rev. Neurother. 15 (2015) 477–491. https://doi.org/10.1586/14737175.2015.1028369.
[37] J.T. Trevino, R.C. Quispe, F. Khan, V. Novak, Non-Invasive Strategies for Nose-to-Brain Drug Delivery., J. Clin. Trials 10 (2020).
[38] J. Wang, Z. Li, M. Pan, M. Fiaz, Y. Hao, Y. Yan, L. Sun, F. Yan, Ultrasound-mediated blood–brain barrier opening: An effective drug delivery system for theranostics of brain diseases, Adv. Drug Deliv. Rev. 190 (2022) 114539. https://doi.org/10.1016/j.addr.2022.114539.
[39] E. Perolina, S. Meissner, B. Raos, B. Harland, S. Thakur, D. Svirskis, Translating ultrasound-mediated drug delivery technologies for CNS applications, Adv. Drug Deliv. Rev. 208 (2024) 115274. https://doi.org/10.1016/j.addr.2024.115274.
[40] S. Gänger, K. Schindowski, Tailoring formulations for intranasal nose-to-brain delivery: A review on architecture, physico-chemical characteristics and mucociliary clearance of the nasal olfactory mucosa, Pharmaceutics 10 (2018) 116. https://doi.org/10.3390/pharmaceutics10030116.
[41] Q. Liu, Q. Zhang, 10 - Nanoparticle systems for nose-to-brain delivery, in: H. Gao, X. Gao (Eds.), Brain Target. Drug Deliv. Syst., Academic Press, 2019: pp. 219–239. https://doi.org/10.1016/B978-0-12-814001-7.00010-X.
[42] Z. Wang, G. Xiong, W.C. Tsang, A.G. Schätzlein, I.F. Uchegbu, Nose-to-Brain Delivery, J. Pharmacol. Exp. Ther. 370 (2019) 593–601. https://doi.org/10.1124/jpet.119.258152.
[43] S.-H. Jeong, J.-H. Jang, Y.-B. Lee, Drug delivery to the brain via the nasal route of administration: exploration of key targets and major consideration factors, J. Pharm. Investig. 53 (2023) 119–152. https://doi.org/10.1007/s40005-022-00589-5.
[44] A. Alu, L. Chen, H. Lei, Y. Wei, X. Tian, X. Wei, Intranasal COVID-19 vaccines: From bench to bed, eBioMedicine 76 (2022). https://doi.org/10.1016/j.ebiom.2022.103841.
[45] Y. Ozsoy, S. Güngör, Nasal route: an alternative approach for antiemetic drug delivery, Expert Opin. Drug Deliv. 8 (2011) 1439–1453. https://doi.org/10.1517/17425247.2011.607437.

[46] D. Kim, Y.H. Kim, S. Kwon, Enhanced nasal drug delivery efficiency by increasing mechanical loading using hypergravity, Sci. Rep. 8 (2018) 168. https://doi.org/10.1038/s41598-017-18561-x.
[47] P. Arora, S. Sharma, S. Garg, Permeability issues in nasal drug delivery, Drug Discov. Today 7 (2002) 967–975. https://doi.org/10.1016/S1359-6446(02)02452-2.
[48] P. Henriques, A. Fortuna, S. Doktorovová, Spray dried powders for nasal delivery: Process and formulation considerations, Eur. J. Pharm. Biopharm. 176 (2022) 1–20. https://doi.org/10.1016/j.ejpb.2022.05.002.
[49] S. Grassin-Delyle, A. Buenestado, E. Naline, C. Faisy, S. Blouquit-Laye, L.-J. Couderc, M. Le Guen, M. Fischler, P. Devillier, Intranasal drug delivery: An efficient and non-invasive route for systemic administration: Focus on opioids, Pharmacol. Ther. 134 (2012) 366–379. https://doi.org/10.1016/j.pharmthera.2012.03.003.
[50] L.-A. Keller, O. Merkel, A. Popp, Intranasal drug delivery: opportunities and toxicologic challenges during drug development, Drug Deliv. Transl. Res. 12 (2022) 735–757. https://doi.org/10.1007/s13346-020-00891-5.
[51] M.L. Formica, D.A. Real, M.L. Picchio, E. Catlin, R.F. Donnelly, A.J. Paredes, On a highway to the brain: A review on nose-to-brain drug delivery using nanoparticles, Appl. Mater. Today 29 (2022) 101631. https://doi.org/10.1016/j.apmt.2022.101631.
[52] R. Boyuklieva, B. Pilicheva, Micro- and Nanosized Carriers for Nose-to-Brain Drug Delivery in Neurodegenerative Disorders, Biomedicines 10 (2022) 1706. https://doi.org/10.3390/biomedicines10071706.
[53] Q. Huang, Y. Chen, W. Zhang, X. Xia, H. Li, M. Qin, H. Gao, Nanotechnology for enhanced nose-to-brain drug delivery in treating neurological diseases, J. Controlled Release 366 (2024) 519–534. https://doi.org/10.1016/j.jconrel.2023.12.054.
[54] R. Awad, A. Avital, A. Sosnik, Polymeric nanocarriers for nose-to-brain drug delivery in neurodegenerative diseases and neurodevelopmental disorders, Acta Pharm. Sin. B 13 (2023) 1866–1886. https://doi.org/10.1016/j.apsb.2022.07.003.
[55] N. Montegiove, E. Calzoni, C. Emiliani, A. Cesaretti, Biopolymer Nanoparticles for Nose-to-Brain Drug Delivery: A New Promising Approach for the Treatment of Neurological Diseases, J. Funct. Biomater. 13 (2022) 125. https://doi.org/10.3390/jfb13030125.
[56] C.P. Costa, J.N. Moreira, J.M. Sousa Lobo, A.C. Silva, Intranasal delivery of nanostructured lipid carriers, solid lipid nanoparticles and nanoemulsions: A current overview of in vivo studies, Acta Pharm. Sin. B 11 (2021) 925–940. https://doi.org/10.1016/j.apsb.2021.02.012.
[57] M. Chaturvedi, M. Kumar, K. Pathak, A review on mucoadhesive polymer used in nasal drug delivery system, J. Adv. Pharm. Technol. Res. 2 (2011) 215–222. https://doi.org/10.4103/2231-4040.90876.
[58] K. Zhao, Y. Xie, X. Lin, W. Xu, The Mucoadhesive Nanoparticle-Based Delivery System in the Development of Mucosal Vaccines, Int. J. Nanomedicine 17 (2022) 4579–4598. https://doi.org/10.2147/IJN.S359118.
[59] D. Lee, T. Minko, Nanotherapeutics for nose-to-brain drug delivery: An approach to bypass the blood brain barrier, Pharmaceutics 13 (2021) 2049. https://doi.org/10.3390/pharmaceutics13122049.
[60] S.U. Islam, A. Shehzad, M.B. Ahmed, Y.S. Lee, Intranasal Delivery of Nanoformulations: A Potential Way of Treatment for Neurological Disorders, Molecules 25 (2020) 1929. https://doi.org/10.3390/molecules25081929.

[61] D.H. Jo, J.H. Kim, T.G. Lee, J.H. Kim, Size, surface charge, and shape determine therapeutic effects of nanoparticles on brain and retinal diseases, Nanomedicine Nanotechnol. Biol. Med. 11 (2015) 1603–1611. https://doi.org/10.1016/j.nano.2015.04.015.
[62] Y. Liu, J. Tan, A. Thomas, D. Ou-Yang, V.R. Muzykantov, The shape of things to come: importance of design in nanotechnology for drug delivery, Ther. Deliv. 3 (2012) 181–194. https://doi.org/10.4155/tde.11.156.
[63] M. Handa, A. Singh, D. Bisht, P. Kesharwani, R. Shukla, Potential of particle size less than 15 nm via olfactory region for direct brain delivery via intranasal route, Health Sci. Rev. 4 (2022) 100038. https://doi.org/10.1016/j.hsr.2022.100038.
[64] C.Y.J. Wong, A. Baldelli, H. Gholizadeh, H. Oguzlu, Y. Guo, H. Xin Ong, A.P. Rodriguez, G. Singhera, A. Thamboo, A. Singh, A. Pratap-Singh, D. Traini, Engineered dry powders for the nose-to-brain delivery of transforming growth factor-beta, Eur. J. Pharm. Biopharm. 189 (2023) 202–211. https://doi.org/10.1016/j.ejpb.2023.06.015.
[65] J. Koo, C. Lim, K.T. Oh, Recent Advances in Intranasal Administration for Brain-Targeting Delivery: A Comprehensive Review of Lipid-Based Nanoparticles and Stimuli-Responsive Gel Formulations, Int. J. Nanomedicine (2024) 1767–1807. https://doi.org/10.2147/IJN.S439181.
[66] S.-S. Hong, K.T. Oh, H.-G. Choi, S.-J. Lim, Liposomal Formulations for Nose-to-Brain Delivery: Recent Advances and Future Perspectives, Pharmaceutics 11 (2019) 540. https://doi.org/10.3390/pharmaceutics11100540.
[67] J. Rejman, V. Oberle, I.S. Zuhorn, D. Hoekstra, Size-dependent internalization of particles via the pathways of clathrin- and caveolae-mediated endocytosis, Biochem. J. 377 (2004) 159–169. https://doi.org/10.1042/BJ20031253.
[68] G. Rassu, E. Soddu, M. Cossu, E. Gavini, P. Giunchedi, A. Dalpiaz, Particulate formulations based on chitosan for nose-to-brain delivery of drugs. A review, J. Drug Deliv. Sci. Technol. 32 (2016) 77–87. https://doi.org/10.1016/j.jddst.2015.05.002.
[69] A. Maaz, I.S. Blagbrough, P.A. De Bank, In Vitro Evaluation of Nasal Aerosol Depositions: An Insight for Direct Nose to Brain Drug Delivery, Pharmaceutics 13 (2021) 1079. https://doi.org/10.3390/pharmaceutics13071079.
[70] J.L. Sobiesk, S. Munakomi, Anatomy, Head and Neck, Nasal Cavity, in: StatPearls, StatPearls Publishing, Treasure Island (FL), 2023. http://www.ncbi.nlm.nih.gov/books/NBK544232/ (accessed August 22, 2023).
[71] C.R. Chen, C. Kachramanoglou, D. Li, P. Andrews, D. Choi, Anatomy and Cellular Constituents of the Human Olfactory Mucosa: A Review, J. Neurol. Surg. Part B Skull Base 75 (2014) 293–300. https://doi.org/10.1055/s-0033-1361837.
[72] C. Moon, S. Jun Yoo, H. Soo Han, Smell, in: M.J. Aminoff, R.B. Daroff (Eds.), Encycl. Neurol. Sci. Second Ed., Academic Press, Oxford, 2014: pp. 216–220. https://doi.org/10.1016/B978-0-12-385157-4.00072-5.
[73] C.K. Lankford, J.G. Laird, S.M. Inamdar, S.A. Baker, A Comparison of the Primary Sensory Neurons Used in Olfaction and Vision, Front. Cell. Neurosci. 14 (2020). https://www.frontiersin.org/articles/10.3389/fncel.2020.595523.
[74] C. Huart, P. Rombaux, T. Hummel, Plasticity of the Human Olfactory System: The Olfactory Bulb, Molecules 18 (2013) 11586–11600. https://doi.org/10.3390/molecules180911586.
[75] T. Shirai, D. Takase, J. Yokoyama, K. Nakanishi, C. Uehara, N. Saito, A. Kato-Namba, K. Yoshikawa, Functions of human olfactory mucus and age-dependent changes, Sci. Rep. 13 (2023) 971. https://doi.org/10.1038/s41598-023-27937-1.

[76] C. Crespo, T. Liberia, J.M. Blasco-Ibáñez, J. Nácher, E. Varea, Cranial Pair I: The Olfactory Nerve, Anat. Rec. 302 (2019) 405–427. https://doi.org/10.1002/ar.23816.
[77] E. Ruysseveldt, K. Martens, B. Steelant, Airway Basal Cells, Protectors of Epithelial Walls in Health and Respiratory Diseases, Front. Allergy 2 (2021). https://www.frontiersin.org/articles/10.3389/falgy.2021.787128.
[78] T. Huff, L.J. Weisbrod, D.T. Daly, Neuroanatomy, Cranial Nerve 5 (Trigeminal), in: StatPearls, StatPearls Publishing, Treasure Island (FL), 2023. http://www.ncbi.nlm.nih.gov/books/NBK482283/ (accessed August 29, 2023).
[79] Y. Li, C. Wang, S. Zong, J. Qi, X. Dong, W. Zhao, W. Wu, Q. Fu, Y. Lu, Z. Chen, The Trigeminal Pathway Dominates the Nose-to-Brain Transportation of Intact Polymeric Nanoparticles: Evidence from Aggregation-Caused Quenching Probes, J. Biomed. Nanotechnol. 15 (2019) 686–702. https://doi.org/10.1166/jbn.2019.2724.
[80] L. Illum, Is nose-to-brain transport of drugs in man a reality?, J. Pharm. Pharmacol. 56 (2004) 3–17. https://doi.org/10.1211/0022357022539.
[81] T. Tashima, Shortcut Approaches to Substance Delivery into the Brain Based on Intranasal Administration Using Nanodelivery Strategies for Insulin, Molecules 25 (2020) 5188. https://doi.org/10.3390/molecules25215188.
[82] F. Erdő, L.A. Bors, D. Farkas, Á. Bajza, S. Gizurarson, Evaluation of intranasal delivery route of drug administration for brain targeting, Brain Res. Bull. 143 (2018) 155–170. https://doi.org/10.1016/j.brainresbull.2018.10.009.
[83] R.M. Lu, Y.C. Hwang, I.J. Liu, C.C. Lee, H.Z. Tsai, H.J. Li, H.C. Wu, Development of therapeutic antibodies for the treatment of diseases, J. Biomed. Sci. 27 (2020). https://doi.org/10.1186/s12929-019-0592-z.
[84] K. Tsumoto, Y. Isozaki, H. Yagami, M. Tomita, Future perspectives of therapeutic monoclonal antibodies, Immunotherapy 11 (2019). https://doi.org/10.2217/imt-2018-0130.
[85] B. Dealmakers, A view into the central nervous system disorders market, Biopharma Deal. (2020). https://doi.org/10.1038/d43747-020-01119-8.
[86] K. Wojtunik-Kulesza, M. Rudkowska, A. Orzeł-Sajdłowska, Aducanumab—Hope or Disappointment for Alzheimer's Disease, Int. J. Mol. Sci. 24 (2023) 4367. https://doi.org/10.3390/ijms24054367.
[87] U. Julku, M. Xiong, E. Wik, S. Roshanbin, D. Sehlin, S. Syvänen, Brain pharmacokinetics of mono- and bispecific amyloid-β antibodies in wild-type and Alzheimer's disease mice measured by high cut-off microdialysis, Fluids Barriers CNS 19 (2022) 99. https://doi.org/10.1186/s12987-022-00398-w.
[88] W.M. Pardridge, Treatment of Alzheimer's Disease and Blood–Brain Barrier Drug Delivery, Pharmaceuticals 13 (2020) 394. https://doi.org/10.3390/ph13110394.
[89] A.R. Rezai, P.-F. D'Haese, V. Finomore, J. Carpenter, M. Ranjan, K. Wilhelmsen, R.I. Mehta, P. Wang, U. Najib, C. Teixeira Vieira Ligo, T. Arsiwala, A. Tarabishy, P. Tirumalai, D.O. Claassen, S. Hodder, M.W. Haut, Ultrasound Blood–Brain Barrier Opening and Aducanumab in Alzheimer's Disease, N. Engl. J. Med. 390 (2024) 55–62. https://doi.org/10.1056/NEJMoa2308719.
[90] J.J. Sabatino, S.S. Zamvil, S.L. Hauser, B-Cell Therapies in Multiple Sclerosis, Cold Spring Harb. Perspect. Med. 9 (2019) a032037. https://doi.org/10.1101/cshperspect.a032037.
[91] S. Gupta, S.S. Zamvil, Can Systemic Anti-CD20 B Cell-Depleting Antibodies Eliminate Meningeal Follicles in Multiple Sclerosis?, Neurol. Neuroimmunol. Neuroinflammation 8 (2021) e1000. https://doi.org/10.1212/NXI.0000000000001000.

[92] L. Han, C. Liu, H. Qi, J. Zhou, J. Wen, D. Wu, D. Xu, M. Qin, J. Ren, Q. Wang, L. Long, Y. Liu, I. Chen, X. Yuan, Y. Lu, C. Kang, Systemic Delivery of Monoclonal Antibodies to the Central Nervous System for Brain Tumor Therapy, Adv. Mater. 31 (2019) 1805697. https://doi.org/10.1002/adma.201805697.
[93] V. Sifniotis, E. Cruz, B. Eroglu, V. Kayser, Current advancements in addressing key challenges of therapeutic antibody design, manufacture, and formulation, Antibodies 8 (2019) 36us. https://doi.org/10.3390/antib8020036.
[94] A. Amiri, G. Barreto, T. Sathyapalan, A. Sahebkar, siRNA Therapeutics: Future Promise for Neurodegenerative Diseases, Curr. Neuropharmacol. 19 (2021) 1896. https://doi.org/10.2174/1570159X19666210402104054.
[95] S. Guo, M. Zhang, Y. Huang, Three 'E' challenges for siRNA drug development, Trends Mol. Med. 30 (2024) 13–24. https://doi.org/10.1016/j.molmed.2023.10.005.
[96] M. Moazzam, M. Zhang, A. Hussain, X. Yu, J. Huang, Y. Huang, The landscape of nanoparticle-based siRNA delivery and therapeutic development, Mol. Ther. 32 (2024) 284–312. https://doi.org/10.1016/j.ymthe.2024.01.005.
[97] D.A. Quinteros, J.M. Bermúdez, S. Ravetti, A. Cid, D.A. Allemandi, S.D. Palma, Therapeutic use of monoclonal antibodies: general aspects and challenges for drug delivery, Nanostructures Drug Deliv. (2017) 807–833. https://doi.org/10.1016/B978-0-323-46143-6.00025-7.
[98] M.L. Borrajo, M.J. Alonso, Using nanotechnology to deliver biomolecules from nose to brain — peptides, proteins, monoclonal antibodies and RNA, Drug Deliv. Transl. Res. 12 (2022) 862–880. https://doi.org/10.1007/s13346-021-01086-2.
[99] T. Musumeci, G. Di Benedetto, C. Carbone, A. Bonaccorso, G. Amato, M.J. Lo Faro, C. Burgaletto, G. Puglisi, R. Bernardini, G. Cantarella, Intranasal Administration of a TRAIL Neutralizing Monoclonal Antibody Adsorbed in PLGA Nanoparticles and NLC Nanosystems: An In Vivo Study on a Mouse Model of Alzheimer's Disease, Biomedicines 10 (2022) 985. https://doi.org/10.3390/biomedicines10050985.
[100] N.N. Ferreira, S. Granja, F.I. Boni, F.G. Prezotti, L.M.B. Ferreira, B.S.F. Cury, R.M. Reis, F. Baltazar, M.P.D. Gremião, Modulating chitosan-PLGA nanoparticle properties to design a co-delivery platform for glioblastoma therapy intended for nose-to-brain route, Drug Deliv. Transl. Res. 10 (2020) 1729–1747. https://doi.org/10.1007/s13346-020-00824-2.
[101] Z.H. Wang, Z.Y. Wang, C.S. Sun, C.Y. Wang, T.Y. Jiang, S.L. Wang, Trimethylated chitosan-conjugated PLGA nanoparticles for the delivery of drugs to the brain, Biomaterials 31 (2010) 908–915. https://doi.org/10.1016/j.biomaterials.2009.09.104.
[102] L. Chu, A. Wang, L. Ni, X. Yan, Y. Song, M. Zhao, K. Sun, H. Mu, S. Liu, Z. Wu, C. Zhang, Nose-to-brain delivery of temozolomide-loaded PLGA nanoparticles functionalized with anti-EPHA3 for glioblastoma targeting, Drug Deliv. 25 (2018) 1634–1641. https://doi.org/10.1080/10717544.2018.1494226.
[103] C. Gruber-Traub, J. Ullrich, »N2B-Patch« – Nose-To-Brain Delivery of an Active Pharmaceutical Ingredient via the Olfactory Region, Drug Des. Intellect. Prop. Int. J. (2018). https://doi.org/10.32474/DDIPIJ.2018.01.000116.
[104] N.G. Türeli, A.E. Türeli, Chapter 11 - Upscaling and GMP production of pharmaceutical drug delivery systems, in: R. Shegokar (Ed.), Drug Deliv. Trends, Elsevier, 2020: pp. 215–229. https://doi.org/10.1016/B978-0-12-817870-6.00011-0.

[105] R.K. Thapa, J.O. Kim, Nanomedicine-based commercial formulations: current developments and future prospects, J. Pharm. Investig. 53 (2023) 19–33. https://doi.org/10.1007/s40005-022-00607-6.
[106] R. Paliwal, R.J. Babu, S. Palakurthi, Nanomedicine Scale-up Technologies: Feasibilities and Challenges, AAPS PharmSciTech 15 (2014) 1527–1534. https://doi.org/10.1208/s12249-014-0177-9.
[107] T. Patel, J. Zhou, J.M. Piepmeier, W.M. Saltzman, Polymeric nanoparticles for drug delivery to the central nervous system, Adv. Drug Deliv. Rev. 64 (2012) 701–705. https://doi.org/10.1016/j.addr.2011.12.006.
[108] A. Zielinska, F. Carreiró, A.M. Oliveira, A. Neves, B. Pires, D. Nagasamy Venkatesh, A. Durazzo, M. Lucarini, P. Eder, A.M. Silva, A. Santini, E.B. Souto, Polymeric Nanoparticles: Production, Characterization, Toxicology and Ecotoxicology, Molecules 25 (2020) 3731-. https://doi.org/10.3390/molecules25163731.
[109] S. Ding, N. Anton, T.F. Vandamme, C.A. Serra, Microfluidic nanoprecipitation systems for preparing pure drug or polymeric drug loaded nanoparticles: an overview, Expert Opin. Drug Deliv. (2016) 1447–1460. https://doi.org/10.1080/17425247.2016.1193151.
[110] R. Rietscher, C. Thum, C.-M. Lehr, M. Schneider, Semi-automated nanoprecipitation-system—an option for operator independent, scalable and size adjustable nanoparticle synthesis, Pharm. Res. 32 (2015) 1859–1863. https://doi.org/10.1007/s11095-014-1612-z.
[111] S. Schiller, A. Hanefeld, M. Schneider, C.-M. Lehr, Focused Ultrasound as a Scalable and Contact-Free Method to Manufacture Protein-Loaded PLGA Nanoparticles, Pharm. Res. 32 (2015) 2995–3006. https://doi.org/10.1007/s11095-015-1681-7.
[112] P.M. Valencia, O.C. Farokhzad, R. Karnik, R. Langer, Microfluidic technologies for accelerating the clinical translation of nanoparticles, Nat. Nanotechnol. 7 (2012) 623–629. https://doi.org/10.1038/nnano.2012.168.
[113] D.D. Ojeda-Hernández, A.A. Canales-Aguirre, J. Matias-Guiu, U. Gomez-Pinedo, J.C. Mateos-Díaz, Potential of Chitosan and Its Derivatives for Biomedical Applications in the Central Nervous System, Front. Bioeng. Biotechnol. 8 (2020) 389. https://doi.org/10.3389/fbioe.2020.00389.
[114] Y. Wang, B. Qin, G. Xia, S.H. Choi, FDA's Poly (Lactic-Co-Glycolic Acid) Research Program and Regulatory Outcomes, AAPS J. 23 (2021) 92. https://doi.org/10.1208/s12248-021-00611-y.
[115] B. Gabold, F. Adams, S. Brameyer, K. Jung, C.L. Ried, T. Merdan, O.M. Merkel, Transferrin-modified chitosan nanoparticles for targeted nose-to-brain delivery of proteins, Drug Deliv. Transl. Res. 13 (2023) 822–838. https://doi.org/10.1007/s13346-022-01245-z.
[116] A.-T. Chatzitaki, S. Jesus, C. Karavasili, D. Andreadis, D.G. Fatouros, O. Borges, Chitosan-coated PLGA nanoparticles for the nasal delivery of ropinirole hydrochloride: In vitro and ex vivo evaluation of efficacy and safety, Int. J. Pharm. 589 (2020) 119776. https://doi.org/10.1016/j.ijpharm.2020.119776.
[117] L.M. Spindler, A. Feuerhake, S. Ladel, C. Günday, J. Flamm, N. Günday-Türeli, E. Türeli, G.E.M. Tovar, K. Schindowski, C. Gruber-Traub, Nano-in-Micro-Particles Consisting of PLGA Nanoparticles Embedded in Chitosan Microparticles via Spray-Drying Enhances Their Uptake in the Olfactory Mucosa, Front. Pharmacol. 12 (2021). https://doi.org/10.3389/fphar.2021.732954.
[118] A. Haasbroek-Pheiffer, S. Van Niekerk, F. Van der Kooy, T. Cloete, J. Steenekamp, J. Hamman, In vitro and ex vivo experimental models for evaluation

of intranasal systemic drug delivery as well as direct nose-to-brain drug delivery, Biopharm. Drug Dispos. 44 (2023) 94–112. https://doi.org/10.1002/bdd.2348.
[119] M.A. Albarki, M.D. Donovan, Bigger or Smaller? Size and Loading Effects on Nanoparticle Uptake Efficiency in the Nasal Mucosa, AAPS PharmSciTech 21 (2020) 294. https://doi.org/10.1208/s12249-020-01837-3.
[120] S. Vachhani, C. Kleinstreuer, Numerical analysis of enhanced nano-drug delivery to the olfactory bulb, Aerosol Sci. Technol. 55 (2021) 1343–1358. https://doi.org/10.1080/02786826.2021.1959018.
[121] J. Smith, E. Wood, M. Dornish, Effect of chitosan on epithelial cell tight junctions, Pharm. Res. 21 (2004) 43–49. https://doi.org/10.1023/b:pham.0000012150.60180.e3.
[122] G. Kali, B. Özkahraman, F. Laffleur, P. Knoll, R. Wibel, K. Zöller, A. Bernkop-Schnürch, Thiolated Cellulose: A Dual-Acting Mucoadhesive and Permeation-Enhancing Polymer, Biomacromolecules 24 (2023) 4880–4889. https://doi.org/10.1021/acs.biomac.3c00577.
[123] O.I. Martínez-Muñoz, L.F. Ospina-Giraldo, C.E. Mora-Huertas, O.I. Martínez-Muñoz, L.F. Ospina-Giraldo, C.E. Mora-Huertas, Nanoprecipitation: Applications for Entrapping Active Molecules of Interest in Pharmaceutics, in: Nano-Microencapsul. - Tech. Appl., IntechOpen, 2020. https://doi.org/10.5772/intechopen.93338.
[124] S. Salatin, J. Barar, M. Barzegar-Jalali, K. Adibkia, F. Kiafar, M. Jelvehgari, Development of a nanoprecipitation method for the entrapment of a very water soluble drug into Eudragit RL nanoparticles, Res. Pharm. Sci. 12 (2017) 1–14. https://doi.org/10.4103/1735-5362.199041.
[125] C. Draheim, F. de Crécy, S. Hansen, E.-M. Collnot, C.-M. Lehr, A Design of Experiment Study of Nanoprecipitation and Nano Spray Drying as Processes to Prepare PLGA Nano- and Microparticles with Defined Sizes and Size Distributions, Pharm. Res. 32 (2015) 2609–2624. https://doi.org/10.1007/s11095-015-1647-9.
[126] K. Krishnamoorthy, M. Mahalingam, Selection of a Suitable Method for the Preparation of Polymeric Nanoparticles: Multi-Criteria Decision Making Approach, Adv. Pharm. Bull. 5 (2015) 57–67. https://doi.org/10.5681/apb.2015.008.
[127] H.K. Makadia, S.J. Siegel, Poly Lactic-co-Glycolic Acid (PLGA) as biodegradable controlled drug delivery carrier, Polymers 3 (2011) 1377–1397. https://doi.org/10.3390/polym3031377.
[128] B. Gaba, T. Khan, M.F. Haider, T. Alam, S. Baboota, S. Parvez, J. Ali, Vitamin E Loaded Naringenin Nanoemulsion via Intranasal Delivery for the Management of Oxidative Stress in a 6-OHDA Parkinson's Disease Model, BioMed Res. Int. 2019 (2019) e2382563. https://doi.org/10.1155/2019/2382563.
[129] N. Günday Türeli, A.E. Türeli, M. Schneider, Counter-ion complexes for enhanced drug loading in nanocarriers: Proof-of-concept and beyond, Int. J. Pharm. 511 (2016) 994–1001. https://doi.org/10.1016/j.ijpharm.2016.08.004.
[130] K.Y. Hernández-Giottonini, R.J. Rodríguez-Córdova, C.A. Gutiérrez-Valenzuela, O. Peñuñuri-Miranda, P. Zavala-Rivera, P. Guerrero-Germán, A. Lucero-Acuña, PLGA nanoparticle preparations by emulsification and nanoprecipitation techniques: Effects of formulation parameters, RSC Adv. 10 (2020) 4218–4231. https://doi.org/10.1039/c9ra10857b.
[131] T. Pulingam, P. Foroozandeh, J.-A. Chuah, K. Sudesh, Exploring Various Techniques for the Chemical and Biological Synthesis of Polymeric

Nanoparticles, Nanomaterials 12 (2022) 576. https://doi.org/10.3390/nano12030576.
[132] K. Lim, Z.A.A. Hamid, 10 - Polymer nanoparticle carriers in drug delivery systems: Research trend, in: Inamuddin, A.M. Asiri, A. Mohammad (Eds.), Appl. Nanocomposite Mater. Drug Deliv., Woodhead Publishing, 2018: pp. 217–237. https://doi.org/10.1016/B978-0-12-813741-3.00010-8.
[133] S. Rezvantalab, N.I. Drude, M.K. Moraveji, N. Güvener, E.K. Koons, Y. Shi, T. Lammers, F. Kiessling, PLGA-Based Nanoparticles in Cancer Treatment, Front. Pharmacol. 9 (2018) 1260. https://doi.org/10.3389/fphar.2018.01260.
[134] M. Alvi, A. Yaqoob, K. Rehman, S.M. Shoaib, M.S.H. Akash, PLGA-based nanoparticles for the treatment of cancer: current strategies and perspectives, AAPS Open 8 (2022) 12. https://doi.org/10.1186/s41120-022-00060-7.
[135] K. Huanbutta, K. Suwanpitak, N. Weeranoppanant, P. Sriamornsak, K. Garg, S. Sharma, I. Singh, T. Sangnim, Continuous flow synthesis: A promising platform for the future of nanoparticle-based drug delivery, J. Drug Deliv. Sci. Technol. 91 (2024) 105265. https://doi.org/10.1016/j.jddst.2023.105265.
[136] S.J. Shepherd, D. Issadore, M.J. Mitchell, Microfluidic formulation of nanoparticles for biomedical applications, Biomaterials 274 (2021) 120826. https://doi.org/10.1016/j.biomaterials.2021.120826.
[137] C.J. Martínez Rivas, M. Tarhini, W. Badri, K. Miladi, H. Greige-Gerges, Q.A. Nazari, S.A. Galindo Rodríguez, R.Á. Román, H. Fessi, A. Elaissari, Nanoprecipitation process: From encapsulation to drug delivery, Int. J. Pharm. 532 (2017) 66–81. https://doi.org/10.1016/j.ijpharm.2017.08.064.
[138] N.J. Caggiano, S.K. Nayagam, L.Z. Wang, B.K. Wilson, P. Lewis, S. Jahangir, R.D. Priestley, R.K. Prud'homme, K.D. Ristroph, Sequential Flash NanoPrecipitation for the scalable formulation of stable core-shell nanoparticles with core loadings up to 90%, Int. J. Pharm. 640 (2023) 122985. https://doi.org/10.1016/j.ijpharm.2023.122985.
[139] X. Zhang, L.Y. Chau, H.W. Chan, J. Weng, K.W. Wong, S.F. Chow, A.H.L. Chow, Physical stability and in vivo brain delivery of polymeric ibuprofen nanoparticles fabricated by flash nanoprecipitation, Int. J. Pharm. 598 (2021) 120224. https://doi.org/10.1016/j.ijpharm.2021.120224.
[140] M.B. Kulkarni, S. Goel, Microfluidic devices for synthesizing nanomaterials—a review, Nano Express 1 (2020) 032004. https://doi.org/10.1088/2632-959X/abcca6.
[141] M.I. Teixeira, M.H. Amaral, P.C. Costa, C.M. Lopes, D.A. Lamprou, Recent Developments in Microfluidic Technologies for Central Nervous System Targeted Studies, Pharmaceutics 12 (2020) 542. https://doi.org/10.3390/pharmaceutics12060542.
[142] K. Wang, U.S. Kumar, N. Sadeghipour, T.F. Massoud, R. Paulmurugan, A Microfluidics-Based Scalable Approach to Generate Extracellular Vesicles with Enhanced Therapeutic MicroRNA Loading for Intranasal Delivery to Mouse Glioblastomas, ACS Nano 15 (2021) 18327–18346. https://doi.org/10.1021/acsnano.1c07587.
[143] E. Samaridou, H. Walgrave, E. Salta, D.M. Álvarez, V. Castro-López, M. Loza, M.J. Alonso, Nose-to-brain delivery of enveloped RNA - cell permeating peptide nanocomplexes for the treatment of neurodegenerative diseases, Biomaterials 230 (2020) 119657. https://doi.org/10.1016/j.biomaterials.2019.119657.
[144] F. Mohebichamkhorami, M. Faizi, M. Mahmoudifard, A. Hajikarim-Hamedani, S.S. Mohseni, A. Heidari, Y. Ghane, M. Khoramjouy, M. Khayati, R. Ghasemi, H. Zali, S. Hosseinzadeh, E. Mostafavi, Microfluidic Synthesis of Ultrasmall

Chitosan/Graphene Quantum Dots Particles for Intranasal Delivery in Alzheimer's Disease Treatment, Small Weinh. Bergstr. Ger. 19 (2023) e2207626. https://doi.org/10.1002/smll.202207626.
[145] C. Martins, F. Araújo, M.J. Gomes, C. Fernandes, R. Nunes, W. Li, H.A. Santos, F. Borges, B. Sarmento, Using microfluidic platforms to develop CNS-targeted polymeric nanoparticles for HIV therapy, Eur. J. Pharm. Biopharm. 138 (2019) 111–124. https://doi.org/10.1016/j.ejpb.2018.01.014.
[146] M.C. Operti, A. Bernhardt, V. Sincari, E. Jager, S. Grimm, A. Engel, M. Hruby, C.G. Figdor, O. Tagit, Industrial Scale Manufacturing and Downstream Processing of PLGA-Based Nanomedicines Suitable for Fully Continuous Operation, Pharmaceutics 14 (2022) 276. https://doi.org/10.3390/pharmaceutics14020276.
[147] S.F. Tehrani, P. Bharadwaj, J. Leblond Chain, V.G. Roullin, Purification processes of polymeric nanoparticles: How to improve their clinical translation?, J. Control. Release Off. J. Control. Release Soc. 360 (2023) 591–612. https://doi.org/10.1016/j.jconrel.2023.06.038.
[148] N.K. Shah, R. Ivone, J. Shen, S.A. Meenach, A comparison of centrifugation and tangential flow filtration for nanoparticle purification: A case study on acetalated dextran nanoparticles, Particuology 50 (2020) 189–196. https://doi.org/10.1016/j.partic.2019.06.004.
[149] G. Dalwadi, H.A.E. Benson, Y. Chen, Comparison of diafiltration and tangential flow filtration for purification of nanoparticle suspensions, Pharm. Res. 22 (2005) 2152–2162. https://doi.org/10.1007/s11095-005-7781-z.
[150] P. Fonte, S. Reis, B. Sarmento, Facts and evidences on the lyophilization of polymeric nanoparticles for drug delivery, J. Controlled Release 225 (2016) 75–86. https://doi.org/10.1016/j.jconrel.2016.01.034.
[151] K. Sampathkumar, B.A. Kerwin, Roadmap for Drug Product Development and Manufacturing of Biologics, J. Pharm. Sci. 113 (2024) 314–331. https://doi.org/10.1016/j.xphs.2023.11.004.
[152] T.M. Amis, J. Renukuntla, P.K. Bolla, B.A. Clark, Selection of Cryoprotectant in Lyophilization of Progesterone-Loaded Stearic Acid Solid Lipid Nanoparticles, Pharmaceutics 12 (2020) 892. https://doi.org/10.3390/pharmaceutics12090892.
[153] N. Garti, R. Lutz, Chapter 14 - Recent progress in double emulsions, in: D.N. Petsev (Ed.), Interface Sci. Technol., Elsevier, 2004: pp. 557–605. https://doi.org/10.1016/S1573-4285(04)80016-4.
[154] M. Iqbal, N. Zafar, H. Fessi, A. Elaissari, Double emulsion solvent evaporation techniques used for drug encapsulation, Int. J. Pharm. 496 (2015) 173–190. https://doi.org/10.1016/j.ijpharm.2015.10.057.
[155] Y. Su, B. Zhang, R. Sun, W. Liu, Q. Zhu, X. Zhang, R. Wang, C. Chen, PLGA-based biodegradable microspheres in drug delivery: recent advances in research and application, Drug Deliv. 28 (n.d.) 1397–1418. https://doi.org/10.1080/10717544.2021.1938756.
[156] N. Prichapan, D.J. McClements, U. Klinkesorn, Encapsulation of Iron within W1/O/W2 Emulsions Formulated Using a Natural Hydrophilic Surfactant (Saponin): Impact of Surfactant Level and Oil Phase Crystallization, Food Biophys. 15 (2020) 346–354. https://doi.org/10.1007/s11483-020-09628-w.
[157] J. Andrade, M. Corredig, Vitamin D3 and phytosterols affect the properties of polyglycerol polyricinoleate (PGPR) and protein interfaces, Food Hydrocoll. 54 (2016) 278–283. https://doi.org/10.1016/j.foodhyd.2015.10.001.
[158] A. Lamprecht, N. Ubrich, M. Hombreiro Pérez, C.-M. Lehr, M. Hoffman, P. Maincent, Influences of process parameters on nanoparticle preparation

performed by a double emulsion pressure homogenization technique, Int. J. Pharm. 196 (2000) 177–182. https://doi.org/10.1016/S0378-5173(99)00422-6.
[159] M.F. Zambaux, F. Bonneaux, R. Gref, P. Maincent, E. Dellacherie, M.J. Alonso, P. Labrude, C. Vigneron, Influence of experimental parameters on the characteristics of poly(lactic acid) nanoparticles prepared by a double emulsion method, J. Controlled Release 50 (1998) 31–40. https://doi.org/10.1016/S0168-3659(97)00106-5.
[160] D. Deepika, H.K. Dewangan, L. Maurya, S. Singh, Intranasal Drug Delivery of Frovatriptan Succinate–Loaded Polymeric Nanoparticles for Brain Targeting, J. Pharm. Sci. 108 (2019) 851–859. https://doi.org/10.1016/j.xphs.2018.07.013.
[161] A.T. Alex, A. Joseph, G. Shavi, J.V. Rao, N. Udupa, Development and evaluation of carboplatin-loaded PCL nanoparticles for intranasal delivery, Drug Deliv. 23 (2016) 2144–2153. https://doi.org/10.3109/10717544.2014.948643.
[162] Z. Lu, J. Bei, S. Wang, A method for the preparation of polymeric nanocapsules without stabilizer, J. Controlled Release 61 (1999) 107–112. https://doi.org/10.1016/S0168-3659(99)00112-1.
[163] H.K. Sah, R. Toddywala, Y.W. Chien, Biodegradable microcapsules prepared by a w/o/w technique: Effects of shear force to make a primary w/o emulsion on their morphology and protein release, J. Microencapsul. 12 (1995) 59–69. https://doi.org/10.3109/02652049509051127.
[164] D.L. Priwitaningrum, J. Jentsch, R. Bansal, S. Rahimian, G. Storm, W.E. Hennink, J. Prakash, Apoptosis-inducing peptide loaded in PLGA nanoparticles induces anti-tumor effects in vivo, Int. J. Pharm. 585 (2020) 119535. https://doi.org/10.1016/j.ijpharm.2020.119535.
[165] Y. Zhu, G. Zhang, H. Yang, X. Hong, Influence of surfactants on the parameters of polylactide nanocapsules containing insulin, J. Surfactants Deterg. 8 (2005) 353–358. https://doi.org/10.1007/s11743-005-0368-9.
[166] A.R. Ahmed, R. Bodmeier, Preparation of preformed porous PLGA microparticles and antisense oligonucleotides loading, Eur. J. Pharm. Biopharm. 71 (2009) 264–270. https://doi.org/10.1016/j.ejpb.2008.09.007.
[167] M. Igartua, R.M. Hernández, J.E. Rosas, M.E. Patarroyo, J.L. Pedraz, γ-Irradiation effects on biopharmaceutical properties of PLGA microspheres loaded with SPf66 synthetic vaccine, Eur. J. Pharm. Biopharm. 69 (2008) 519–526. https://doi.org/10.1016/j.ejpb.2007.12.014.
[168] T.K. Giri, C. Choudhary, Ajazuddin, A. Alexander, H. Badwaik, D.K. Tripathi, Prospects of pharmaceuticals and biopharmaceuticals loaded microparticles prepared by double emulsion technique for controlled delivery, Saudi Pharm. J. SPJ 21 (2013) 125–141. https://doi.org/10.1016/j.jsps.2012.05.009.
[169] S. Saffarionpour, One-step preparation of double emulsions stabilized with amphiphilic and stimuli-responsive block copolymers and nanoparticles for nutraceuticals and drug delivery, JCIS Open 3 (2021) 100020. https://doi.org/10.1016/j.jciso.2021.100020.
[170] S. Mohammadi, A. Harvey, K.V.K. Boodhoo, Synthesis of TiO2 nanoparticles in a spinning disc reactor, Chem. Eng. J. 258 (2014) 171–184. https://doi.org/10.1016/j.cej.2014.07.042.
[171] C.Y. Tai, Y.-H. Wang, C.-T. Tai, H.-S. Liu, Preparation of Silver Nanoparticles Using a Spinning Disk Reactor in a Continuous Mode, Ind. Eng. Chem. Res. 48 (2009) 10104–10109. https://doi.org/10.1021/ie9005645.
[172] M. Stoller, J.M. Ochando-Pulido, ZnO Nano-Particles Production Intensification by Means of a Spinning Disk Reactor, Nanomaterials 10 (2020) 1321. https://doi.org/10.3390/nano10071321.

[173] N. Anantachoke, M. Makha, C.L. Raston, V. Reutrakul, N.C. Smith, M. Saunders, Fine tuning the production of nanosized beta-carotene particles using spinning disk processing, J. Am. Chem. Soc. 128 (2006) 13847–13853. https://doi.org/10.1021/ja063545n.
[174] S. Zamani, M.R. Rahimi, M. Ghaedi, Photocatalytic Degradation of Penicillin v Using Bi2O3/Ag/TiO2 Thin Film in a Spinning Disc Photoreactor under Blue LED Illumination, Iran. J. Chem. Chem. Eng. 41 (2022) 3032–3044. https://doi.org/10.30492/ijcce.2022.525941.4604.
[175] S. Zamani, M.R. Rahimi, M. Ghaedi, Spinning disc photoreactor based visible-light-driven Ag/Ag2O/TiO2 heterojunction photocatalyst film toward the degradation of amoxicillin, J. Environ. Manage. 303 (2022) 114216. https://doi.org/10.1016/j.jenvman.2021.114216.
[176] S. Fallahizadeh, M. Gholami, M.R. Rahimi, A. Esrafili, M. Farzadkia, M. Kermani, Enhanced photocatalytic degradation of amoxicillin using a spinning disc photocatalytic reactor (SDPR) with a novel Fe3O4@void@CuO/ZnO yolk-shell thin film nanostructure, Sci. Rep. 13 (2023) 16185. https://doi.org/10.1038/s41598-023-43437-8.
[177] G. Vilardi, M. Stoller, L. Di Palma, K. Boodhoo, N. Verdone, Metallic iron nanoparticles intensified production by spinning disk reactor: Optimization and fluid dynamics modelling, Chem. Eng. Process. - Process Intensif. 146 (2019) 107683. https://doi.org/10.1016/j.cep.2019.107683.
[178] A.J. Zander, Development of nanoparticulate drug delivery systems for cytostatic application in PIPAC, 2021. doi:10.22028/D291-35188.
[179] M. Akhtar, B.S. Murray, E.I. Afeisume, S.H. Khew, Encapsulation of flavonoid in multiple emulsion using spinning disc reactor technology, Food Hydrocoll. 34 (2014) 62–67. https://doi.org/10.1016/j.foodhyd.2012.12.025.
[180] S. Gandhi, D.H. Shastri, J. Shah, A.B. Nair, S. Jacob, Nasal Delivery to the Brain: Harnessing Nanoparticles for Effective Drug Transport, Pharmaceutics 16 (2024) 481. https://doi.org/10.3390/pharmaceutics16040481.
[181] A.E. Türeli, Nanoparticle preparation process using novel microjet reactor technology for enhancing dissolution rates of poorly water soluble drugs, Johannes Gutenberg-Universität Mainz, 2015. https://doi.org/10.25358/OPENSCIENCE-1833.
[182] N. Günday Türeli, A.E. Türeli, M. Schneider, Optimization of ciprofloxacin complex loaded PLGA nanoparticles for pulmonary treatment of cystic fibrosis infections: Design of experiments approach, Int. J. Pharm. 515 (2016) 343–351. https://doi.org/10.1016/j.ijpharm.2016.10.025.
[183] E.L.J. Moya, S.M. Lombardo, E. Vandenhaute, M. Schneider, C. Mysiorek, A.E. Türeli, T. Kanda, F. Shimizu, Y. Sano, N. Maubon, F. Gosselet, N. Günday-Türeli, M.-P. Dehouck, Interaction of surfactant coated PLGA nanoparticles with in vitro human brain-like endothelial cells, Int. J. Pharm. 621 (2022) 121780. https://doi.org/10.1016/j.ijpharm.2022.121780.
[184] J.M. Lü, X. Wang, C. Marin-Muller, H. Wang, P.H. Lin, Q. Yao, C. Chen, Current advances in research and clinical applications of PLGA-based nanotechnology, Expert Rev. Mol. Diagn. 9 (2009) 325–341. https://doi.org/10.1586/erm.09.15.
[185] Y. Hua, Y. Su, H. Zhang, N. Liu, Z. Wang, X. Gao, J. Gao, A. Zheng, Poly(lactic-co-glycolic acid) microsphere production based on quality by design: a review, Drug Deliv. 28 (2021) 1342–1355. https://doi.org/10.1080/10717544.2021.1943056.
[186] M.C. Operti, A. Bernhardt, S. Grimm, A. Engel, C.G. Figdor, O. Tagit, PLGA-based nanomedicines manufacturing: Technologies overview and challenges in

industrial scale-up, Int. J. Pharm. 605 (2021) 120807. https://doi.org/10.1016/j.ijpharm.2021.120807.
[187] G.K. Tripp, K.L. Good, M.J. Motta, P.H. Kass, C.J. Murphy, The effect of needle gauge, needle type, and needle orientation on the volume of a drop, Vet. Ophthalmol. 19 (2016) 38–42. https://doi.org/10.1111/vop.12253.
[188] T.P.T. Dao, T.H. Nguyen, V.V. To, T.H. Ho, T.A. Nguyen, M.C. Dang, A new formulation of curcumin using poly (lactic-co-glycolic acid)—polyethylene glycol diblock copolymer as carrier material, Adv. Nat. Sci. Nanosci. Nanotechnol. 5 (2014) 035013. https://doi.org/10.1088/2043-6262/5/3/035013.
[189] K.H. Lee, F.N. Khan, L. Cosby, G. Yang, J.O. Winter, Polymer Concentration Maximizes Encapsulation Efficiency in Electrohydrodynamic Mixing Nanoprecipitation, Front. Nanotechnol. 3 (2021). https://doi.org/10.3389/fnano.2021.719710.
[190] M. Danaei, M. Dehghankhold, S. Ataei, F. Hasanzadeh Davarani, R. Javanmard, A. Dokhani, S. Khorasani, M.R. Mozafari, Impact of Particle Size and Polydispersity Index on the Clinical Applications of Lipidic Nanocarrier Systems, Pharmaceutics 10 (2018) 57. https://doi.org/10.3390/pharmaceutics10020057.
[191] S. Ding, N. Anton, T.F. Vandamme, C.A. Serra, Microfluidic nanoprecipitation systems for preparing pure drug or polymeric drug loaded nanoparticles: an overview, Expert Opin. Drug Deliv. 13 (2016) 1447–1460. https://doi.org/10.1080/17425247.2016.1193151.
[192] N. Lababidi, V. Sigal, A. Koenneke, K. Schwarzkopf, A. Manz, M. Schneider, Microfluidics as tool to prepare size-tunable PLGA nanoparticles with high curcumin encapsulation for efficient mucus penetration, Beilstein J. Nanotechnol. 10 (2019) 2280–2293. https://doi.org/10.3762/bjnano.10.220.
[193] E. Türeli, K. Krauel-Göllner, Agilent NanoDis System Method Development Guide, 2020.
[194] S. Bolte, F.P. Cordelières, A guided tour into subcellular colocalization analysis in light microscopy, J. Microsc. 224 (2006) 213–232. https://doi.org/10.1111/j.1365-2818.2006.01706.x.
[195] K. Pearson, A. Lee, On the Laws of Inheritance in Man: I. Inheritance of Physical Characters, Biometrika 2 (1903) 357–462. https://doi.org/10.2307/2331507.
[196] E.M.M. Manders, J. Stap, G.J. Brakenhoff, R.V. Driel, J.A. Aten, Dynamics of three-dimensional replication patterns during the s-phase, analysed by double labelling of dna and confocal microscopy, J. Cell Sci. 103 (1992) 857–862. https://doi.org/10.1242/jcs.103.3.857.
[197] B.P. Peters, S. Ebisu, I.J. Goldstein, M. Flashner, Interaction of wheat germ agglutinin with sialic acid, Biochemistry 18 (1979) 5505–5511. https://doi.org/10.1021/bi00591a038.
[198] A. Katsikari, Chr. Patronidou, C. Kiparissides, M. Arsenakis, Uptake and cytotoxicity of poly(d,l-lactide-co-glycolide) nanoparticles in human colon adenocarcinoma cells, Mater. Sci. Eng. B 165 (2009) 160–164. https://doi.org/10.1016/j.mseb.2009.09.007.
[199] M.J. Mitchell, M.M. Billingsley, R.M. Haley, M.E. Wechsler, N.A. Peppas, R. Langer, Engineering precision nanoparticles for drug delivery, Nat. Rev. Drug Discov. 20 (2021) 101–124. https://doi.org/10.1038/s41573-020-0090-8.
[200] S. Hernando, E. Santos-Vizcaíno, M. Igartua, R.M. Hernandez, Targeting the central nervous system: From synthetic nanoparticles to extracellular vesicles—Focus on Alzheimer's and Parkinson's disease, WIREs Nanomedicine Nanobiotechnology 15 (2023) e1898. https://doi.org/10.1002/wnan.1898.

6.2. Scientific Output

Articles

Published Article

- Akpinar Adscheid, A.E. Türeli, N. Günday-Türeli, M. Schneider, Nanotechnological approaches for efficient N2B delivery: from small-molecule drugs to biopharmaceuticals, Beilstein J. Nanotechnol. 15 (2024) 1400–1414. https://doi.org/10.3762/bjnano.15.113.
- S. Akpinar Adscheid, M. Rojas-Rodríguez, S.M. Abdel-Hafez, F.S. Pavone, M. Schneider, A.E. Türeli, M. Calamai, N. Günday-Türeli, Scalable Manufacturing Method for Model Protein-Loaded PLGA Nanoparticles: Biocompatibility, Trafficking and Release Properties, Pharmaceutics 17 (2025) 87. https://doi.org/10.3390/pharmaceutics17010087.

Submitted Articles & Book Chapters

Book chapter:

- Akpinar Adscheid, S.; Türeli, A.E.; Günday-Türeli, N. Industrial Aspects to be considered for drug delivery for brain. Taylor & Francis: Oxfordshire, UK., 2024

Oral presentations

- MSCA ITN Bio2Brain scientific meeting, oral presentation, “Bio(polymer)-based particulate formulations for intranasal transmucosal delivery of biopharmaceuticals”, August 2022, Biberach, Germany

- MSCA ITN Bio2Brain scientific meeting, oral presentation, “Bio(polymer)-based particulate formulations for intranasal transmucosal delivery of biopharmaceuticals”, February 2023, Stuttgart, Germany
- MSCA ITN Bio2Brain scientific meeting, oral presentation as part of work package 1 session, “Bio(polymer)-based particulate formulations for intranasal transmucosal delivery of biopharmaceuticals”, June 2023, City of London, UK.
- UK Colloids 2023, oral presentation as part of Polymer Colloid Engineering session, “Manufacturing of PLGA-W/O/W Double Emulsions with a Novel Spray-Reactor-System for Nose-to-Brain Delivery Applications” July 2023, Liverpool, UK
- MSCA ITN Bio2Brain scientific meeting, oral presentation as part of work package 1 session, “Bio(polymer)-based particulate formulations for intranasal transmucosal delivery of biopharmaceuticals”, January 2024, Florence, Italy

Poster presentations

- Controlled Release Society German Chapter Meeting, poster presentation, “Development of Polymeric Nanoparticles with an Innovative Continuous Manufacturing Method”, March 2023, Würzburg, Germany
- PhD Students' Day “Development of Polymer-based Particulate Formulations with an Innovative Continuous Manufacturing Method”, May 2023, Saarbrücken, Germany
- Controlled Release Society German Chapter Meeting, poster presentation, “Manufacturing PLGA Nanoparticles with Novel-spray-reactor system for Nose-to-brain Delivery”, January 2024, Bad Dürkheim, Germany

6.3. Curriculum Vitae

Name: Selin Akpinar Adscheid

Date of birth: 27.02.1995, in Yüregir, Adana, Türkiye

Education

Doctoral Candidate in Pharmacy Oct 2021-Present

Biopharmaceutics and Pharmaceutical Technology, Department of Pharmacy

Saarland University, Saarbrücken, Germany

MSc. in Nanomedicine and Drug Delivery Graduated in Jul 2021 *(with High Honors)*

Department of Pharmacy, Pharmaceutical Technology

University of Paris Cité (Paris, France), University of Angers (Angers, France), University of Pavia (Pavia, Italy) and University of Patras (Patras, Greece)

- As part of Erasmus Mundus Joint Master´s Degree (EMJMD) Nanomedicine for Drug Delivery (NANOMED) program with an EU-funded EMJMD scholarship

BSc. in Chemistry Graduated in Jun 2019 *(with Honors)*

Department of Chemistry

Middle East Technical University, Ankara, Türkiye

Professional Experience

Postdoctoral Research Associate April 2025-Present

Johannes Gutenberg-Universität Mainz, Institute for Pharmaceutical and Biomedical Sciences, Department of Pharmacology and Toxicology, Mainz, Germany

Process Engineer Oct 2024-March 2025

Procter & Gamble (P&G), Gross Gerau, Germany

Marie Skłodowska-Curie Early-Stage Researcher (Scientist) Oct 2021-Sep 2024

MyBiotech GmbH, Überherrn, Germany

- As part of Marie Skłodowska-Curie Actions (MSCA), Innovative Training Network (ITN) Bio2Brain project, funded by EU Horizon 2020 with a fellowship
- As part of the MSCA ITN Bio2Brain project, a month-long-secondment at **Queen Mary University of London (QMUL)** at Resmini lab and a month-long-secondment at **European Laboratory of Non-linear Spectroscopy, LENS** at Calamai Lab have been performed for collaboration, research and training purposes.

6.4. Acknowledgements

I am sincerely thankful to everyone who made it possible to complete this thesis throughout the past three years and for their endless support for many years; without them, it would not have been possible. This list can only show a small fraction of the support I receive and the people I am thankful for.

I would like to express my gratitude to my supervisors at MyBiotech, Dr. Nazende Günday-Türeli and Dr. Emre Türeli, for their help, time, and endless support during the past years. I consider coming to Überherrn and working with you as one of the best decisions I have made, thanks to your countless support. Thank you for everything from the bottom of my heart!

I also would like to thank my supervisor, Prof. Dr. Marc Schneider, for his guidance, time, support, and valuable feedback during my doctoral studies. Thank you for including me in your team, which I am very happy and grateful to be part of. I am also very happy that you always created time for me and the project, even with your busy schedule.

I would like to thank the European Union H2020 Marie Skłodowska-Curie Actions for funding and the MSCA ITN Bio2Brain project consortium for their support. I feel fortunate to be part of such an international and brilliant project and to have the Bio2Brain team as my colleagues. I will always miss our time together in international meetings all around Europe.

Especially to everyone at MyBiotech GmbH, I would like to thank you for supporting me as a PhD student and as a member of the team. I have always felt at home here and am very lucky to have you call my colleagues and friends.

Especially thanks to every past and current member of AG Schneider at Saarland University for including me in the team and not making me feel like an outsider. I always enjoyed our time together. I also would like to extend my thanks to Dr. Salma M Abdel-Hafez for our collaboration, her time, and our nice discussions.

My very special gratitude goes to fellow early-stage researchers in the MSCA ITN Bio2Brain project, who made the journey very special and fun at the same time! I would also like to thank the QMUL and LENS team members, especially for hosting me during my secondments in London and Florence and for their time and support. I would also

like to thank all ESRs who visited MyB as part of their secondments for their valuable contribution to the project and scientific exchange.

I would also like to thank LENS team members Marta Rojas Rodríguez and Dr. Martino Calamai once again for our fruitful collaboration during the Bio2Brain project, which led to exciting results. Working with you was a pleasure, and I am happy to see that our hard work has paid off!

I would like to especially extend my thanks to MyB team once again. I would like to thank Cemre Günday for her help, endless support, and friendship without hesitation during my doctoral work since the beginning, for which I will always be grateful. I would also like to thank Zeliha Yetiren-Isoglu, especially for her friendship and support in the lab. My thanks are extended to my friends and colleagues Eleonora Rizzi and Gökalp Isoglu for their support and friendship. I am looking forward to many more adventures and fun times!

I would also like to thank my colleague Felix Penth for his time, effort, and his vision in re-establishing the SDS and for the very nice collaborations. I would also like to thank Dr. Ailing Qiao for their support in the lab.

Another very special gratitude goes to all the master's and undergraduate interns/students I had the opportunity to work with: Shehneela Jamil, Mohamed Saqawa, Beyda Bilim, and Francisco Branco, for working together, their help during the experiments and being fun lab mates. I truly enjoyed working with you and am thankful for your time on this project.

I would like to thank all my friends from all over the world for supporting me, sending me PhD memes, and being there for me in good and hard times. I would like to thank Ann, Yigit, Bilal and Esra for their kind friendship and support. I look forward to creating many more memories and having many more adventures.

Finally, in the next parts, I would like to thank my family. Without the support of all my family in Türkiye and Germany, none of this would have been possible.

To my Mutti, Renate, for her love and support and for making me feel at home, far away from home.

To everyone back in Türkiye, including all my friends and relatives, for their support and for rooting for me since I was a little child. Your support made all this journey possible!

Of course, to my father, Mehmet, and my mother, Belgin, for supporting me since I was little, for every decision I made, and for being the best parents that I can ask for. Without your support, none would be possible. Thank you for supporting me by taking a journey all around the world, even if this includes lots of missing. Thank you for always supporting my curiosity and creating opportunities for me. This is also your thesis and success. Love you so much!

And to my dear Toni, for being an amazing partner, soulmate and now husband. You have supported me endlessly since the beginning of my PhD, and you were there for me in each step. I can't wait to create many more memories with you all around the world and spend a lifetime together. Love you so much!

Selin Akpinar Adscheid